Engineering a 3D composite hydrogel with antibacterial activity for skin regeneration

Ana Moura Vieira Faria Brites

Thesis to obtain the Master of Science Degree in

Biological Engineering

Supervisors: Prof. Dr. Catarina Ferreira dos Santos

Prof. Dr. Joana Marques Marto

Examination Committee

Chairperson: Prof. Dr. Cláudia Alexandra Martins Lobato da Silva

Supervisor: Prof. Dr. Catarina Ferreira dos Santos

Member of the Committee: Prof. Dr. Maria Helena Raposo Fernandes

November 2021

Declaration

I declare that this document is an original work of my own authorship and that it fulfils all the requirements of the Code of Conduct and Good Practices of the Universidade de Lisboa.

Preface

This document was written and made publicly available as an institutional academic requirement and as a part of the evaluation of the MSc thesis in Biological Engineering of the author at Instituto Superior Técnico. The work described herein was initially performed at the Pharmaceutical Development Lab, Faculty of Pharmacy, University of Lisbon (Lisbon, Portugal) and at the CDP2T group, Polytechnic Institute of Setúbal (Setúbal, Portugal), during the period April-May 2021, under the supervision of Prof. Dr. Catarina Santos and Prof. Dr. Joana Marto. The termination of the work was performed at the Bone Lab, Faculty of Dental Medicine, University of Porto (Porto, Portugal), during the period June-September 2021, under the supervision of Prof. Dr. Maria Helena Fernandes. The thesis was co-supervised at Instituto Superior Técnico by Prof. Dr. Catarina Santos (CQE, Instituto Superior Técnico) and Prof. Dr. Joana Marto.

Acknowledgments

First, I would like to express my gratitude to my supervisors, for all the knowledge transmitted and the help along the way. To Prof. Catarina Santos, who always encouraged me to have a positive attitude when facing adversity and to think outside the box, when needed. To Prof. Joana Marto, for her accessibility during this time and for always providing me the tools to succeed.

To 3DGelComp Group, at Polytechnic Institute of Setúbal (Setúbal, Portugal), I want to thank for giving me the opportunity to use the 3D printer, utilized during the work.

To Marta, just like you said, words are not enough. I never thought I would leave with such a great friendship. Thank you for all the support and help when I felt hopeless.

To Sara, thank you for all the patience, for teaching me how to use the printer and for all the help; to Daniel, Prof. Ricardo Cláudio and Engineer Gonçalo Torres for their kindness and availability and for always being ready to solve all problems.

To Bone Lab, Faculty of Dental Medicine, University of Porto, thank you for providing me every tool to successfully conclude my work and for the contribution given during the biological characterization part of this process. To the Bone Lab team, Prof. Dr. Maria Helena, Prof. Dr. Pedro, Prof. Dr. Liliana, Víctor, Carla, Laura, Sanjana, Rita and Lorena, I want to thank you all for the heart-warming welcome and for always making me feel at home.

A special thank you to Prof. Maria Helena for welcoming me in her Lab and for supporting me during all the process; to Prof. Pedro Gomes for the availability and all the help provided. I would also like to specially thank Prof. Liliana Grenho who, most definitely, is the most patient person in this world and was always available to help me in my work, frustrations, in everything.

To my friends, who were always there for me, no matter what, thank you for the strength, for all the laughs and cries and the emotional support during the toughest times.

At last, I want to thank my family. To my parents who never let me give up and encourage me to be a better and stronger person. For all the patience and motivation when I had none left. To the rest of my family, thank you for all the support and encouragement. To my grandparents, this is for you.

Abstract

Wound care is a huge burden in worldwide health care expenses and the progress in new therapeutics for topical applications is crucial. One of the development approaches combines composite hydrogels with three-dimensional (3D) printing technology.

The main goal of this work was to produce 3D printed gelatine-based hydrogels displaying antibacterial properties, for topical applications. To achieve this, 40% Manuka Honey (MH), a potent antimicrobial monofloral honey, was incorporated into the gelatine-based hydrogel. The increase in gelatin concentration from 30% to 40%, as well as the incorporation of MH, were studied through rheological and printing tests. In both cases, an increase in ink viscosity and in printing temperature, from 34 ºC to 43 ºC, occurred. The remaining printing conditions, printing pressure (25 Psi), layer heigh (0.15 mm), line width (0.6 mm) and printing velocity (30 mm/s) were maintained for all inks. Reproducible three-layered patches, with high shape fidelity and adequate porosity were obtained.

The incorporation of MH in the hydrogels caused a significant antibacterial effect against *S. aureus*, *S. epidermidis* and *E. coli*, but not *P. aeruginosa*, after 24h. A higher impact on gram-positive bacteria was perceived. Gelatine-based patches were not cytotoxic against human dermal fibroblasts and human epidermal keratinocytes, after 24h. Furthermore, the concentration of the incorporated MH was a determinant factor in the cytotoxic tests. Additionally, the 3D patches showed no irritation in the HET-CAM tests and did not increase angiogenesis. The results suggest that the proposed 3D printed hydrogels are suitable for topical applications with therapeutic properties.

Keywords: Gelatine-based hydrogel; Manuka honey; topical application; 3D printing; antibacterial activity.

Resumo

O tratamento de feridas representa um custo muito elevado na saúde pública, sendo crucial o desenvolvimento de novas terapias, para aplicação tópica. Neste âmbito, o desenvolvimento de hidrogéis recorrendo a impressão 3D é uma das abordagens desenvolvidas.

O principal objetivo deste trabalho consistiu na produção de hidrogéis 3D à base de gelatina e com propriedades antibacterianas, para aplicações tópicas. Para tal, 40% de mel de Manuka (MH), um potente antimicrobiano monofloral, foi incorporado no hidrogel. O aumento da concentração da gelatina de 30% para 40% e a incorporação de MH foram estudados, recorrendo-se a testes reológicos e testes de impressão. Em ambos os casos, um aumento da viscosidade e temperatura de impressão (34 ºC para 43 ºC) foi percetível. As restantes condições de impressão, pressão de extrusão (25 Psi), altura da camada (0.15 mm), largura da linha (0.6 mm) e velocidade de impressão (30 mm/s) mantiveram-se constantes para os 3 hidrogéis.

Os hidrogéis com MH incorporado demonstraram propriedades antibacterianas significativas contra *S. aureus, S. epidermidis* e *E. coli,* contrariamente ao observado em *P. aeruginosa,* após 24h. Os hidrogéis de gelatina não provocaram citototoxicidade em fibroblastos humanos da derme e queratinócitos humanos da epiderme e a concentração de MH foi um fator determinante nos testes de citotoxicidade, após 24h. Adicionalmente, os hidrogéis não provocaram irritabilidade no teste HET-CAM, nem promoveram angiogénese. Estes resultados sugerem que os hidrogéis produzidos por impressão 3D à base de gelatina e MH podem ser adequados para o desenvolvimento de novos adesivos com propriedades terapêuticas.

Palavras-chave: Hidrogel à base de gelatina; mel de Manuka; aplicação tópica; impressão 3D; atividade antibacteriana.

Table of Content

List of Figures

List of Tables

List of Abbreviations

% - Percent

µL – Microlitre

µm – micrometre

µM – Micromolar

2D – Two Dimensional

2MH-P30 – Gelatin Based Patch with Layer 1&3 Of MH-P30 Ink and Layer 2 Of P30 Control Ink

3D – Three Dimensional

3MH-P30 – Gelatin Based Patch with 3 Layers of MH-P30 ink

5(6)-CDCFDA – 5(6)-Carboxy-2',7'-Dichloroflourescein Diacetate

AA – Ascorbic Acid

ATP - Adenosine Triphosphate

ATR-FTIR - Attenuated Total Reflectance-Fourier Transform Infrared Spectroscopy

BG – Borat Bioactive Glass

BSA – Bovine Serum Albumin

CAD – Computer-Aided Design

CFU - Colony-Forming Unit

cm – Centimetre

CO_2 – Carbon Dioxide

DMSO – Dimethyl Sulfoxide Solution

EC_{05} – Cytotoxic Effect In 5% of the Population

EC_{50} – Cytotoxic Effect In 50% of the Population

ECM – Extracellular Matrix

FBS-HI – Heat-Inactivated Fetal Bovine Serum

FDA - US Food and Drug Administration

FGF-2 - Fibroblast Growth Factor 2

g – Gram

G’ – Storage Modulus

G’’ – Loss Modulus

Gen – Gentamicin

h – Hours

H_2O_2 – Hydrogen Peroxide

HDF – Human Dermal Fibroblasts

HEK – Human Epidermal Keratinocytes

HET-CAM - Hen's Egg Test on the Chorioallantoic Membrane

HPL – Human Platelet Lysate

Hz – Hertz

ID – Identification

kV - Kilovolts

LCST - Lower Critical Solution Temperature

M – Molar

MBC – Minimum Bactericidal Concentration

MDRP - Multidrug-resistant *P. aeruginosa*

mg – Milligram

MGO – Methylglyoxal

MH - Manuka Honey

MH-P30 – Gelatin Based Ink Incorporated with 40% MH

MIC - Minimum Inhibitory Concentration

min – Minutes

mL – Millilitre

mm – Millimetre

mm/s – Millimetre per Second

MMPs – Matrix Metalloproteinases

MRSA - Methicillin-Resistant *Staphylococcus aureus*

MTT – 3-(4,5-Dimethylthiazol-2-Yl)-2,5-Diphenyl-2H-Tetrazolium Bromide

NaCl – Sodium Chloride

NADPH - Nicotinamide Adenine Dinucleotide Phosphate

NaOH – Sodium Hydroxide

nm – Nanometre

º – Degree

ºC – Degree Celsius

OD – Optical Density

P30 – Gelatin Based Ink with 30% Gelatine

P40 - Gelatin Based Ink with 40% Gelatine

Pa – Pascal

PBS - Phosphate-Buffered Saline

Psi - Pound-Force per Square Inch

RFU – Relative Units of Fluorescence

RGD - Arg-Gly-Asp

ROS – Reactive Oxygen Species

rpm – Rotation Per Minute

S.D. – Standard Deviation

SEM – Scanning Electron Microscopy

T – Temperature

TEM - Transmission Electron Microscopy

TSB – Tryptic Soy Broth

Tsol-gel – Sol-Gel Transition Temperature

UCST – Upper Critical Solution Temperature

UMF – Unique Manuka Factor

UV – Ultraviolet

v/v – Volume per Volume

VEGF - Vascular Endothelial Growth Factor

w/v – Weight per Volume

α-MEM – Alpha-Minimum Essential Medium

β – Beta

ΔT – Temperature Difference

ρ – Density

Chapter 1: Introduction

1. Introduction

Tissue damage and injury, especially skin wounds, is a severe health problem and a rapidly growing burden in worldwide health care expenses [1]. Over the last three decades, the fields of tissue engineering and regenerative medicine have made big efforts to try and meet the needs for alternatives to artificial tissues and organs for transplant. The treatment options for damaged tissue and organs currently rely on obtaining tissue from the patient itself or transplantation from cadavers. These treatments are very limited, moreover, limitations like donor site morbidity and donor scarcity support the urgent need for the development of biological substitutes [2].

Skin is the largest organ in our body and is responsible for several key functions such as protecting the body from trauma, shielding internal tissues from microbial infections, regulating body temperature and protection against ultraviolet radiation, perceiving stimuli, maintaining water and electrolyte balance [3]. Most importantly, it serves as a barrier, protecting the body from the external environment. As a result, skin is constantly exposed to possible injury and trauma, where wound healing and skin regeneration are vital in recovering from the lesion. Besides the impact on the individual patient, its account for around half of the world's annual health care expenses, being a significant burden to the healthcare system [4,5]. Furthermore, skin injuries and skin healing can be highly affected by external conditions, such as obesity, diabetes, stress, and aging. This can result in abnormal wound healing with high healing times, which leads to long-term sequalae and chronic low-level inflammatory states in the wound [4,6,7].

Currently, several solutions such as dressings and ointments are used with the purpose of managing skin wounds, but not to fully regenerate the tissues, thus, persisting a clinical challenge in certain cases such as diabetic ulcers, chronic wounds, burns and post-surgical wounds, due to their variable healing [6]. Patches seeded with autologous adult stem cells are seen as a promising treatment for skin injuries, but this approach is considered very expensive and time-consuming, needing development to become a viable alternative [8]. Thus, there is a need for more effective therapies and new approaches have been developed to try and tackle this problem.

1.1. The Wound Healing Process

To understand wound healing and the therapeutics used for this purpose, we must first look at the structural components of the skin.

The human skin consists of three sequential layers: the epidermis, dermis, and hypodermis, with different functions and cellular constituents (Table 1.1).

Table 1.1 - Location and presentation of the cellular constituents of the human skin and their main functions [9-11].

Skin Layer	Cell Type	Main Functions
Epidermis	Keratinocytes	Produce keratin, that provides skin with strength and protection, and lamellar granules (secreting several compounds that contribute to the barrier function)
	Melanocytes	Produce the pigment melanin, that confers skin coloration and protection from UV radiation
	Merkel and Langerhans cells	Sensing and immunological defence
Dermis	Fibroblasts	Production of ECM components
	Mast cells and immune cells	Immune and inflammatory response
Hypodermis	Adipocytes	Energy storage

The epidermis corresponds to the outer, avascular, and impermeable layer of the skin, that endures the external conditions. It contains the sebaceous and sweat glands, hair follicles and is mainly composed of keratinocytes, melanocytes, Merkel cells and Langerhans cells. The second layer corresponds to the dermis, that is rich in extracellular matrix (ECM), blood vessels and mechanoreceptors, providing the skin strength, nutrients, and immunity as well. The predominant cells in the dermis are heterogeneous populations of fibroblasts, and other cells like mast cells and macrophages are also present. The third and inner-most layer is the subcutaneous adipose tissue or hypodermis. It mostly functions as energy reservoir, providing growth factors to the dermis and is mainly composed of adipocyte cells [4,10,11].

The wound healing mechanism is an immediate protective process that intervenes after the body suffers injury [12]. Injury, including surgery, activates and initiates a cascade of coordinated physiological responses, which if successful results in wound repair, termed acute wounds. Whereas wounds that fail to heal due to interruption and/or delay in wound healing, caused by infection or an underlying disease, are termed chronic or indolent wounds [12]. This wound healing cascade is characterized by four stages, including haemostasis, inflammation, proliferation, and remodelling phases (Figure 1.1).

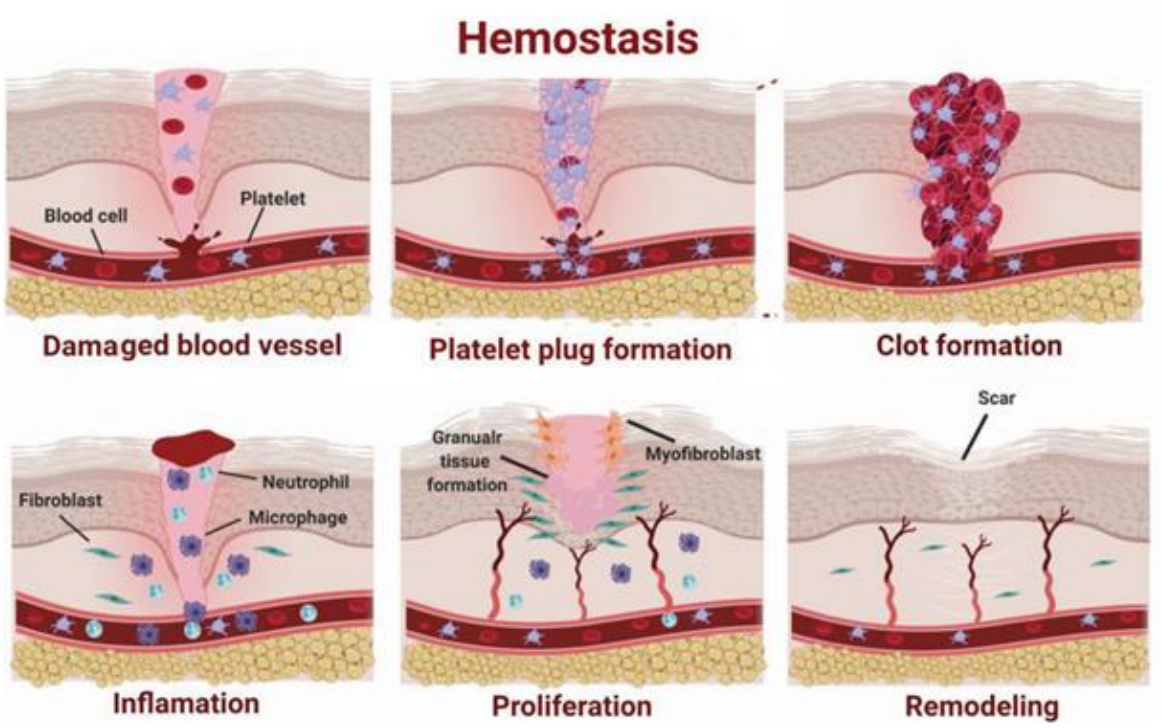

Figure 1.1 - Schematic of the process of wound healing adapted from [13]. It includes the four wound healing stages: haemostasis, inflammation, proliferation, and remodelling.

1.1.1. Haemostasis

Briefly, haemostasis lasts 2-3 hours and is the mechanism that leads to the cessation of bleeding from a blood vessel and involves multiple interlinked steps. Sometimes this phase is also called ‘lag-phase’, in which the organism needs to manage the recruitment of many cells and factors for the healing process in the absence of mechanical strength of the wound [14]. It begins with trauma to the lining of the blood vessel and the formation of a platelet plug [13]. This is followed by the generation of a network of insoluble fibrin, which allows inflammatory cells such as leukocytes, macrophages and neutrophils to invade into the wounding site. The cells and platelets release compounds like cytokines and growth factors to activate the next step of the cascade, the inflammatory process [14]. Finally, self-polymerization of the fibrin monomers leads to the formation of protofibrils, aggregating laterally to make fibres and branches resulting in the formation of a 3D network. Intra and interfibre crosslinking later lead to increasing clot stiffness of the fibrin plug [13]. Thus, it culminates into the formation of a fibrin plug that closes the damaged site of the blood vessel and controls the bleeding [13].

1.1.2. Inflammation

The Inflammatory phase begins immediately after haemostasis and lasts from hours to days in acute wounds, while in chronic wounding it can last for weeks or even months, caused by the underlying disease’s effects [15]. In this phase, the platelets formed during haemostasis release proinflammatory mediators, like cytokines (prostaglandins, histamine, and other amines), and growth factors that

increase local vasodilatation and vessel permeability. This allows the migration and attraction of inflammatory cells like neutrophils, which are engaged in infection control; macrophages, capable of removing damaged cells and tissue debris from the wound area; and activation of endothelial cells, into the wound bed. It is also the first time that fibroblasts appear at the site of injury [8,15]. Serous fluid also leaks into the wound bed and surrounding tissue, creating oedema, the build-up of fluid in the body, causing swelling in the trauma area [12].

1.1.3. Proliferation

The proliferative phase is the rebuilding phase of the wound healing process, characterized by major processes including granulation tissue formation, wound contraction, and epithelialization. In granulation tissue formation, once fibroblast cells migrate into the wound site, they proliferate, fill the skin defect and secrete ECM proteins such as fibronectin, fibrin, collagen and other components to form a provisional ECM [13]. When fibroblasts interact with the ECM, they also induce intracellular/extracellular cytoskeleton tension [16]. The old matrix is degraded by matrix metalloproteinases (MMPs proteases), which promote the self-destruction of debris and cell migration in wounds. The proteases levels increase after the tissue damage and decrease after inflammation stops in normal wounds, but on chronic wounds it increases abnormally [15]. When the wound site is covered with granulation tissue, wound edges begin to be contacted by myofibroblasts, thereby decreasing the size of the wound. Later, during the epithelialization phase, epithelial cells migrate from the wound edges across the wound bed and seal the wound [13]. The differentiation of keratinocytes helps to restore the function of the epidermis [15].

1.1.4. Remodelling

During the remodelling phase, the last wound healing phase, the matrix is constantly being reconstructed by myofibroblasts. It occurs the maturation of granulation tissue into scar, where the microfilaments attached to the ECM are reorganized and rearranged, maximizing tensile strength and contracting in the wound. Besides, the proportion of the different types of collagen changes, increasing collagen type I (80-90%) and decreasing collagen type III (10-20%) [12,15]. Lastly, the density of the myofibroblasts is reduced by apoptosis, allowing fibroblasts to strengthen the ECM and increase its resistance [15]. However, it is found that the resulting scar only has 80% of the tensile strength, compared to the normal dermis. Depending on the wound type, this phase of the wound healing process can last for months, a year or longer [13,15].

1.2. Crosstalk between keratinocytes and dermal fibroblasts modulates wound healing

Fibroblasts and keratinocytes are considered two of the major cell types present during the inflammatory phase of wound healing. Several inflammatory signals trigger the proliferation, differentiation, and maturation of these cells, which is essential in the repair process.

Briefly, fibroblasts are present in the healthy healing wound, from the late inflammatory phase, as described, until full epithelialisation has occurred. In granulation tissue formation, once fibroblast cells migrate into the wound site, they proliferate, fill the skin defect, and secrete ECM proteins such as fibronectin, fibrin, collagen, and other components to form a provisional ECM [13]. When fibroblasts interact with the ECM, they also induce intracellular/extracellular cytoskeleton tension [16]. The old fibrin clot is also degraded by MMPs proteases also produced by fibroblasts. This promotes the self-destruction of debris and cell migration in wounds [15]. Furthermore, when the wound site is covered with granulation tissue, wound edges begin to be contacted by myofibroblasts, differentiated fibroblast cells, thereby decreasing the size of the wound [13].

Taking a closer look at the keratinocytes' function, these are the most dominant cell type constituting the epidermis and are the initiators of the re-epithelialization process, where keratinocytes migrate, proliferate, and differentiate to repair the epidermal barrier [13]. Being present in the first layer of the skin, they are in direct contact with the environment and form the first line of defence against environmental threats and contribute to the preservation of the immune barrier [17]. In normal epidermis, resting keratinocytes employ basal anti-inflammatory actions by producing antimicrobial peptides. When the skin barrier is disrupted, an imbalance arises and these cells recruit, stimulate, and coordinate the actions of multiple other cell types involved in healing and repair the epidermal layer of the skin. In response to the disruption of the barrier, keratinocytes release a prestored cytokine, interleukin 1, which acts as both an autocrine and paracrine signal, activating and increasing both keratinocyte migration and proliferation and surrounding cells, to aid the regeneration of the wound. Keratinocytes also secrete angiogenic growth factors, which are key during endothelial cell migration and angiogenesis in the wound [18].

Besides their separate importance during wound healing, these two cell types are known to communicate with each other through a dynamic and reciprocal crosstalk. This communication is designated as a double paracrine signalling loop, which coordinate their actions. After the skin suffers the injury, the inflammatory cells at the wound site signal the fibroblasts in the wound margins and promote its migration inward. This response, cause the fibroblasts to secrete several paracrine factors, such as basic fibroblast growth factor, keratinocyte growth factor, vascular endothelial growth factor, among others, that trigger adjacent keratinocytes. This response causes a paracrine signalling response from keratinocytes and inflammatory cells, causing fibroblasts to synthesize collagen and promote crosslinking to form the ECM, and differentiate into myofibroblast, cells that facilitate wound closure [18].

As described, in normal skin, the several secreted products by fibroblasts and keratinocytes are important for maintaining tissue homeostasis, and in wounds, this coordinated crosstalk starts the recruitment of cells necessary for complete wound healing and closure. Therefore, it is of most importance to study in detail these cell lineages and the impact of the developed wound therapies in these cells.

1.3. The role of oxygen and angiogenesis process in wound healing

Two important factors to achieve complete wound healing are oxygenation and the angiogenesis process.

Oxygenation is a key factor in cell metabolism, especially energy production by means of adenosine triphosphate, ATP, and is critical for almost every wound healing process. It prevents wounds from infection, promotes angiogenesis, enhances keratinocyte differentiation, migration, and re-epithelialization; fibroblast proliferation and collagen synthesis, and promotes the contraction of the wound. The disruption of blood vessels in early wounds provokes acute hypoxia, the deprivation of adequate oxygen supply to the tissue. It is this hypoxia that triggers the activation of platelets and endothelium formation, induction of reactive oxygen species (ROS) and the release of cytokines. However, this process must be transient since oxygen is crucial in further phases [19]. Temporary hypoxia after injury triggers the healing process, but its prolongation, creating chronic hypoxia can delay wound healing. Several factors, including advancing age and diabetes, can cause decreased vascular flow, thus setting the stage for poor tissue oxygenation. In wounds where oxygenation is not restored, healing is impaired. When pathogen phagocytosis occurs, oxygen is used by NADPH-linked oxygenase's present in leukocytes to produce peroxide anions, that are transformed into ROSs that suffer several reactions and allow the production of hypochlorous acid, promoting bacterial death in the wounds and avoids infection [19]. The reactive species produced in this phase also have an active role in other processes like coagulation, cytokine release, cell proliferation, re-epithelization, angiogenesis, and matrix formation [19,7]. During the proliferative phase, where cells consume high levels of energy, oxygen, the final electron acceptor in the aerobic metabolism of glucose, is used to generate energy, in the form of ATP. Oxygen is also necessary for the production of mature collagen, where the hydroxylation of proline and lysine residues of procollagen allow the stabilization of the triple helices of collagen, and fibroblast differentiation into contractile myofibroblasts [19].

The formation of new blood vessels from pre-existing ones is called angiogenesis or neovascularization. This process is mainly regulated by vascular endothelial growth factor (VEGF), mainly expressed during the formation of granulation tissues, and fibroblast growth factor 2 (FGF-2). The first is released by platelets, macrophages, endothelial cells, activated epidermal cells and fibroblasts. The latter is released by fibroblasts, keratinocytes, endothelial cells, smooth muscle cells, and chondrocytes at the beginning of the healing process. VEGF enhances the permeability of vessels, promotes migration of smooth muscle cells and endothelial cells, promoting as well the mitogenic stimulation of the latter, required to form new blood vessels [19]. 3-5 days after the injury, new capillaries become visible in the wound bed as granulation tissue, however, in chronic wounds defects in this process can occur, being a very important aspect to take in consideration when wound healing therapies are developed.

1.4. The influence of the presence of bacteria on the wound healing process

Delayed healing has been attributed to the presence of specific pathogenic microorganisms. After skin injury, microorganisms that are normally present at the skin surface gain access to the underlying tissues. Moreover, bacterial invasion risk is higher in a wound resulting from poor local factors (arterial insufficiency, venous hypertension, trauma) or systemic disease, such as diabetes mellitus and rheumatoid arthritis [20,21].

This interaction varies from contamination to colonization on to local infection, and lastly to spreading infection, which is formed through cellulitis or septicaemia. Contamination is the presence of non-replicating organisms on a wound, while colonization is corresponding to the presence of replicating microorganisms on the wound, but without causing damage in the tissues. Local infection or critical colonization corresponds to the intermediate stage of microorganism replication and the starting of tissue reaction. Invasive infection is associated with the presence of replicating organisms in a wound that cause wound damage and injury [20,21].

The interactions between host and the microbials present in the wound determine the wound healing process, specifically the amount of bacteria per gram of tissue, the virulence and pathogenicity of the present organisms, and the efficacy of the host's immune response. Normal skin flora consists of 10^5 microcolonies without clinical problems. In open wounds, where the epithelium damage provides a good environment for bacteria, this bacterial load is frequently associated with infection. Even though 10^5 bacteria count is theoretically representing clinical infection, the infective dose of a particular organism can vary with the type of organism, as well as being affected by the organism's interactions with surrounding microflora. Moreover, bacterial species like *β-Haemolytic streptococci* can cause infection at even lower levels than 10^5, and their detection in a wound biopsy can indicate the presence of infection and a delayed healing response, regardless of bacterial load [20,21].

Inflammation, as mentioned, is part of the wound-healing mechanism and is key in the removal of contaminating microorganisms. If a successful decontamination does not occur, inflammation may be prolonged. Like other infective processes, the bacteria in infected wounds occur in biofilms, which are aggregated bacteria embedded in an extracellular polysaccharide matrix, secreted by the bacteria. Mature biofilms can create secure microenvironments for bacteria and allow antibiotic-resistance to be established. Interestingly, rather than the bacterial species found in a wound, it is the number of different bacterial species present that relates to wound healing. It has been shown that the presence of four or more bacterial species in such wounds has a huge impact on nonhealing [20].

In general, all wounds, especially chronic wounds, are susceptible to contamination by microorganisms. *Staphylococcus aureus* is the most dominant pathogen (39.28%); *Pseudomonas aeruginosa* (19.64%), *Escherichia coli* (30.35%), among other bacterial species have also been identified as causes of these infections [22].

Staphylococcus aureus is a coagulase-positive staphylococci and is present in 60% of the biofilms of chronic wounds [23]. It has various virulence factors that cause mild to severe infections, varying from cutaneous to systemic infections. *S. aureus* also comprises surface components such as Protein A and extracellular adhesion proteins, allowing an evasion from the inhibitory activity of antibiotics and host immune system recognition [24]. Thus, the emergence of antibiotic-resistant strains has reduced treatment options. Methicillin-resistant *Staphylococcus aureus* (MRSA) is the most common hospital-borne infection affecting millions of patients daily. Moreover, *S. aureus* is a major causative agent of chronic wounds such as diabetic foot ulcers, venous leg ulcers, and pressure ulcers [25]. The slow or non-healing of these wounds increase the risk of sepsis and can lead to invasive inflammatory diseases such as infective endocarditis, the infection of the endocardial surfaces of the heart, associated with high mortality and morbidity [25].

Pseudomonas aeruginosa is an opportunist pathogen particularly present in moist environments. In wounds, it is a virulent wound pathogen and is commonly isolated from polymicrobial biofilms found in chronic wounds [26]. Infections caused by *P. aeruginosa* are difficult to treat due to its inherent antibiotic resistance mechanisms, giving rise to persistent infections in burns patients and chronic venous leg ulcers. The progress of novel antimicrobial interventions is needed [27,28]. The developed resistance mechanisms comprise multi-drug efflux pumps that eliminate the antibiotics from inside the cell prior to its action. In addition, the physical structure of the produced extracellular biofilm matrix hampers the access into the biofilm [28]. Because *P. aeruginosa* is only susceptible to only a few antibiotic agents, infections caused by this organism are difficult to cure and often require combination therapy. Multidrug-resistant *P. aeruginosa* (MDRP) has been described as resistant to several antibiotics such as imipenem, amikacin, and ciprofloxacin, employed in infected wounds. The increasing resistance of *P. aeruginosa* is a growing threat to the clinical management of such infections, thus, new approaches must be developed [26].

Another common pathogen presents in wounds, especially chronic wounds, is *Escherichia coli. E. coli* is a gram-negative bacterium, and its strains are typically not pathogenic to humans. However, numerous strains of *E. coli* have evolved to opportunistic and commensal, being able to impair wound healing. Moreover, various bacterial strains have become resistant to antimicrobial agents, posing as well a health and economical risks to society [29].

Polymicrobial interactions may well play a crucial role in wound healing, for example less invasive microorganisms can be synergistic with more virulent forms [20]. Previously, *Staphylococcus epidermidis* was only considered an innocuous commensal microorganism present on the human skin. This bacterial specie is defined as coagulase-negative staphylococci, different from coagulase-positive staphylococci such as *S. aureus* for having an enzyme coagulase deficiency. Most *S. epidermidis* infections are hospital-acquired that include indwelling foreign devices, surgical wound infections, and bacteraemia, the presence of viable bacteria in the bloodstream, in immunocompromised patients. It is also seen as an important opportunistic pathogen, that is thought to provide a reservoir of resistance genes to other infective agents. *S. epidermidis* infections hardly progress into life-threatening diseases,

however, their frequency and its extremely difficult treatment represent a serious burden for the public health system. Treatment is complex due to specific antibiotic resistance genes and the appearance of biofilms, multicellular bacterial aggregates that exhibit intrinsic resistance to antibiotics and mechanisms of host defence. Furthermore, recent investigation has identified specific molecular determinants that facilitate *S. epidermidis* immune evasion and ability to cause chronic diseases [30,31].

1.5. Gelatine-Based Hydrogel for Wound Healing

Due to the increase of injuries and diseases derived from wounds and related to infection in the past few years, a variety of wound care products have been developed to try to tackle this problem. Before 1960, wound dressings were regarded as passive products and had a minimal role in the healing process. Winter et al. introduced the concept of an optimal environment for wound repair and a shift from passive to an active involvement of a wound dressing in the establishment and maintenance of said environment occurred [32].

An ideal wound dressing must maintain a local moist environment around the wound and stop wound desiccation; allow good gases circulation; offer a protective role against harmful bacteria and contaminants; remove wound exudates and promote tissue regeneration; possess mechanical protection and improve the overall quality of wound healing [33]. Taking the above factors into consideration, hydrogels are great candidates for wound dressings.

Hydrogels were the first biomaterials designed for use in the human body and are 3D networks formed by crosslinking hydrophilic polymer chains embedded in a water-rich environment. Its large surface network allows a physical and chemical tunability of its properties, through several mechanisms that include physical and chemical crosslinking and ionic interaction. It also allows the hydrogels to absorb up to thousands times of their equivalent weight in water until the process reaches an equilibrium state [34,35].

The physical methods of gelation of the hydrogels depend on the intrinsic properties of the polymers and this dependence can limit the ability to fine-tune the hydrogels' properties. However, gelation is easily achievable without the need to modify the polymer chains and is easy to reverse when necessary. Most natural polymers form thermally driven hydrogels, where the physical alterations of the polymer chains occur in response to a temperature change. The gelation mechanism can vary according to the type of polymer: polymers in which the transition temperature is defined as lower critical solution temperature (LCST), such as poly(N-isopropylacrylamide), gel only above the LCST, as opposed to polymers with an upper critical solution temperature (UCST), such natural polymers as gelatin as well as synthetic polymers such as poly-acrylic acid that gel as the temperature drops below the UCST. Non-covalent molecular self-assembly, spontaneous physical gelation, by chelation or electrostatic interactions, and chemical crosslinking are also other employed gelation methods [34].

Different types of biomaterials can constitute the matrixes of the hydrogels, such as polymers derived from natural sources or synthetic sources (Table 1.2)

Table 1.2 - Some of the most commonly used natural and synthetic hydrogel polymers in wound healing applications, retrieved from [8,36].

Natural Hydrogels' Components	Synthetic Hydrogels' Components
Alginate	Polyethylene glycol
Gelatine	Poly (methacrylates)
Collagen	Poly-vinylpyrrolidine
Chitosan	Polyurethane
Fibrin	Polyvinyl alcohol
Hyaluronic Acid	

In this work, gelatine will be used as the primary constituent of the hydrogel matrix. Gelatine, a form of hydrolysed collagen, is an easily dissolvable polymer, exhibiting amphoteric behaviour, because of the presence of alkaline amino acids and acid functional groups. It is seen as a promising material as a scaffold with therapeutic and regenerative characteristics due to its similarities to the ECM in the native tissues. Conventionally, gelatine is extracted from porcine, bovine, or fish skin collagen (mostly type I). The hydrolysis of collagen into protein fragments by acidic or basic treatment produces type A or type B gelatine, respectively, that differ in characteristics, like the composition of aminoacids, gel strength, isoelectric point and charge [36,37]

As wound dressing material, gelatine contains Arg-Gly-Asp (RGD) peptides sequences for the recognition of integrin receptors in the cells, which are crucial for cell adhesion. RGD sequence can not only increase the cellular bioactivity of scaffolds but also promote cell adhesion and migration. It also tends to form a nanofiber structure, that due to its large specific surface area, high porosity, and good permeability, can biomimic the ECM and favour cell adhesion, migration, and proliferation. It is also a polymer characterized by its biocompatibility, biodegradability, low antigenicity, low cost, abundance, and has accessible functional groups that easily allow chemical modifications [37,38].

Most importantly, the US Food and Drug Administration (FDA) has approved its use in biomedical applications [37]. Due to these characteristics, an FDA approved commercial gelatine-based biomaterial, Gelform, has also been developed and successfully used in tissue engineering, and more importantly, in wound healing applications [36]. One of the most promising applications of gelatine is also its use to stop bleeding, creating a haemostatic effect, where gelatine can not only activate and aggregate platelets causing the acceleration of blood coagulation, but also it can swell upon contact with blood, and provide a tamponade effect [13].

Previous reports have studied gelatine-based hybrid hydrogels and their wound healing applications. Hsu et al., fabricated gelatine-hyaluronic acid hybrid hydrogels encapsulated with recombinant thrombomodulin by chemical crosslinking and followed by freeze-drying. Thrombomodulin is a surface transmembrane glycoprotein present in endothelial cells and epidermal keratinocytes. It regulates blood coagulation, inflammation, and cell-cell adhesion. These hydrogels were developed with the aim to be

applied in diabetic wounds. The hydrogels had good absorption rates, which is beneficial for drug incorporation, absorbing wound exudates, and allowing a moist environment for the wound [16]. Moreover, the evaluation of fibroblast adhesion and proliferation on alginate-gelatine crosslinked hydrogels has also been previously studied [39]. Alginate is a good biomaterial base scaffold, due to its biocompatibility and rapid ionic gelation, however, alone it has a very uncontrollable and slow degradation and is not able to promote cell adhesion, in physiological conditions. The addition of gelatine to the hydrogel increased the viability, attachment, spreading and proliferation of human dermal fibroblast. Additionally, the *in vitro* cytocompatibility increased with increasing gelatine content [39].

The use of gelatine-based hydrogels has also been studied *in vivo*, which is a very important step to the translation of the developed therapies to its use in patients. Balakrishnan et al. investigated an oxidized alginate- and gelatin-based hydrogel for wound dressing applications. The obtained hydrogels presented improved water retention when compared with commercially available wound dressings and good water absorptivity. These characteristics facilitated the development of a moist environment that is conducive to wound healing and increased cell migration and re-epithelialization in an *in vivo* study, in a rat model [36].

1.6. 3D printing and its prospective use in skin regeneration

3D printing is a process for constructing 3D structures from digital models through the layer-by-layer deposition of a myriad of biomaterials, that include natural and synthetic polymers, living cells, metals, among others. Its application in the biomedical engineering field can be separated into four main areas: the manufacturing of permanent implants; production of organ models; printing of completely bioactive tissues and organs; and creation of local bioactive and biodegradable patches [40]. The latter is the application highlighted during this work, specifically for its use in wound healing and skin regeneration (Figure 1.2).

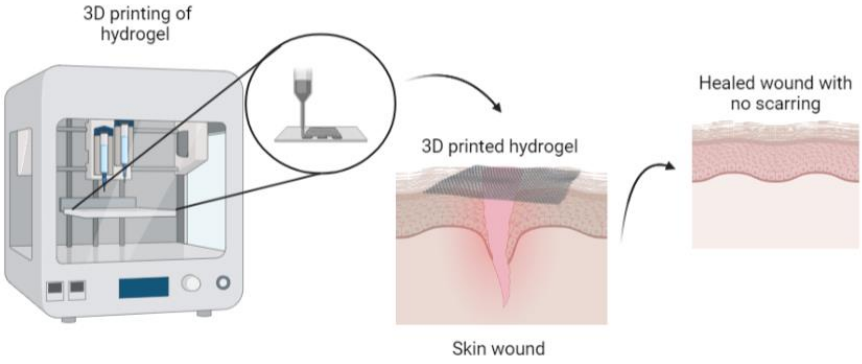

Figure 1.2 - Process of 3D printing of hydrogels to create bioactive patches for wound healing and skin regeneration applications. Figure created with Biorender.com [41].

Thus, 3D printing can be described as an innovative fabrication strategy that can comprise biological components, like living cells, bioactive molecules, signalling molecules, growth factors, organic molecules, among others, in a 3D organization with the final goal of creating suitable biological constructs. This method permits the printing of flexible hydrogels with several layers through the conversion of computer-aided design (CAD) models into 3D complex structures [42,43].

These biological structures aim to reproduce the architectural, physiological, and mechanical properties of the native tissue/organ. Moreover, when compared to other preparing methods, such as thermally induced phase separation and electrospinning, the use of 3D printing allows a more flexible, personalized, and repeatable structure [5].

It is important to note that 90% of the polymers used in printing processes come from natural sources, even though they may lack mechanical stability. Their ability to mimic the ECM's structure and chemical balance allows an improvement in the adhesion, migration, proliferation, and differentiation process of cells [5].

The three main used printing techniques in biomedical applications are: inkjet, laser-assisted, and extrusion printing. Inkjet printing was the first developed printing technology and is very similar to conventional 2D inkjet printing. Briefly, the solution is introduced into a cartridge which is connected to a printer head. During printing, the printer heads are deformed by a thermal or piezoelectric actuator and squeezed to generate droplets of controllable size. The advantages are its low cost, high printing speed and relatively high cell viability (from 80% to 90%), however, high viscosity materials and bioinks with high cell density result in clogging of the head printer [43]. Laser-assisted printing works with a donor layer a "ribbon" structure with an energy-absorbing layer at the top and an ink solution layer at the bottom, that responds to laser stimulation. During printing, a laser pulse is applied and stimulates a small area of the absorbing layer. The laser vaporizes a portion of the donor layer, producing a high-pressure bubble at the interface of the bottom layer, propelling the suspended ink. After the impulse, the solution droplet is stored on the receiving substrate and, thus, crosslinked [43]. Finally, the extrusion printing technique is a modification of inkjet printing. This was the applied 3D printing technique in this project, due to it being the most efficient when a hydrogel is utilized [43]. In this technique, the hydrogels are loaded into cartridges and extruded using pneumatic pressure or mechanical forces through a nozzle into a predefined point, onto a platform. The cartridges are positioned onto an XYZ stage, with temperature and pressure being set (piston speed and rotational speed in the case of piston-driven and screw driven) through a computer software. The advantages of this printing technique are its ability to extrude inks with different compositions. Moreover, one of the most important advantages, is that extrusion-based printing has become relatively affordable and is highly customizable with respect to the desired structure or ink. Currently, the extrusion printers can be customized for specific applications that enable core-shell printing, combined extrusion, electrospinning, and UV curing during and post-printing in addition to other emerging tissue engineering technologies [44].

Even though 3D printing is not currently applied in clinical settings, this technology has made impressive advances towards clinical translation and personalized medicine. In 3D printing, gelatine is a very commonly used polymer in combination with other polymers. However, at low temperatures (<25 ºC), gelatin is in the gel state, while at around 30 ºC, it can start to shift to a more liquid state, depending on the gelatine concentration, resulting in difficulties in preserving the printed structure stable at physiological temperatures. This corresponds to a sol-gel transition process, which translates the gelation process. During this transition, the reorganisation of the gelatine molecules happens and non-specific bonds, like hydrogen, electrostatic and hydrophobic bonds are formed. This provides the hydrogel thermo-reversible property, meaning the nonspecific bonds can be easily broken by heating [45]. At higher temperatures than the sol-gel temperature, it also has weak mechanical strength and low viscosity. For that reason, it is often mixed with other natural biopolymers like alginate and silk-fibroin to overcome these limitations [5].

Rheological studies of inks are crucial to find the best extrusions conditions for printing, including viscosity, gelation and melting temperature. Rheology is the study of flow and deformation of a substance under the effect of an external force, which is very relevant to an extrusion-based 3D printing process. Many studies have been carried out to evaluate the printability of a hydrogel through rheological experiments [46].

Additionally, some parameters which may have significant influence on the printability of a hydrogel are viscosity, temperature, printing pressure, diameter of the nozzle, printing accuracy, shear thinning, among others. Viscosity is the resistance of a fluid to flow under a stress. Inks should maintain their shape once they leave the tip of the printing nozzle. The viscosity of a hydrogel is mostly determined by its excipients' concentration, and molecular weight and sufficient viscosity must be attained to maintain the desired shape of a printed structure [46]. Overall, proper ink viscosity guarantees high shape fidelity and reduces the chance of structural collapse after printing [5]. Shear-thinning is another critical parameter as inks should have excellent shear-thinning properties to avoid clogging during the printing process. It is also important for the ink to regain immediate consistency after printing and to be able to support the next layer [5]. He et al. studied the printability of hydrogels by starting with printing lines followed by printing 2D films and finally achieving 3D printed structures, studying in attention the accuracy of the prints. The one-dimensional printing experiments allowed them to find optimized printing parameters, such as air pressure, feed rate and even printing distance [47].

For the temperature-sensitive gelatine used in 3D printing, the relations between printing parameters (printing speed, nozzle shape and diameter, and temperature) and hydrogel consistency (like gelation point, viscosity, and viscoelasticity), are key factors. They strongly impact the hydrogel's strength rate during printing, resolution, and shape fidelity after printing. To achieve reproducible and high-quality prints, a high enough initial viscosity with good flow is decisive [46]. Moreover, the study of other rheological parameters, such as storage modulus (G') and loss modulus (G''), are equally important, defining whether the material can produce mechanically strong hydrogels, with enough elasticity to be bendable and not breakable, while maintaining its viscosity. Inks with higher G' values could provide a

higher resistance to deformations, thus providing increased stability of the printed structures [48]. For example, Chung et al. performed temperature sweep tests on alginate-gelatin blends of variable concentrations. Pre-crosslinked alginate alone was liquid-like during printing. However, by controlling the temperature and adding gelatin, the formulations had higher viscosity, storage modulus and consistency which facilitated higher print resolution and consequently, precision [49].

Although previous works have demonstrated that rheological properties of a hydrogel are important in controlling the printability of a hydrogel, the effect of the extrusion process on the rheological behaviour and the resultant quality of a printed 3D structure is still not clear and needs further studying.

In addition, printing can be used to design the porosity of scaffolds and introduce interconnected channels [48]. When pores are too small, it can cause a lack of nutrition and oxygen supply. This leads to low cell viability into the wound bed and an impaired migration [5]. Choi et al. developed 3D printed gelatine scaffolds and studied the effect of gelatine pore size on cell behaviour. They found that the proliferation rate of human dermal fibroblasts (HDFs) increased by 14% in pore size of 580 μm compared to 435 μm after 14 days [50].

3D printed gelatin-based hydrogels specifically for wound healing applications are not very portrayed in previous works. The reasons could rely on the fact that gelatin-based materials only can reveal poor mechanical properties, low thermal stability, and shorter degradation rates. When used in long-term studies, such as drug release, cell differentiation, and wound healing, these materials may not last through the study [51]. Moreover, although gelatin hydrogels have high rheological properties, all the found gelatin studies have examined the use of different crosslinking agents and blending with other polymers. As an example, Jing Liu et al. studied the effect of 3D printed gelatin-alginate scaffolds on the full-thickness skin wound healing on a mouse back and observed the histopathological changes that occurred. The application of the developed 3D printed hydrogels reduced the healing time from 16±1 days (control mice) to 14±1 days and the histological analysis also revealed improved healing in the treatment mice [52].

1.7. Manuka Honey Added to Hydrogels as Antibacterial Agent

From ancient times until nowadays, honey was applied to treat wounds, due to its unique properties, especially its antibacterial and antioxidant activities, immunomodulatory effect, and wound healing properties. However, since the development of penicillin and the emergence of other antibiotics, its use and clinical application have significantly decreased. But recently, due to the increase in antibiotic resistance, the search for natural alternative treatments, such as honey, has returned [53,54].

Leptospermum honey from New Zealand, commonly known as manuka honey (MH), has a high osmolarity and sugar content, that is able to provide a powerful antibacterial effect and microbial growth inhibition. Its low pH (3.5 - 4.5), besides contributing to microbial growth inhibition, can also stimulate macrophages and its bactericidal activity, increase fibroblast activity, increase oxygenation, and induce angiogenesis [55].

MH is known to be effective against a panoply of bacteria, like *Enterobacter aerogenes*, *Helicobacter pylori*, *Staphylococcus aureus* (*S. aureus*), and *Escherichia coli* (*E. coli*), *Pseudomonas aeruginosa* (*P. aeruginosa*) and against biofilm formation [56]. Previous studies have discovered that MH does not induce the same structural changes in *P. aeruginosa* as those observed in staphylococci. The staphylococcal target site of MH has been demonstrated to be involved in cell division. These structural changes were previously discovered and found with Transmission Electron Microscopy (TEM) imaging, where honey-treated cells failed to progress normally through the cell cycle and accumulated with fully formed septa, the cell wall that forms between two daughter cells as a result of cell division but were unable to separate. Sugars were discovered to not be implicated in this effect [27,57]. The observation of cellular debris in TEM images indicated that *P. aeruginosa* had lysed and whole cells in Scanning Electron Microscopy (SEM) images were short, distorted and displayed cell surface abnormalities [27]. This indicates that MH will have different actions depending on the bacterial strain present in the wound.

Besides its antibacterial effect, MH is also an inflammation modulation component, which promotes wound repair and avoids the extension of inflammatory phases. The distinct anti-bacterial activity of MH is mostly due to its high amount of methylglyoxal (MGO), also referred to as the “Unique Manuka Factor” (UMF), a non-peroxide antibacterial compound. The UMF grading system indicates the MGO concentration in MH sold commercially [24,57].

Wounds, in particular chronic wounds, are characterized by an uncontrollable inflammatory stage, high levels of oxidative stress, protease activity and infections, as previously mentioned. The production of excessive amounts of reactive oxygen species (ROS) are known to be deleterious to the cells, due to their high reactivity. Thus, apart from the antibacterial effects of honey, its antioxidant properties are also considered important. This activity of honey is attributed mainly to its polyphenols (flavonoids and phenolic acids, for example), antioxidant enzymes, like catalase and peroxidase, vitamins, Maillard reaction products, carotenoids, and amino acids [53]. Furthermore, MH has the highest value in terms of phenolic content and antioxidant capacity, for example compared to Acacia, wild carrot and Portobello honeys [58]. Additionally, recently published research has concluded that the UMF rating for MH correlates with its antioxidant capacity and with the total phenol content analysed [59].

During degradation of MH inside the human body, low levels of hydrogen peroxide (H_2O_2) are produced, due to wound exudates interaction with glucose oxidase present in honey. While this increases its antibacterial effect if in high amounts, it can also have a nefarious effect on cells and tissues. Previous studies have concluded that the possible cytotoxicity produced by MH in the cells is directly dependent on MH concentration used [60]. Thus, its study independently and when incorporated must also be performed for cells, to understand how they behave when in contact with the substances. Honey additionally provides topical needed nutrition to the wound and stimulates wound epithelialization [58, 61].

The limitations encountered due to its physical features, like high viscosity and low mechanical stability, difficult its direct use in wounds, but can be overcome by incorporating honey in a hydrogel form [61].

Due to its properties, honey impregnated dressings are already available in the market, e.g. MediHoney® , Activon Tulle® , Algivon® , and Actilite®, and clinical trials have shown honey's beneficial effects on wound healing [7].

Few works have previously been developed with the incorporation of MH in gelatin-based hydrogels. However, it is important to highlight the work of Abd El-Malek, et al. who developed a hydrogel film composed of chitosan and gelatin, loaded with manuka honey. The produced structure showed antibacterial activity against pathogenic isolates of *Staphylococcus aureus*, *Streptococcus pyogenes*, *Acinetobacter baumannii*, *Pseudomonas aeruginosa* and *Proteus mirabilis*. The results also demonstrated that the produced hydrogels can prevent bacterial growth for 12 h, thus it must be replaced twice a day. This study introduces an alternative to conventional antibiotic therapy and shows potential as wound dressing for the treatment of infected wounds [62].

Regarding 3D printing, no studies with gelatine and MH were found on its application in wound healing. However, this study has been previously made with other polymers as base. Katharina Schuhladen et al. explored the incorporation of MH in methylcellulose-based hydrogels, that formed thermo-sensitive scaffolds and studied the effect of borate bioactive glass (BG) on the printability of the hydrogels [63]. Regarding MH, it was found to allow natural crosslinking connections with methylcellulose, thus, was determined as being a good natural crosslinking agent. Moreover, the addition of the bioactive agents MH and BG had no significant impact on the viability of human dermal fibroblasts (HDFs) in comparison to the control, indicating their biocompatibility. Another study also contributed with the evaluation of the physic and mechanical properties of 3D printable alginate-methylcellulose hydrogels incorporated with several bioactive components, including MH [64]. Concerning the incorporation of MH, the rheological properties of the hydrogel inks showed that an increase in the concentration of MH resulted in decrease in the storage modulus, G' value, of the hydrogels and decreased viscosity [64]. The *in vitro* wound healing efficacy of the different hydrogel compositions was also assessed in HDFs migration. Hydrogels containing MH significantly enhanced cell migration, and this effect was more pronounced for the highest concentration used at 24 h post treatment. Antimicrobial studies against *S. aureus* and *E. coli* also showed higher antibiofilm activity was achieved for the MH-containing hydrogels, with a higher susceptibility for *S. aureus* compared to *E. coli* and this susceptibility was highest when the highest concentration of MH was used [64].

These results reported in literature indicate that it is possible to incorporate MH in 3D printed structures, while maintaining its pretended effects, such as its antibacterial activity, wound regeneration capacities and modulation of the hydrogels properties. Moreover, this work can help advance the study of incorporation of MH in gelatin-based hydrogel and in 3D printed hydrogels.

1.8. Objectives and Deliverables

The current work focuses on the establishment of a three-dimensional (3D) printed gelatine-based hydrogel containing an antibacterial agent, Manuka honey (MH), crucial for wound treatment and skin regeneration. Moreover, the developed patches must display the fundamental properties to be used in topical applications.

First, a brief explanation of the hydrogels' development will be provided, focusing on the investigation of their morphological appearance, rheological properties, and physico-chemical changes due to gelatine increase and the incorporation of MH. Moreover, the 3D hydrogel's viscous properties and elastic properties will be assessed via storage (G') and loss (G'') moduli. Afterwards, a description of the optimization of the hydrogels' printing process will be presented, where the goal was to form reproducible, and structurally accurate 3D hydrogel patches. An attenuated total reflectance-Fourier transform infrared spectroscopy (ATR-FTIR) analysis was also performed to evaluate the 3D printed patches' composition.

The decision of which hydrogels should be printed, regarding their composition, was made according to the following presumptions:

1. To understand if the increase in gelatine concentration can induce any physico-chemical differences in the printed patches.
2. If the addition of MH induces changes in the physico-chemical properties of the base hydrogel.
3. If MH, when incorporated in the patch, was able to promote the antibacterial effect and possibly regeneration abilities, without impairing cell viability. Moreover, to study the effect of its concentration.

Finally, a biological characterization was performed, to understand if the hydrogels' composition had the pretended antibacterial activity against *S. aureus, S. epidermidis, E. coli* and *P. aeruginosa* bacteria known to be able to infect wounds and impair healing. Moreover, in a future perspective to utilize the 3D patches *in vivo* and consequently, in patients, indirect cytotoxicity tests, regeneration ability as well as antioxidant activity in human dermal fibroblasts and human epidermal keratinocytes were also performed. *In vivo* irritability and angiogenesis tests using the hen's egg test on the chorioallantoic membrane (HET-CAM test), were additionally presented to conclude the work. These tests are of extreme importance to assess the patches biocompatibility.

The results of the different experiments were evaluated to assess if the 3D patches produced demonstrated to be an effective and promising therapeutical alternative for topical applications.

Chapter 2: Materials and Methods

2. Materials and Methods

2.1. Materials

Gelatine was obtained from Acopharma (Spain), glycerine was purchased from Lacrilar (Torres Vedras, Portugal) and sucrose from Fisher Scientific (Hampton, United States). The bioactive compound, Manuka Honey (MH), was purchased from Pure Gold (New Zealand). Purified water, used in the hydrogel formulations was attained by reverse osmosis and electrodeionization (Millipore®, Elix 3), followed by filtration (filter pore 0.22 µm) and sterilization. Sodium methylparaben and sodium propylparaben, known commercially as nipagin and nipazol, respectively, were purchased from Fagron (Spain).

2.2. Preparation of Gelatine Hydrogel and Gelatine-Manuka honey hydrogel ink

The gelatine-based hydrogels inks were produced using a method developed in-house at the Faculty of Pharmacy, University of Lisbon, and using the amount of excipients described in Table 2.1. The technique's steps will be summarized next.

Table 2.1 - Qualitative and quantitative composition of gelatine hydrogel inks and gelatine-Manuka honey hydrogel inks. Control (-) – Ink with lower concentration of gelatine (less viscous ink); MH – Manuka honey; Control (+) – Ink with higher concentration of gelatine (more viscous ink).

		Composition (%, w/w)						
Gelatine-Based Ink	**Identification (ID)**	Gelatine	Glycerine	Sucrose	Water	MH	Nipagin	Nipazol
Control (-)	P30	30	8	2	59.8	-	0.18	0.02
MH	MH-P30	30	8	-	19.8	40	0.18	0.02
Control (+)	P40	40	10	10	39.8	-	0.18	0.02

First, a certain amount of glycerine (Table 2.1) was weighted with distilled water and the mixture was heated at 40 ºC for 5 minutes in the water bath. This step allows a more homogeneous incorporation of gelatine and prevents its immediate gelling and the appearance of lumps. For the gelatine-based hydrogel with Manuka honey (MH-P30), the incorporation of the honey was also made during this step.

Afterwards, gelatine, sucrose, nipagin and nipazol were weighted (Table 2.1), added to the previous mixture, and stirred gently, avoiding the appearance of bubbles. Nipagin and nipazol are broad spectrum antimicrobial agents designed for preservation of a wide range of products and are commonly used in the pharmaceutical field [65]. Then, the hydrogel was kept in a water bath at 40 °C for 45 min, to guarantee the homogenization of the ink. For easy recording, Manuka honey is abbreviated as MH below and the inks with low concentration of gelatine in the composition, P30, and high concentration, P40. Thus, the P30, P40 and MH-P30 inks were obtained.

2.3. Rheological Characterization of Gelatine-Based Inks

To determine the gelation temperature of the prepared formulations, a single frequency strain-controlled temperature event sequence was designed. The measurements were carried out with a plate–plate geometry and a gap of 0.5 mm (patch height simulation) in a stress Kinexus Lab+ Rheometer (Malvern Instruments, Malvern, UK). The onset of gelation temperature was defined as the crossover, where the data point showed the sol-gel transition (G'>G"). All measurements were performed from 50 °C to 25 °C at a rate of 2.5 ºC/min; frequency was kept at 1 Hz and the shear strain at 1%.

2.4. Production and Characterization of 3D printed Gelatine-Manuka Hydrogel patch

The core objective of this work was to print gelatine-based hydrogel patches using an extruder printer. For that purpose, a 3D bioprinter, Allevi 2, was used (Figure 2.1).

Figure 2.1 - Allevi 2 3D bioprinter retrieved from [66].

The printer has two extruders and is built around a compressed air pneumatic system, the pressure ranges between 1 and 120 Psi and allows the use of a wide range of viscous materials. The temperature can be controlled from room temperature to 160 °C, thus, allowing the printing of numerous types of inks [66].

The printing process occurred after 24h of ink stabilization in a heating chamber and final heating for 45 min in a water bath at 40 ºC. Then, the gelatine-based hydrogel inks were transferred to the inside of the cartridge and after the target temperature was achieved and ink stabilization occurred. The inks were extruded through specific nozzles, Figure 2.2, with 27 Gauge and an inner diameter of 0.200 mm (white tip) and 25 Gauge and an inner diameter of 0.250 mm (red tip), depending on the ink composition. Ink stabilization occurred always in no less than 30 minutes and extrusion was performed to see if the filament extrusion was made with proper gelation.

Figure 2.2 - Plastic nozzles used for printing of the 3D hydrogel inks. The red and white nozzles are tapered plastic tips with 25 Gauge and an inner diameter of 0.250 mm and 27 Gauge and an inner diameter of 0.200 mm, respectively. Pictures retrieved from [66].

For P30 ink, the nozzle selected due to rheological properties and low viscosity of the hydrogel was the small diameter nozzle (0.200 mm). For the high viscosity of the gelatine-based hydrogel inks (MH-P30 and P40), a nozzle with a higher inner diameter was required (0.250 mm), thus, the red tapered plastic tip was the chosen one.

After extruders' calibration and gelatine-based hydrogel stabilization, firstly, a standing extrusion was performed, to see if extrusion can happen without any issues, as an example, nozzle clogging, homogeneous extrusion and premature gelling of the ink.

Before printing starts, a cold plastic plate, that serves as the base for the hydrogel deposition, was placed under the extruders. When in contact with the cold surface, the ink rapidly gels, allowing better control of filament spreading and more reproducible results.

Concerning the importance to create adequate porosity in the 3D patches a three-layered structure was designed, each layer with a different angle, to create porosity in the patch. The first layer has an angle of 45º, the second layer an angle of 90º, and the last layer an angle of 135º. All the layers were printed with a 0.15 mm layer height, 0.6 mm line width and 30 mm/s printing velocity and were maintained constant for every ink. An illustration of the design can be seen in Figure 2.3. Table 2.2 resumes the optimized printing parameters used for each gelatine-based hydrogel ink.

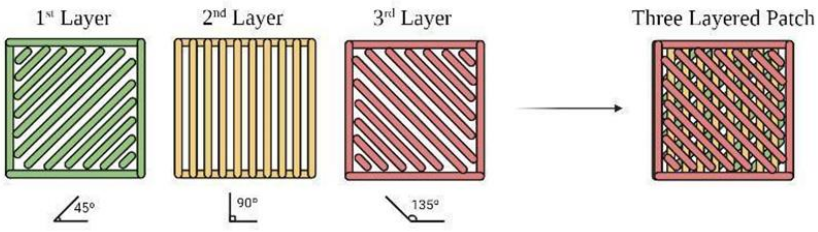

Figure 2.3 - Illustration of the three layers individually and the final three-layered patch. The first, second and third layers have an angle of 45°, 90°, 135°, respectively. All layers were printed with 0.15 mm layer height, 30 mm/s printing velocity and 0.6 mm line width.

Table 2.2 - Printing parameters used for each ink: $T_{chamber}$ (ºC), $T_{cartridge}$ (ºC), Pressure (Psi), Line Width (mm), Layer Height (mm) and Printing Velocity (mm/s).

Identification	$T_{chamber}$ (ºC)	$T_{cartridge}$ (ºC)	Pressure (Psi)	Line Width (mm)	Layer Height (mm)	Printing Velocity (mm/s)
P30	26	34	25	0.6	0.15	30
MH-P30	26	43	25	0.6	0.15	30
P40	26	43	25	0.6	0.15	30

2.4.1. 3D hydrogel patches physico-chemical characterization

The morphology of the 3D hydrogel patches as well as the porous geometry, distribution and size were examined using a scanning electron microscope (SEM Hitachi, Tokyo, Japan). To increase the conductivity, the 3D patches were coated with a thin layer of gold/palladium and examined using an acceleration voltage of 20 kV. The pore size diameter of the 3D patches was analysed using ImageJ® software and the pore size distribution was determined as mean pore size (µm) ± S.D.

To identify the functional groups of the 3D patches, attenuated total reflectance-Fourier transform infrared spectroscopy (ATR-FTIR) spectra were acquired using a Nicolet FTIR spectrometer (Thermo Electron, Thermo Fisher Scientific, Waltham, MA, USA). The 3D patches and respective raw materials were placed on the ATR diamond crystal, and spectra were obtained in the range of 500 to 4500 cm^{-1} with a resolution of 8 cm^{-1}. The recorded signals were reported as transmittance.

2.5. Biological Characterization of bioactive 3D patches

After the optimization and characterization of the gelatine-based inks and the printing conditions, the characteristics and composition of each patch ought to be studied were selected. The gelatine-based hydrogels used in the following tests are described in Table 2.3.

Table 2.3 - Characterization and a detailed description of all the 3D printed hydrogels ought to be studied.

Identification	Layers Description
P30	3 layers of P30 control ink
3MH-P30	3 layers of MH-P30 ink
2MH-P30	Layer 1&3 of MH-P30 ink and layer 2 of P30 control ink
P40	3 layers of P40 control ink

For the biological characterization, the focus was on the hydrogels' composition, to confirm its possible antibacterial activity and regeneration capacities. Prior to its use in these tests, the 3D printed hydrogels were sterilized under UV light for 30 minutes, on each side.

2.5.1. *In vitro* antibacterial evaluation of bioactive 3D patches

Dose-Response Curve of Manuka Honey

The minimum inhibitory concentration (MIC) and minimum bactericidal concentration (MBC) of 4 bacterial strains were assessed for the incorporated bioactive substance, Manuka honey (MH). The gram-negative bacteria *Escherichia coli* ATCC 25922 and *Pseudomonas aeruginosa* PA01 and gram-positive bacteria *Staphylococcus epidermidis* RP62A and *Staphylococcus aureus* ATCC 25923 were the chosen strains, due to their importance in the wound healing environment.

For MIC determination, MH was serially diluted 1:2 in Tryptic Soy Broth (TSB, Liofilchem) growth medium in microdilution trays, with concentrations ranging from 0.024 to 0.500 mL MH/mL and in a total volume of 100 µL. Each well was inoculated with 50 µL of bacteria, to yield a final bacterial concentration of $5x10^5$ CFU/mL [67]. Afterwards, the plaques were incubated at 37 °C for approx. 24 h. The MIC was defined as the lowest concentration that completely inhibited the growth of the bacterial isolates as detected by the unaided eye (first well where no turbidity was seen).

MBCs were determined by subculturing, onto agar plates 10 µL of aliquots from wells containing antimicrobial concentrations greater than or equal to the MIC. Plates were incubated at 37 °C for 24 h, and viable colonies were counted. The MBC was defined as the lowest concentration at which there was no visible bacterial growth. The entire test was performed in triplicates and the results were presented admitting a MH density of ρ_{MH} = 1.42 g/mL [68].

Antibacterial evaluation of the 3D printed hydrogel patches

The antibacterial evaluation of the 3D patches controls and incorporated with Manuka honey (MH) was examined *in vitro*. Wells without the 3D printed hydrogels were selected as the contrastive group (positive control) and Tryptic Soy Broth (TSB, Liofilchem) was used as a source of culture nutrients.

Three methods of antibacterial activity assessment were performed: spectrophotometer method of optical density (OD) measurement, culture-based counting for colony-forming units (CFU) and *in vitro* metabolization of resazurin. The OD method measures turbidity associated directly with bacterial growth and measures live as well as dead bacterial cell debris [69]. CFU determination quantifies viable bacteria that can grow on solid media [69]. Resazurin is a cell permeable redox indicator that is used to monitor the number of viable cells. When added directly to the wells and dissolved in TSB, resazurin results in a deep blue coloured solution. Viable cells with active metabolism can reduce resazurin into the resorufin product which is pink and fluorescent. For this matter, it is important to add the resazurin and read the fluorescence in a dark room, since resorufin is sensitive to light [70].

Onto each well, 0.5 mL of a $1x10^5$ CFU/mL bacterial suspension was added into a 24-well plate. Next, the patches were added to each respective well and incubated for 3h, 6h and 24h at 37 °C, with continuous shaking (100 rpm). At each time point, 50 µL of the bacterial suspension of each sample was collected and transferred to a 96-well plate, to measure cell density, DO, and resazurin reduction. Another 20 µL were collected for colony forming units (CFU) count. At each time point, the DO was measured at 600 nm using a microplate reader (BioTek® Synergy HT) to monitor bacterial growth. After OD reading, to each well, 10 µL of resazurin solution (Sigma) were added and the plaques were incubated at 37 °C, with continuous shaking (100 rpm), until a shift in colour was perceived. The fluorescence was read at a microplate fluorometer (BioTek® Synergy HT) equipped with a 530 nm excitation / 590 nm emission filter set. At each time point, 20 µL of the bacterial suspensions were also retrieved and placed in a 96-well plate, where sequential dilutions were performed (between 10^0 -10^{-8}) for CFU count. 10 µL of the undiluted and diluted suspensions were plated on agar Petri dishes and incubated in culture at 37°C until visible colony growth. 70 µL of TSB medium were introduced to substitute the removed medium, at each time point. Positive and negative controls were maintained throughout the study for comparison. All samples were performed in triplicates.

Data from OD measurement is represented as bacterial growth (%), calculated by Equation 2.1; from resazurin metabolization as relative units of fluorescence (RUF) and fluorescence average, calculated by Equation 2.2; and for CFU count as CFU's/mL.

$$Bacterial\ Growth\ (\%) = \frac{OD\ (600\ nm)_{sample}}{OD\ (600\ nm)_{control}}\ x\ 100 \qquad 2.1$$

Where OD_{sample} and $OD_{control}$ correspond to the optical density at 600 nm of the respective sample and the control, respectively.

$$RFU\ = \frac{Fluorescence\ of\ exposed\ cells}{Fluorescence\ of\ non-exposed\ cells} \qquad 2.2$$

Where the fluorescence of exposed bacterial cells and non-exposed cells corresponds to the fluorescence read at 530 nm excitation / 590 nm emission of each well incubated with the 3D patches and wells with normal growth conditions, respectively.

Agar disk-diffusion method

The Agar disk-diffusion method is a standardized technique for testing rapidly growing pathogens. This method has been mostly employed to test antibiotics, but a modified version of this method was employed with the 3D patches. Briefly, tryptic soy agar media plates, prepared from TSB (Liofilchem) and powder agar (Liofilchem), are inoculated with a bacterial concentration of $1x10^8$ CFU/mL and spread

uniformly. The tests were done against the previously used strains, *E. coli*. *P. aeruginosa*, *S. aureus* and *S. epidermidis*.

Then, the 3D patches were cut into a circle (10 mm radius). In the agar plates the same was performed, circles of the same diameter were cut into the agar and removed, to add the 3D patches inside. The Petri dishes were incubated under suitable conditions, at 37°C. The evaluation of this test is based on the level of complete and partial growth around the sample. After 24 hours, the diameters of inhibition growth zones are measured. The entire test was performed in triplicate and the values correspond to average ± S.D.

Note that it was necessary to create the holes in the agar because at 37 ºC the formulations are no longer gelled and return to their liquid form.

2.5.2. Cell Culture

Human dermal fibroblasts (HDF) and human epidermal keratinocytes (HEK), kindly provided by BoneLab, Faculty of Dental Medicine U. Porto, were cultured in alpha-minimum essential medium (***α***-MEM) (Gibco,Thermo Fisher Scientific,Inc.), and Ham's Nutrient Mixture F12 (Sigma) , respectively. Both media were supplemented with 10% heat-inactivated fetal bovine serum (FBS-HI, Gibco, Brasil) and 1% Antibiotic-Antimycotic (Anti-Anti, 100X; Gibco®). All the procedures concerning cell cultivation and management were performed inside a safety bench and the instruments were sterilized with 70% (v/v) ethanol prior to being used. Cells cultivated in T-flasks, and well-plates were incubated at 37 °C, 5% CO_2 and in a humidified atmosphere.

Cell proliferation/cytotoxicity assay

The cytotoxicity of the 3D patches was evaluated on both previously mentioned cell lines. In 24-well plates, the cells were seeded in 0.5 mL/well at a concentration of $1x10^5$ cells/mL and incubated for 24h, to allow cell adherence to the wells.

Since the samples easily dissolve at 37 ºC, the preparation of leachates was previously done and then incubated into the cells. Each sample was placed in 0.5 mL of the respective complete medium. After the 24h incubation and adherence to the wells, the culture medium was replaced by the prepared extracts. Afterwards, the cells were incubated for 6h and 24h with the extracts.

MTT Staining Assay

After the incubation periods, the cytotoxicity was evaluated by 3-(4,5-dimethylthiazol-2-yl)-2,5-diphenyl-2H-tetrazolium bromide (MTT) staining assay, where 50 µL (10%) of the MTT labelling reagent was added to each well. The plaques containing the reagent were incubated for 2h. MTT (yellow coloured) staining allows to assess the cell viability since it is metabolized by living cells, forming the violet-coloured product formazan. The samples were documented with a compact stereo microscope (Stemi 305, ZEISS) and a microscope camera (Axiocam 208 color, ZEISS).

Afterwards, to quantify cell viability and dissolve the precipitated formazan dye, 200 µL of dimethyl sulfoxide solution (DMSO, Sigma) was added to the samples for 15 minutes. Absorbance at 550 nm was measured on a microplate reader (BioTek® Synergy HT). The entire test was performed in triplicates and the obtained values correspond to Viability (%) ± S.D. (%), calculated from Equation 2.3.

$$Viability\ (\%)\ =\ \frac{OD\ (550\ nm)_{sample}}{OD\ (550\ nm)_{control}} x100 \qquad 2.3$$

Immunofluorescence staining protocol

In separate 24-well plates, the same assay was performed and after 24h a specific cell marker for each cell line, the cell nuclei, and the F-actin filaments were stained.

The first step of the immunofluorescence staining protocol was to fixate the sample. First, the wells are aspirated and washed once with PBS. After PBS removal, enough formaldehyde (Sigma) to cover the well was added and incubated in the cells for 15 minutes. Afterwards, formaldehyde was removed, and the wells are washed with PBS (Sigma) and if staining is not done immediately after, PBS is left in the well. It is critical from this point on that the cells do not dry out as this will result in increased levels of background staining and difficulty in interpretation of staining results.

The day before image analysis, PBS from the wells was removed and PBS containing 0.1% (v/v) Triton X-100 (Sigma) was added and incubated for 20 minutes, at room temperature. Triton X-100 is a permeabilization reagent that can dissolve the lipids on cell membranes, nuclear membranes and organellar membranes, thus, big molecules such as antibodies can get into cytoplasm and nucleus to bind to antigens.

After Triton removal, cells were incubated with 1% BSA (Sigma) in PBS for 30 min, to block nonspecific binding of the antibodies and to minimize intra- or extracellular background signals. After BSA removal, the rest of the protocol was performed in a dark room. The cells were incubated in the diluted primary antibody in 1% BSA in PBS overnight, at room temperature. For HDF, a mouse monoclonal Ki67 primary antibody (1:100, Santa Cruz Biotechnology, Inc) was used to detect the Ki67 protein of human origin. For HEK a mouse monoclonal cytokeratin 5 primary antibody, CK5 (1:100, Santa Cruz Biotechnology) was chosen for the detection of the cytokeratin 5 protein of human origin.

The next day, the primary cell markers were removed, and the wells were washed 2 times with PBS. Afterwards, cells were incubated with the Alexa Fluor 594 secondary antibody, a goat anti-mouse igG antibody (500 µg/mL, BioLegend), in 1% BSA for 2 h at room temperature. Alexa Fluor 594 is a bright, stable fluorophore that emits fluorescence into the red range of the colour spectrum.

After 1 more wash with PBS, the F-actin filaments were stained for 30 minutes with Alexa Fluor 488 (1:100, BioLegend) in 1% BSA. Alexa Fluor 488 dye is a bright, green-fluorescent dye.

Finally, after F-actin marker removal and 1 PBS wash, the nuclei were also stained for 15 minutes, at room temperature, with Hoechst 33342 antibody (8 µg/mL, Sigma) in PBS. This permits to determine the cell viability by staining in blue the cell nuclei of living cells.

The marker was removed, the wells washed with PBS once more and PBS was added to cover the wells if samples were not immediately visualized. Images of the stained cells were acquired using the Selena S digital imaging system (Logos Biosystems).

Scratch wound healing migration assay

A visual representation of the scratch wound healing essay can be seen in Figure 2.4.

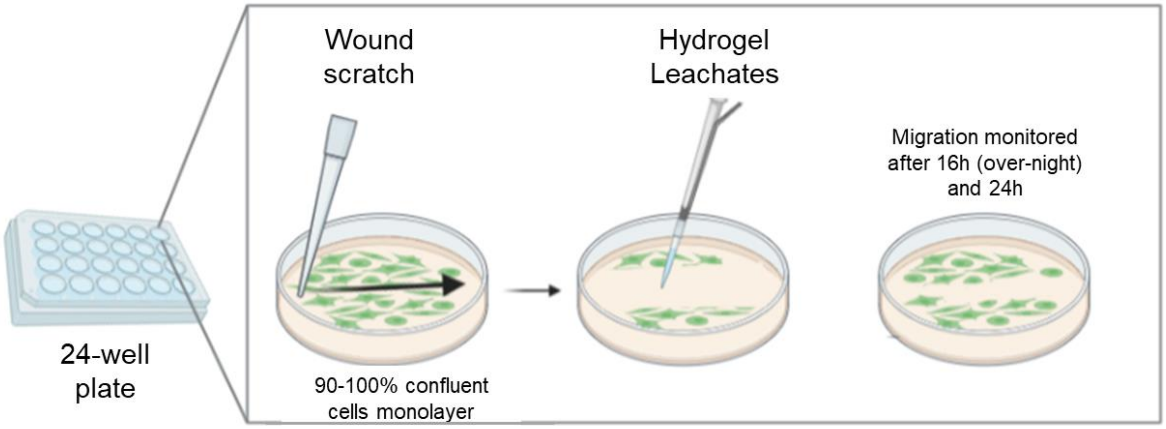

Figure 2.4 – Schematic overview of the scratch wound healing assay and the used test conditions. Picture created with Biorender.com [41].

Cells were seeded onto 24-well plates and cultured until 90-100% confluence. Without removing the medium, the created monolayer was wounded by scraping it with a 10 µL sterile pipette tip. Subsequently, each well was washed 2 times with sterile PBS and one time with non-supplemented culture medium.

As before, the samples were previously diluted until dissolved in 0.5 mL of complete medium and the leachates were added to each well. Wells with only complete medium were selected as the positive control group, to compare the rate of wound healing process.

The migration and regeneration of scratched cell matrix layer (wound healing) was monitored by a microscope for after approx. 16h (over-night) and 24h. The area of the wounds was compared with the wound area at time 0h, to evaluate the migration rate of cells. The distance was determined by measuring the cleared space between the wound edges with image analysis of the pictures obtained with a digital camera from an inverted microscope at 40x objective and the ImageJ® software. The percentage of wound closure was calculated using Equation 2.4,

$$Wound\ Closure\ (\%)\ =\ \left(1-\frac{D_T}{D_0}\right)\ x\ 100 \qquad 2.4$$

Where D_T is the distance between two vertical lines at said time point after adding the extracts and D_0 is the distance between two vertical lines at time 0h in the absence of wound healing compounds.

Triplicate samples were used for this analysis and five random distances of each were used for the quantitative analysis. The results appear as Wound Closure (%) ± S.D. The samples were also stained with MTT reagent after the incubation period, and were documented with a compact stereo microscope (Stemi 305, ZEISS) and a digital camera (Axiocam 208 color, ZEISS).

Antioxidant Activity Assay

The intracellular production of reactive oxygen species (ROS) inside the cells was evaluated using a fluorometric technique by using 5(6)-carboxy-2',7'-dichloroflourescein diacetate (5(6)-CDCFDA), a fluorogenic reagent that detects reactive oxygen species.

The cells were seeded onto 96-well plates at a concentration of $1x10^5$ cells/mL, for a total volume of 100 µL in each well and incubated for 24h to allow adherence to the wells. After the 24h, the cells were incubated for 30 minutes with 10 µM of 5(6)-CDCFDA (Enzo), in the dark at 37 °C.

As before, the samples were previously diluted until dissolved in 0.5 mL of complete medium and the leachates were added to each well. The leachates were placed directly in the wells (100 µL) and ascorbic acid (AA) was used as positive control (1mg/mL). The plaques were incubated for 1h at the previously mentioned conditions.

The oxidative stress was induced by a hydrogen peroxide (H_2O_2, 500 M) solution for 15 minutes and the ROS levels were determined at an excitation wavelength of 485 nm and emission wavelength of 520 nm, using a microplate fluorescence reader. Seven replicates were used for each hydrogel and the data is represented as relative units of fluorescence (RUF) and fluorescence average. Relative units of fluorescence are calculated according to the previously described Eq. 2.2.

The irritation potential and angiogenic test by the HET-CAM Assay

The 3D patches were tested for the irritation and angiogenic potential using the hen's egg test on the chorioallantoic membrane (HET-CAM) assay and according to the Interagency Coordinating Committee on the Validation of Alternative Methods (ICCVAM) [71].

Freshly laid fertilized chicken eggs were incubated horizontally at 37 °C in a 60% humidified atmosphere, using an Octagon Advance incubator (Brinsea) with one hour scheduled rotation. At day 8-post fertilization, a small window was made in the eggshell, under aseptic conditions, to gain access to the CAM beneath. The samples were placed randomly and individually on the CAM of the chicken embryo.

For a contact period of 0.5, 2.0 and 5.0 min, the CAM was assessed by visual inspection and photographed with a stereomicroscope (ZEISS Stemi 305) attached to a digital camera (Axiocam 208 color, ZEISS), for signs of irritation. The irritation potential was evaluated by the occurrence of specific reactions to the membranes and/or vessels (i.e., hyperaemia, haemorrhage, clotting and changes in small vessel diameter) which were then interpreted in comparison to a negative (0.9% NaCl) and a positive (0.5M NaOH) control according to the guideline. Time-dependent scores for irritancy were assigned semi-quantitatively using a grading system according to the Luepke method, from 0 (no-reaction) to 3 (strong reaction). Each test was carried out in duplicates. 10 eggs were used during the experience.

For the angiogenic response, after 8 days, filter paper discs (0.5 cm diameter) impregnated with the extracts were placed on the CAM. The eggs were further incubated for 3 days. The CAM surrounding the discs was cut off and photographed with a stereomicroscope (ZEISS Stemi 305) attached to a digital camera (Axiocam 208 color, ZEISS). Images were processed with the ImageJ® software program for the quantification of blood vessels converging toward the discs. Sterile saline was used as the control.

2.6. Statistical Analysis

Statistical analysis of the results referent to the biological characterization of bioactive 3D patches was performed using Microsoft Excel 365. Comparison of the experimental conditions was performed by the t-test and the comparison of several groups performed by the one-way analysis of variance (ANOVA). P-values ≤0.05 were considered significant.

Chapter 3: Results and Discussion

3. Results and Discussion

3.1. Characterization of Gelatine-Based Hydrogels

3.1.1. Detection of rheological properties of gelatine-based hydrogels inks

After the inks' development and preparation, the rheological properties of the inks were studied, to aid the printing process of the hydrogels.

A rheological study was performed to determine the sol-gel transition temperature from an elastic network formation to a solution of the two hydrogels inks controls (P30 and P40), which can be an indicator of at which temperature the hydrogels should be printed. Figure 3.1. shows the evaluation of the change in the rheological properties with the temperature for the P30 and P40 gelatine-based hydrogel inks.

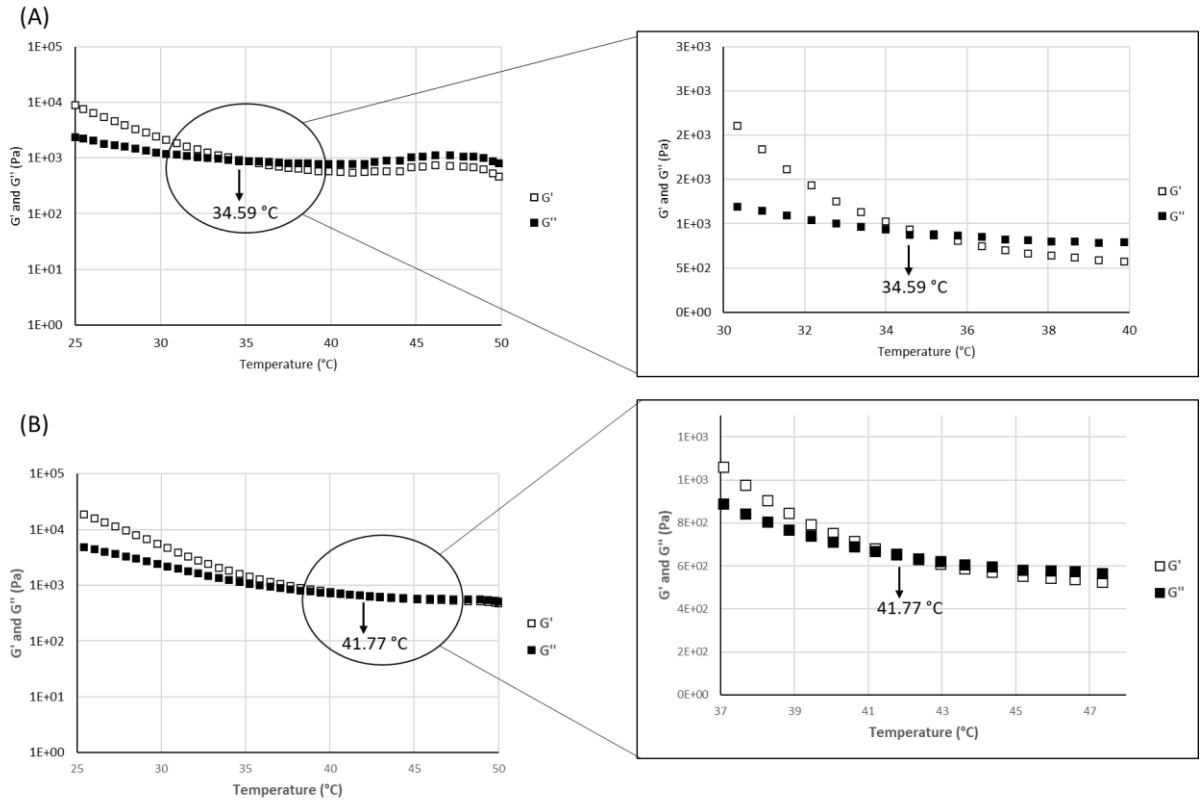

Figure 3.1 - Evaluation of gelatine-based hydrogel formulations' rheological properties, namely its sol-gel transition. Sol-gel transition of P30 hydrogel formulation (A); Sol-gel transition of P40 hydrogel formulation (B). The crossover temperature between G' and G'' corresponds to the sol-gel transition temperature, or gelation temperature.

The changes in storage/elastic (G′) and loss/viscous (G″) moduli for the temperature profile from 25 °C to 50 °C for both gelatine concentrations shows clearly that gelatine displayed liquid behaviour with a higher G″ than G′ at the final temperature of 50 °C. As the temperature decreased, increases in G′ and G″ were observed for both gelatine hydrogels, more pronounced in the case of P40 ink, indicating the

gel formation. The gelation process could be attributed to the shift from single-strands chains to multi/triple-helix of gelatine chains through hydrogen bonding, ionic interaction, Van der Waals forces, self-assembly, and hydrophobic association [72]. Moreover, upon cooling, a crossover occurred for G′ and G″, named the sol-gel transition temperature, Tsol-gel (°C), and the shift from a solution to a gelled state.

Additionally, the results show that an increase in the concentration of the formulation excipients, particularly gelatine, introduced a significant effect in its rheological properties, i.e., the Tsol-gel increased from ~35 ºC in P30 to almost ~42 ºC in P40 ink. The ink viscosity was also increased. This occurrence has been previously described by other authors [73,72]. As an example, the rise from 0-20% w/w in gelatine concentration has shown to increase the critical gelation temperature from 25 ºC to 32.5 ºC [74]. Since here the use of higher gelatine percentages than the ones described, 30% and 40%, respectively, it makes sense that the sol-gel transition is higher and that it increased with the rise in gelatine concentration. However, this is only a suggestion since no results were discovered previously in the literature for gelatine concentrations higher than 20%.

The previous results suggest that the selected temperature inside the cartridge during the printing process should be superior in the P40 ink, as compared to the P30 one. Considering that the temperature difference (ΔT) between the temperature inside the cartridge and the room temperature is ~16 ºC and ~9 ºC for the P40 and P30 respectively, it is expected that the filaments spreading in P40 will be lower than P30, which will lead to a higher printing accuracy and more uniform and reproductible 3D patches [75]. It is also expected the need to use a higher printing temperature for P40 than the indicated, since the high ΔT can cause premature gelling inside the nozzle at sol-gel transition temperature.

The characterization of the inks' behaviour at below sol-gel temperature is also important, to understand its behaviour after extrusion. At room temperature (~26 ºC), both hydrogels are characterized as viscoelastic solids, with storage modulus (G′) values higher than the loss modulus (G″). At this temperature, the G' and G'' moduli are 6.46×10^3 Pa and 2.04×10^3 Pa for P30, and 15.8×10^3 Pa and 4.38×10^3 Pa for P40 inks, respectively. Higher G' and G'' is seen particularly when the gelatine concentration is increased. The higher G' indicates a higher degree of internal structure and that a greater amount of energy must be put into the hydrogel to distort it. As a result, the P40 hydrogel will have higher elastic forces, being able to have more resistance to deformation and will have a more solid like behaviour. Additionally, a higher strength and mechanical rigidity of P40 compared to the P30, at this temperature should be observed [72].

3.1.2. Effects of incorporation of Manuka honey on gelatine-based hydrogel ink

The results for Manuka honey (MH) incorporation on the gelatine-based hydrogel inks revealed that, it was only possible to blend a maximum of 40% MH in the P30 ink, without compromising the hydrogels properties. It was observed (results not showed) that when a higher percentage of MH was added, it

was not possible to fully incorporate the MH into the hydrogel, the inks were not homogeneous and were too viscous.

In relation to P40 ink, due to the higher viscosity, it was not possible to add MH in percentages superiors to 20% since with higher concentrations, gelatine was not able to be dissolved and a lumpy heterogeneous paste was formed (Figure 3.2).

Figure 3.2 - Paste formation after 20% MH incorporation into the P40 ink. A heterogeneous and non-printable paste was formed.

Furthermore, the other formulation excipients, except water and sucrose, already make up a total of 52% of the hydrogel formulation, making it difficult to incorporate high concentrations of honey. Moreover, the goal was to obtain an ink with ≥40 % MH incorporated. Thus, this option was discarded.

Accordingly, to aid the printing process, the rheological characterization of the P30 ink with 40% MH (MH-P30) as shows in Figure 3.3, was performed.

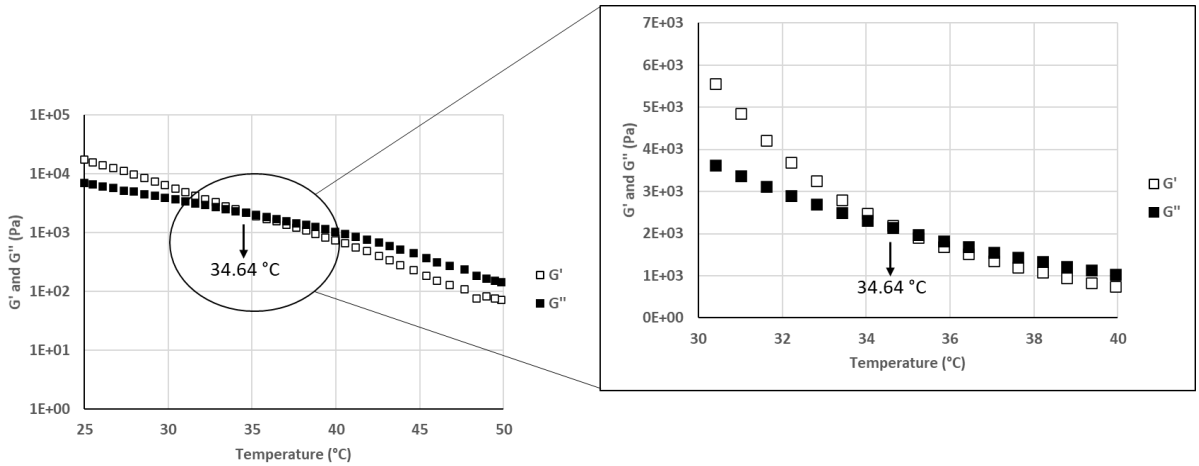

Figure 3.3 - Evaluation of the sol-gel transition of the P30 gelatine-based ink with 40% Manuka honey incorporated (MH-P30). The crossover temperature between G' and G'' corresponds to the sol-gel transition temperature, or gelation temperature.

The addition of MH to the P30 ink (Figure 3.3) did not change the sol-gel transition (~35ºC), when compared to the ink without MH (Figure 3.1) but the shape of the curves is slightly different. At sol-gel

transition of MH-P30, the loss modulus (G'') is much higher than in P30 (2.1 $x10^3$ Pa compared to 0.88$x10^3$ Pa), which correlates with a higher viscosity of the ink at gelation temperature. The storage modulus, G', is also higher for MH-P30, when compared to P30 (2.2$x10^3$ Pa and 0.93 $x10^3$ Pa, respectively). This correlates with a more solid-like behaviour and consequently higher extrusion pressures may be required.

Even though the sol-gel transition was not changed, the previous results suggests that for printing, a higher temperature than the sol-gel must be provided, since with higher viscosities in unstable temperatures, like the sol-gel transition, nozzle clogging, irregular flow rates and inhomogeneity can occur [17]. Hence, a higher temperature than the obtained should be used for MH-P30 ink. Higher mechanical strength and elastic properties should be observed at this temperature, when compared to the P30 ink.

At room temperature, approx. 26 ºC, the MH-P30 ink has G' and G'' higher than P30, i.e.,13.8$x10^3$ Pa and 6.1$x10^3$ Pa compared to 6.5$x10^3$ Pa and 2.0$x10^3$ Pa, respectively. Thus, the addition of MH to the hydrogel, at lower temperatures than the sol-gel transition, indicates an increase in hydrogel strength and rigidity, whilst maintaining a good elasticity and bendability. At T > 40 ºC, the G' and G'' moduli for the P30 and P40 inks are not significantly altered. However, for MH-P30 ink, a decrease in both parameters is seen. This indicates a lower viscosity of the ink, at higher temperatures, when compared to both base inks and the confirmation that high temperatures can provoke mechanical and structural alterations in the hydrogel, when honey is incorporated [76].

Considering that the sol-gel transition is important for setting the printing temperature and knowing that it should not be very high, since it can be deleterious to the various active enzymes and chemicals present in honey, the results indicate that it is possible to print gelatine-based inks with 40% MH incorporation, without impairing the pretended results.

3.1.3. Development of 3D Gelatine-Manuka Honey Hydrogel Patches

Some of the key parameters in the 3D printing process, for successful and reproducible printing 3D patches, are temperature, pressure, printing velocity, line width, spacing (pore size), and layer thickness. Temperature is one of the most critical factors affecting the printability of 3D patches since it changes the material's intrinsic properties [44]. Figure 3.4 shows the effect of printing temperature on strand filament formation at different temperatures.

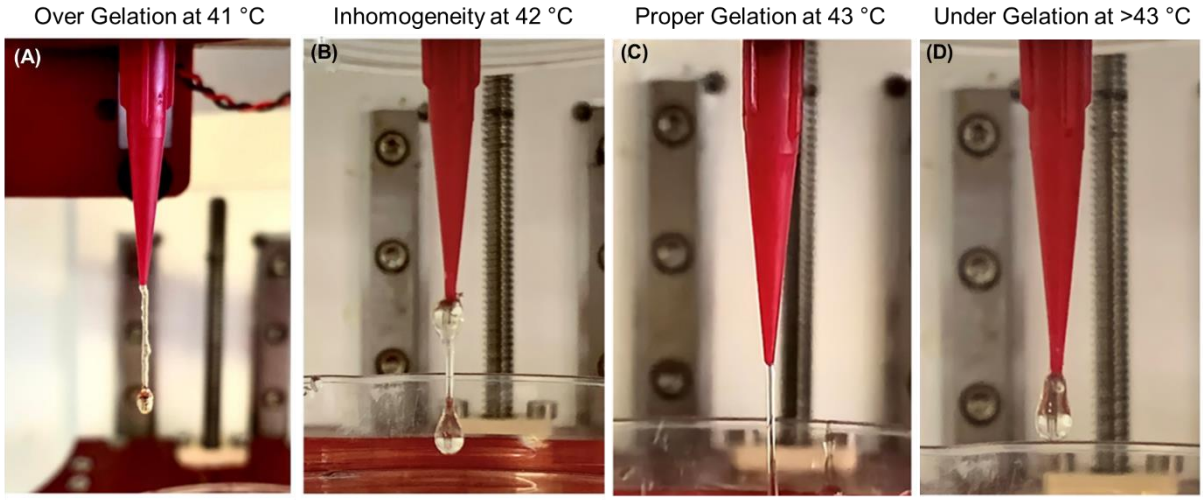

Figure 3.4 - Example of the strand tests performed for P40 ink. Over gelation at T = 41 ºC (A); Inhomogeneity at T = 42 ºC (B); Proper gelation at T = 43 ºC (C); Under gelation at T > 43 ºC (D).

By observing Figure 3.4, before setting the ideal temperature, droplets were extruded, and inhomogeneous filaments were observed (Figure 3.4A-B). But, with the optimized temperatures (34 ºC for P30 and 43 ºC for MH-P30 and P40) a continuous strand was formed, as shown in Figure 3.4C. By printing at a higher temperature than the proper gelation temperature (under gelation) liquid droplets are extruded, and no filament is formed (Figure 3.4D).

For the more viscous inks, P40 (Figure 3.4.) and MH-P30 (results not shown), it was observed that a higher printing temperature translates into an increase in filament homogeneity and quality. These results were in line with the rheological observations, i.e., for high viscous solutions, lower or equal temperatures than sol-gel can induce a gelation inside the nozzle which causes difficulties in the printing process and the formation of inhomogeneous filaments (Figure 3.4.A-B). For MH-P30, due to its viscosity, this difference is even bigger. For the less viscous ink, P30, since the ΔT between the temperature inside the cartridge and the room temperature is much lower (~8º C), the hydrogel is possible to be printed closer to the sol-gel transition temperature, since gelation is not as sudden.

After performing the strand tests for each ink, it was necessary to test the filaments' ability to form structures capable of stacking in layers. Initially, one singular layer was produced, and its behaviour and stability were studied. Figure 3.5. shows in detail an example of the obtained filaments and can be observed that the thickness of the strand relied on the size of the printing nozzle.

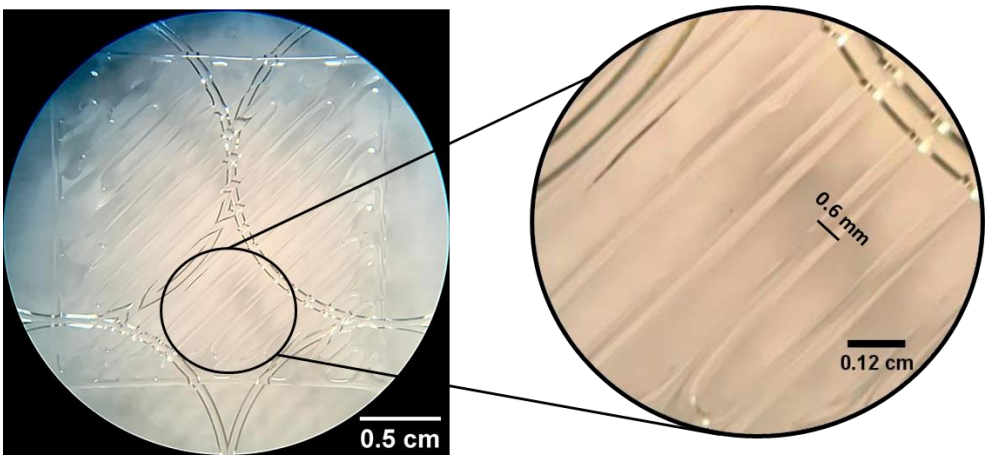

Figure 3.5 – Example of the printed 3D hydrogel monolayer filaments with a line width of 0.6 mm. Printing with P40 ink. Microscopically, the monolayer showed no filament spreading, demonstrated printing accuracy and reproducible results.

At a printing velocity of 30 mm/s, printing pressure of 25 Psi and a line width of 0.6 mm, all the developed hydrogel inks (Figure 3.5) showed stable and consistent results with no spreading of the strands, at the previously established temperatures.

3.2. Physicochemical Characterization of Gelatine-Manuka 3D Patches

Afterwards, 3-layered patches were attained. Figure 3.6A-C microscopically reflected the appearance of the P30 printed hydrogel (Figure 3.6A), MH-P30 printed hydrogel (Figure 3.6B) and P40 printed hydrogel (Figure 3.6C). The P30 patch exhibited a well-designed morphology and a white appearance (Figure 3.6A), whereas the patch changed to yellowish after functionalization with MH (Figure 3.6B) and kept the white colour with addition of gelatine (Figure 3.6C).

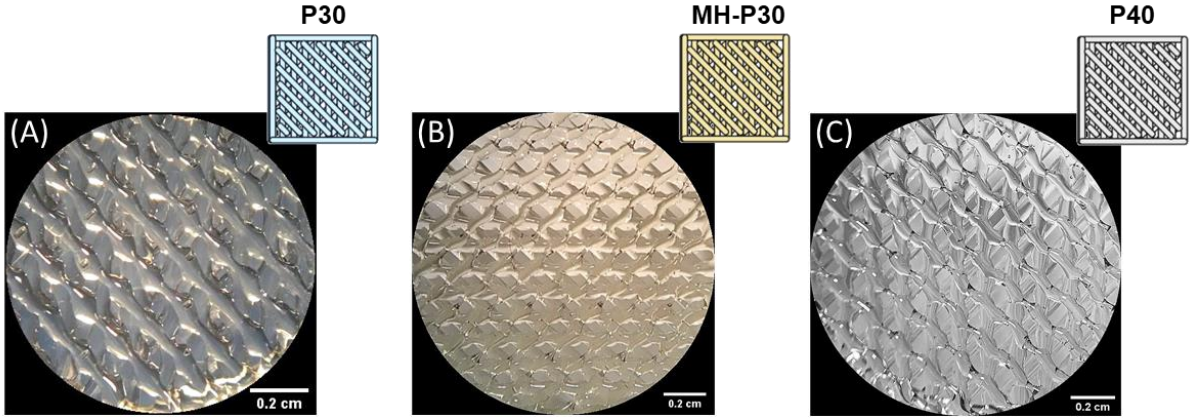

Figure 3.6 - Microscopic images of the developed 3D hydrogel patches. P30 printed patch (A); MH-P30 printed hydrogel (B); P40 printed hydrogel (C). Each hydrogel is composed by 3 layers of each ink. Definition between lines and no substantial filament spreading can be observed.

As demonstrated by the microscopical images, the thickness of the printed strands in the 3rd layer is higher in the P30 patches when compared with MH-P30 and P40, which is translated in a low printing accuracy of the patches. In addition, it was found that the quality of the 3D patches increased after the addition of MH (Figure 3.6B) in MH-P30 and gelatine (Figure 3.6C) in P40 patch. Furthermore, the developed 3D patches had an interconnected 3D structure, with well define geometry. Thus, the pores have better definition in MH-P30 and P40 patches with lower filament spreading, when compared with the P30 patch.

These results are consistent with other studies, where the addition and increased concentration of gelatine reduced the width of printed strands, increased printing accuracy and, consequently, spreading of the ink no longer occurred [77].

These 3-layered structures were able to maintain their structure and stability, without losing quality, for a long period of time (more than 30 days). Additionally, the developed 3-layered 3D patches showed that it is possible, through the previously optimized conditions, to create accurate and reproducible multi-layered porous 3D structures.

To further extend the MH-P30 and P40 patches characterization, the topography of the MH-P30 and P40 obtained by SEM images was obtained and the results are present in Figure 3.7.

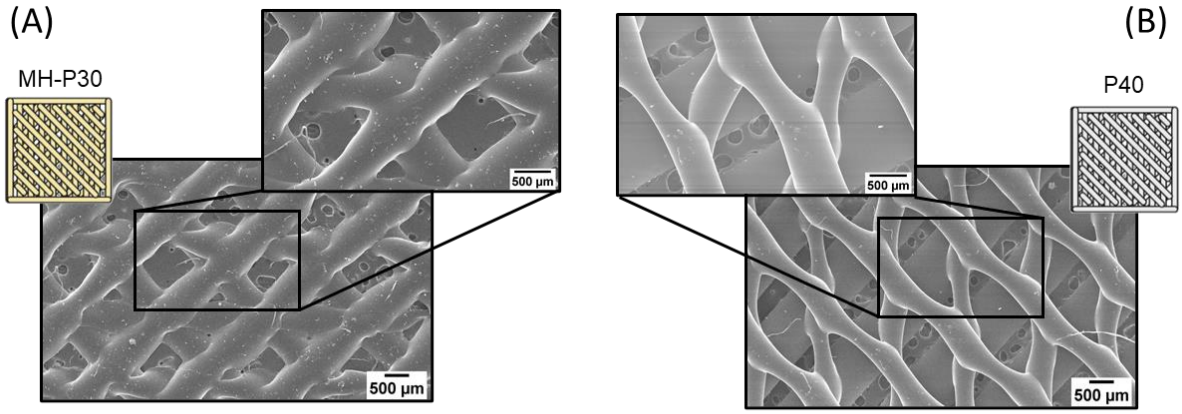

(C)

3D printed hydrogel	Mean Pore Size ± SD (µm)
MH-P30	459 ± 225
P40	517 ± 275

Figure 3.7 - Scanning electron microscopy (SEM) images of MH-P30 and P40 3D printed patches and pore characterization at 20x and 40x. SEM images of MH-P30 patch (A); SEM images of MH-P30 patch (B); Mean pore size distribution of the developed 3D patches (C).

It is instantly noticeable the low filament spreading of the bottom layer of the MH-P30 (Figure 3.7A), compared to the P40 (Figure 3.7B). The MH-P30 shows an expected line width (approx. 0.6 mm), while P40 hydrogel presents a line width of almost double of the expected (approx. 1.1 mm). This behaviour switches in the deposition of the 2nd and 3rd layers. It is important to point out that different materials

have different surface adhesion. Bed adhesion is directly linked to the wettability properties of the hydrogel ink and it has been previously stated that can drastically influence the quality of the final patch [78]. Thus, here, the introduction of MH can be increasing surface adhesion to the plastic plate, whilst in the gelatine-only patch, P40, this adhesion is lower, provoking a superior filament spreading in the first layer and less printing accuracy.

Overall, the MH-P30 hydrogel strands appear to be more uniform between layers and a more homogeneous porous structure is obtained (Figure 3.7A), with a mean pore size of 459± 225 μm. The pores also appear to have the regular pretended shape. Considering the obtained porosity for P40, bigger, with an irregular shape and more heterogenic size pores were obtained, with an average pore diameter of 517± 275 μm. A study by Dong Jin Choi et al. investigated the effect of the pore size in a 3D printed gelatine hydrogels on fibroblast proliferation [50]. All the produced hydrogels had a porous size higher than 435 μm and provided good cell affinity. After 14 days of culture with HDFs, the proliferation was approx. 14% higher in hydrogels with 580 μm rather than 435 μm pore size. The size of the attained porous here are between the previous range, thus, the results suggest that the produced 3D patches can provide a good base for fibroblast affinity and proliferation [50]. Moreover, highly porous biomaterials are very desirable for the easy diffusion of nutrients and waste products. This is a major requirement in hydrogels for wound healing and skin regeneration.

From the obtained results, it can be confirmed that it is possible to develop 3-layered 3D patches, through the previously optimized conditions, to create accurate and reproducible multi-layered porous 3D patches.

To evaluate the possible chemical interaction between the raw materials and the impact of the printing process on the 3D patches' chemical structure, the chemical groups present on powder gelatine, Manuka honey, P30, P40 and MH-P30 patches were qualitatively evaluated through ATR-FTIR analysis (Figure 3.8).

The obtained FTIR spectra indicate the presence of absorption bands characteristic of peptide bonds, present in gelatine (Figure 3.8A). Amide A, one of the most important structural groups in gelatine, appears in a broad band at ~3301 cm^{-1}, mostly due to N-H stretching vibrations [79]. This peak is slightly shifted to the right, when compared to the gelatine powder spectrum (3290 cm^{-1}) and is broader due to the water content of the samples, that provokes a OH stretching band in this area (~3300 cm^{-1}) [79].

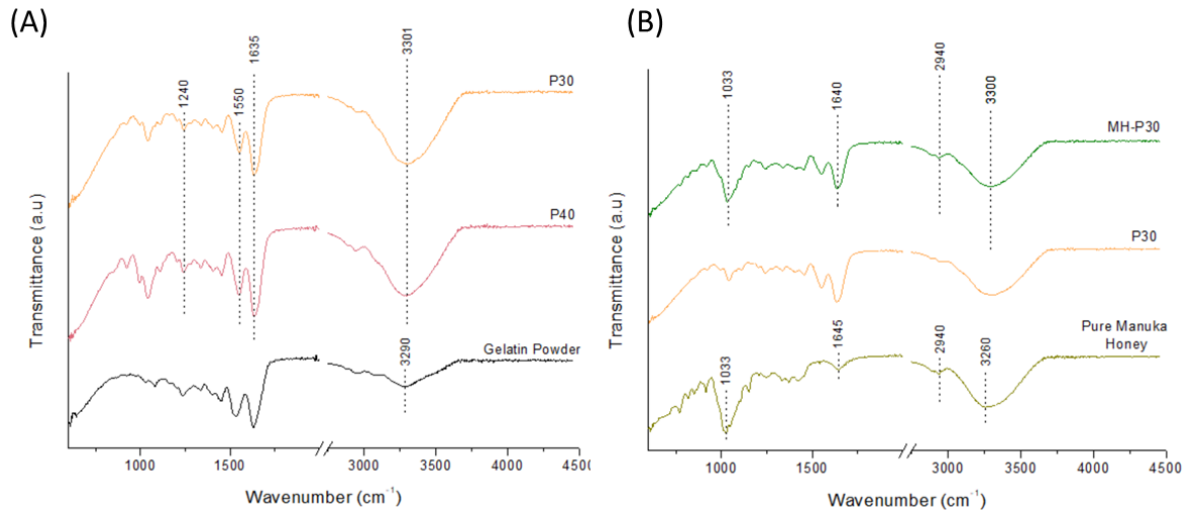

Figure 3.8 – Qualitative ATR-FTIR analysis. ATR-FTIR spectra of gelatine powder, P30 and P40 patches (A); Comparison between the ATR-FTIR spectra of pure Manuka honey, P30 and MH-P30 patches (B).

Other characteristic groups of gelatine present in the hydrogel's structure include amide I (~1635 cm^{-1}), amide II (~1550 cm^{-1}) and amide III (~1240 cm^{-1}). Amide I bands are induced by C = O stretching vibrations, whereas amide II is caused by the bending vibrations of N–H groups and stretching vibrations of C–N groups. Amide III is related to the vibrations stretching of C–N and vibration bending of N–H groups of bound amides [64,79]. No significant peaks specifically related to sucrose or glycerine were found in the spectra (spectra shown in Appendix A1 - Results and Discussion). Additionally, no significant differences are seen between the P30 and P40 spectra. The results show the presence and maintenance of the integrity of gelatine before and after the printing process.

Regarding the incorporated bioactive MH, the presence of the honey in MH-P30 could be observed in Figure 3.8B. The region from about 1500–750 cm^{-1} corresponds to the most sensitive absorption region of the honey's major components, relevant to honey sugars and organic acids [80]. ATR-FTIR spectra of pure MH confirmed the presence of all characteristic peaks of hydrated carbohydrates namely, one broad vibration band at 3260 cm^{-1} identified as OH stretching vibration; a small vibration band at 2940 cm^{-1} corresponds to the C–H stretching of carboxylic acids and NH_3 stretching band of free amino acids [80,81]. Another small band detected at 1645 cm^{-1} characteristic of C=O stretching vibration and an intense peak at 1033 cm^{-1} corresponds to stretching of C-O groups of the C–O–C linkage [80]. ATR-FTIR spectra of MH-P30 shows that particularly the bands at 1033 cm^{-1} and 2940 cm^{-1} confirms the maintenance integrity of the MH. The other two honey distinctive peaks 3300 cm^{-1} and 1640 cm^{-1} in the MH-P30 were overlapped with other components' bands and suffered small shifting, when compared to the spectra of MH.

A previous study tested 63 different honeys, excluding MH, and the other authors obtained the similar peaks found in this work for MH [81]. This suggests that the obtained peaks are characteristic of honey itself, and not to MH specifically [81].

Regarding the ATR-FTIR characterization of patches with MH incorporated, no prior results were discovered for gelatine-based hydrogels. However, data on Manuka honey/gellan gum composite hydrogels for the use in cartilage repair has showed the specific peaks for MH here observed in this work [82].

3.3. Biological Characterization of Bioactive 3D Patches

3.3.1. Antibacterial activity of bioactive 3D Patches

Since one of the set goals was to fabricate a 3D bioactive patch with antibacterial properties, it was first necessary to test if the used 40% MH concentration is enough to provide bacteriostatic and bactericidal activity. To evaluate this assumption, the minimum inhibitory concentration (MIC) and minimum bactericidal concentration (MBC) of MH on each bacterial strain was assessed. Table 3.1. shows the obtained results and a visual representation of the obtained results is present in Appendix A2 - Results and Discussion .

Table 3.1 - Minimum inhibitory concentration (MIC) and minimum bactericidal concentration (MBC) of Manuka honey for each bacterial strain tested: *S. epidermidis*, *S. aureus*, *E. coli* and *P. aeruginosa*.

Bacteria	**MIC (% w/v)**	**MBC (% w/v)**
S. epidermidis	35.5	35.5
S. aureus	17.8	35.5
E. coli	35.5	35.5
P. aeruginosa	35.5	35.5

The results confirm that the bioactive MH has bacteriostatic and bactericidal effect for all the bacterial strains tested. A lower MIC was observed for *S. aureus* (17.8% w/v) and equivalent MICs were found for *S. epidermidis*, *E. coli* and *P. aeruginosa* (35.5% w/v). More diluted solutions did not present activity against the different bacteria. Regarding the MBC concentrations, only at percentages higher than 35.5% w/v, MH was able to provoke a bactericidal effect on the viable bacteria population. No significant differences between gram-negative and gram-positive bacteria susceptibility to MH were encountered. Thus, it is expected that the use of 40% w/v MH in the hydrogels will have both bacteriostatic and bactericidal effect in the studied bacteria, since this value is higher than the MICs and MBCs obtained.

Previous studies indicate that the MIC and MBC concentrations of MH can vary due to the Unique Manuka Factor (UMF) and methylglyoxal (MGO) content present in the honey, but also can vary according to the susceptibility of strains of the same species [83-86].

Prior results have reported a range of inhibition being 20% or less (MIC) on a variety of *S. aureus* strains [56], concordant with the results obtained here. A study by Hern Tze Tan et al. discovered a MIC of

11.25 % w/v for the same studied *S. aureus* strain, using a UMF 10+ MH (with a MGO of >0.261 mg/g). A UMF 10+ corresponds to a UMF factor of 10 or higher. However, for other coagulase-negative *Staphylococci*, the results varied between 8.75 and 15% w/v. The MBC values were also reported for these strains: being 25% w/v for the *S. aureus* here studied and between 22.5-25% w/v for the other strains [83]. When directly compared, a honey of 0.3+ mg/g MGO is used in this work. The MIC and MBC obtained here are higher than the reported in the literature, meaning a higher concentration of MH is necessary to provoke the inhibitory effect. Even though the MGO content is similar in both cases, it would be expected that a higher MGO content would lead to a higher inhibitory effect, however, the contrary occurred. Moreover, other studies with higher MGO concentrations have discovered that diluted solutions of Manuka honey (~4-6% (v/v) MH) can also be bactericidal and bacteriostatic, in different *S. aureus* strains [25,84].

Other studies have shown that MH with lower UMF values, and consequently lower MGO content, increased antimicrobial activity, seemingly due to changes in MGO content of honey over time [85]. Thus, the UMF value by itself may not be a reliable indicator of antibacterial effect. However, other studies have confirmed that MGO content of MH correlates strongly with antistaphylococcal activity [86]. Thus, the study of the relation between MGO content and antibacterial activity needs to be more deepened, since seemingly opposite results have been demonstrated. Moreover, it is also important to note that different growth conditions were used in the essays.

For *S. epidermidis*, no previous work has established MIC or MBC MH concentration for *S. epidermidis* RP62A. However, for other strains, concentrations of 15% v/v (MIC) and <25% v/v (MBC) have been described [56].

Regarding the gram-negative bacteria, MICs and MBCs of MH of up to 33% and 22.5 % w/v, respectively, have been previously reported for *P. aeruginosa* [56]. No direct studies have been made with MH and the *P. aeruginosa* strain studied (*P. aeruginosa* PAO1). However, a study showed that the MIC of MGO for PAO1 was 512 µg/mL [26]. The correspondent MGO concentration to a MIC of 35.5 % w/v is ~107 µg/mL (calculations described in Appendix A3 – Results and Discussion). The results obtained in this work are significantly lower, meaning lower concentrations are needed for the same antibacterial effect. However, these results cannot be directly compared, since MH presents other components that can be synergistically affecting its antibacterial activity. For *E. coli*, a range of inhibition was also observed against a variety of MHs [56]. For *E. coli* ATCC 25922, a MIC and MBC of 13-17.5 and 17.5% w/v, respectively have been described when a UMF 10+ MH (>0.261 mg/g MGO) was used [83]. However, another studied used a UMF 18+ MH (>0.696 mg/g MGO) and obtained MIC and MBC values of 20 and 25 % w/v, respectively [56]. As described before, the MGO content is known to affect the antibacterial activity of MH, but more in-depth studies must be performed, to fully understand its direct impact with antibacterial effect.

After confirming that the used MH percentage can provoke bacterial inhibition, the antibacterial activity of the printed hydrogels was assessed. The use of patches with 2 different MH concentrations was also

studied. Patches with 40% w/v and ~27% w/v of MH were used, corresponding to 3MH-P30 and 2MH-P30 (Figure 3.9). This decision was made to have a condition with a percentage close to the attained in the previous test and a percentage closer to the obtained in the literature.

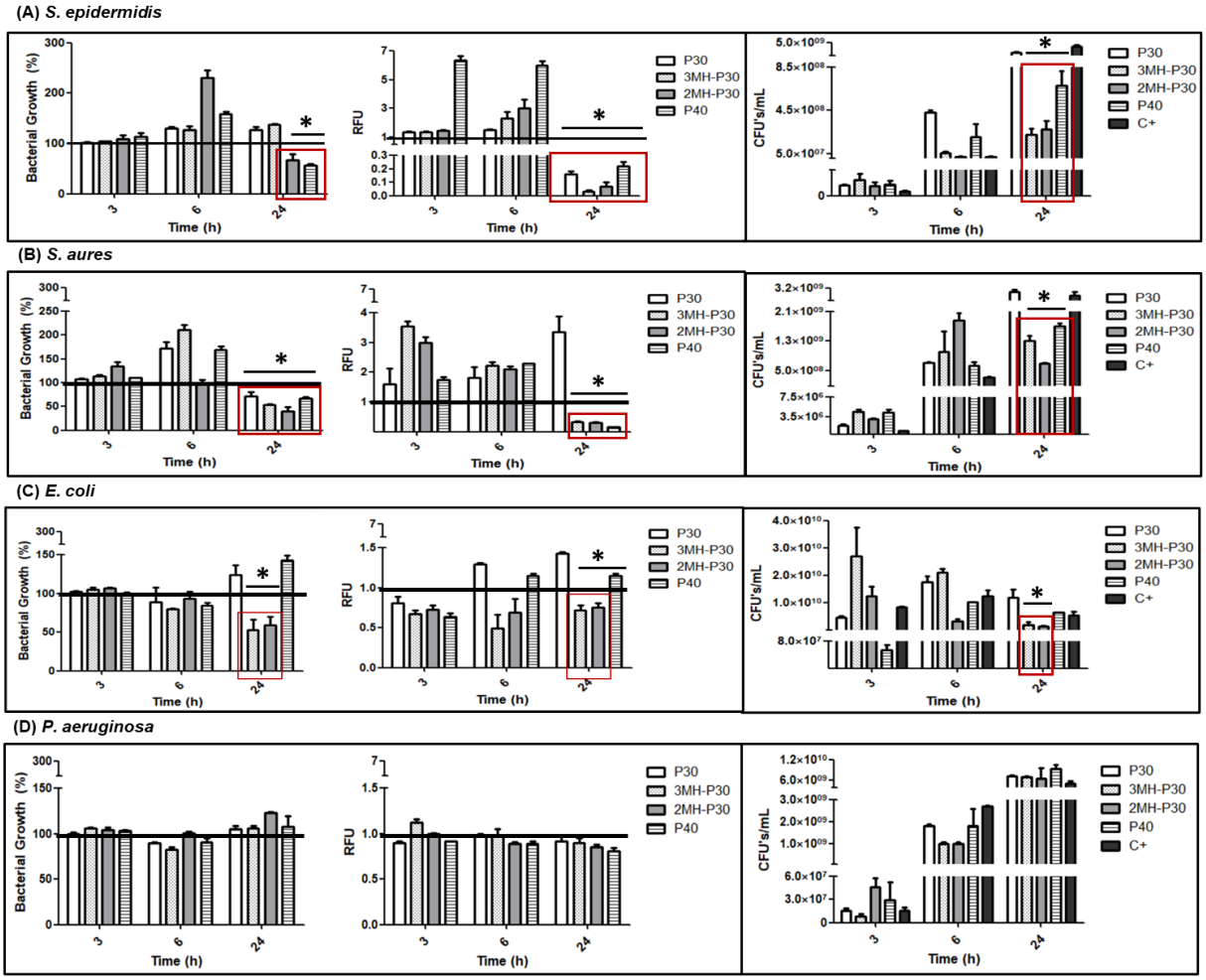

Figure 3.9 - Antibacterial activity of 3D hydrogels against four bacteria strains, after 3h, 6h and 24h of incubation. Bacterial growth in normal culture conditions, positive control, is indicated as 100% of bacterial growth (solid line); Resazurin reduction in normal culture conditions, positive control, is indicated as RFU = 1 (solid line); CFU counting is used to estimate the number of viable bacteria in a sample. Antibacterial activity of *S. epidermidis* (A), *S. aureus* (B), *E. coli* (C) and *P. aeruginosa* (D). * - Results lower and significantly different from the control (C^+) in normal growth medium, at 24h.

A quick overview of the antibacterial activity of the 3D patches (Figure 3.9) indicates that gram-positive bacteria are more susceptible to the patches' composition, than gram-negative.

Regarding *S. epidermidis* (Figure 3.9A), optical density of bacteria shows that at 24h (more relevant results) the microbial growth in the 2MH-P30 and P40 tests is lower, showing a viability of approximately 67% and 56%, respectively, when compared to the control (100%). Concerning the viable bacteria population, even though fluorescence indicates that all patches could have a detrimental effect on the viable population, patches with honey appear to have a higher effect. But with CFU count this is not

seen for P30 patch. One of the disadvantages of the resazurin essay is that if the cell count is too high or incubation is very prolonged, the reduction of resazurin can be amplified, creating a bleaching effect and underestimate the activity of the bacterial suspension [65]. Moreover, it is a more sensitive test than the CFU count. Thus, P30 can be considered as not having antibacterial effect on *S. epidermidis.*

Looking at the results for *S. aureus* (Figure 3.9B), at 24h, normal bacterial growth is impaired with in all imposed conditions, with viability being reduced between 40% and 72%. However, only patches with honey, 3MH-P30 and 2MH-P30, and the P40 control have an impact in the viable bacteria population.

Moreover, only hydrogels with honey appear to have a more pronounced inhibitory and bactericidal effect on *E. coli* at 24h (Figure 3.9C). Regarding P40, contrary to the gram-positive results, the patch does not appear to stress the bacteria.

Finally, for *P. aeruginosa* (Figure 3.9D), the results are not consistent amongst the tests. Even though at 6h in the CFU count, it appears that the patches with honey provoke a significant bactericidal effect, this seems to disappear at 24h of incubation time. Thus, it is assumed that the composition of the patches does not influence *P. aeruginosa.*

Overall, the honey incorporated patches seem to have a negative effect on microbial growth and viability on both gram-positive bacteria and on *E. coli*. Surprisingly, comparing the different honey concentrations incorporated, overall, no differences were observed, the outcomes being very similar for both conditions. It was expected a higher antibacterial effect for the bacterial suspensions incubated with 3MH-P30 than with 2MH-P30, due to honey content decreasing from 40% to ~27%, however, this was not seen. Furthermore, P40 also appears to impact the gram-positive bacteria's normal growth. This can be due to a slower adaptation of the cells to the medium, caused by a higher saturation due to the added excipients, instead of an antibacterial effect. However, none of the 3D patches seem to present an inhibitory effect on *P. aeruginosa*. It is possible that the used MH concentrations in the patches are too low, since the highest concentration used 40% w/v is very close to the MIC obtained (35.5% w/v) and no significantly differences were observed.

It has been previously reported that MH has a higher antibacterial activity against gram-positive bacteria than gram-negative bacteria, which correlates to the present results [87]. Gram-negative bacteria have a 3-layered cell-envelope, comprising a thin peptidoglycan layer arranged between an outer membrane and inner bi-lipid membrane. This membrane arrangement offers additional protection from lysozyme and other agents, like antibiotics and other antibacterial agents [59].

Multiple studies have examined the addition of MH to hydrogel scaffolds for various tissue engineering applications including wound healing and have proved their efficacy against a panoply of bacteria associated with wound healing impairment [62,82,88]. However, not many studies to date have been performed regarding gelatine-based hydrogels with MH incorporated. El-Malek et al. were able to incorporate 20% (v/v), approx. 28.5% (w/v), MH into a chitosan-gelatine hydrogel (40% v/v of each component), resulting in antibacterial properties to several bacterial species such as *S. aureus*, *P.*

aeruginosa, among others. This MH concentration is slightly higher than the used in the 2MH-P30 patch and it presented antibacterial properties against *S. aureus,* like the results present here, and *P. aeruginosa*, contrary to the results for 2MH-P30. However, it is important to note that the hydrogel is also composed of chitosan, which in addition has antibacterial properties. Thus, the antibacterial effect of MH and chitosan combined can be causing the antibacterial effect specially in *P. aeruginosa* and explain the differences in the results [62]. This same synergistic effect between chitosan and MH was observed by Sasikala et al. that stated that incorporating 8% w/v manuka honey into chitosan hydrogel films increased the inhibition of *S. aureus* and *E. coli* growth [88].

By increasing the search to cryogels, a hydrogel fabricated at sub-zero temperatures, the results expanded. A previous work aimed to produce polyvinyl alcohol cryogels physically crosslinked with natural polymers, such as gelatine, infused with MH and showed that the produced cryogels were unable to provoke a growth inhibition in *S. aureus*, however, higher percentages than 25% MH were reported, for it to be effective and inhibit growth [89].

Hence, the used concentrations in this work, 40% and ~27% w/v, when compared to previous works, show that it is possible to incorporated high concentrations of MH and provide the required antibacterial activity. It is also interesting to note that a concentration of 27 % w/v of MH in the 3D patch also has antibacterial effect on the bacterial strains selected, except for *P. aeruginosa*. This value is much lower than the obtained MICs and MBCs. This can indicate that the incorporation of lower MH concentrations than the MIC and MBC in a scaffold, and not its use by itself, can create a synergistic antibacterial environment and allow sub-inhibitory concentrations to be bacteriostatic and bactericidal.

Lastly, the agar diffusion method assay was performed to see if the samples could provoke bacteria inhibition and death, in a different environment (Figure 3.10).

It can be observed in Figure 3.10 that only the patches containing honey showed bacterial inhibition in the agar plate. The behaviour correlates to the antibacterial assay, where the gram-positive bacteria seem to be more susceptible to MH than gram-negative, as observed in Figure 3.9.

3MH-P30 patches provoked a wide full clearance in gram-positive bacteria and partial clearance in *E. coli*. After 24h of incubation, *S. epidermidis* showed the highest susceptibility to honey, with a bacterial clearance radius of 20 mm. For *S. aureus*, the inhibition was lower (17 mm) than for *S. epidermidis*, but full clearance was still attained. For *E. coli* only partial clearance was reached (29±2 mm).

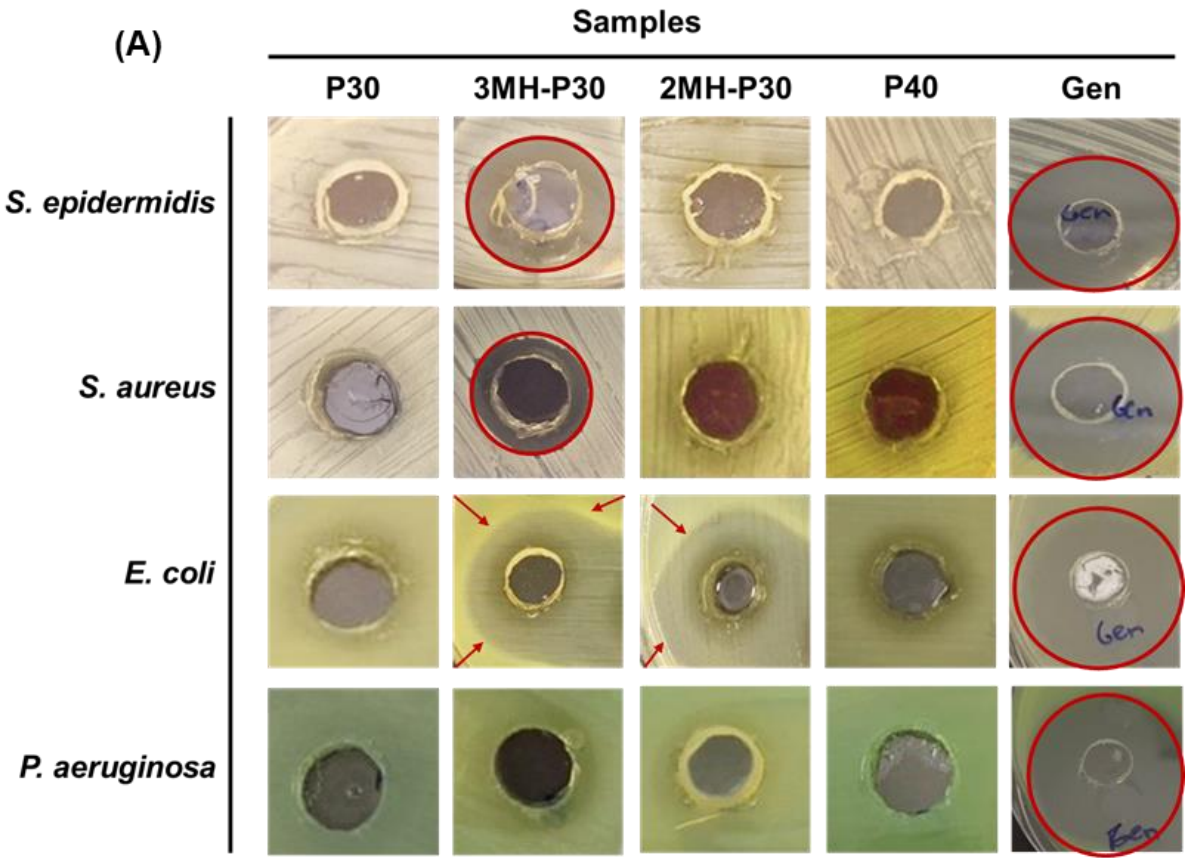

(B)

Bacterial Strain	Studied Samples (mm)				
	P30	3MH-P30	2MH-P30	P40	Gen
S. epidermidis	Ø	20	Ø	Ø	30
S. aureus	Ø	17	Ø	Ø	30
E. coli	Ø	29±2*	29±2*	Ø	27
P. aeruginosa	Ø	Ø	Ø	Ø	35

Figure 3.10 - Agar diffusion test performed with the patches. The patches were placed on plates of *S. epidermidis*, *S. aureus*, *E. coli* and *P. aeruginosa* for 24 h to measure partial and full clearance. Partial clearance is noted with red arrows while full clearance is circled in red (A). Measurement of full and partial (*) bacterial clearance by the 3D patches and gentamicin (B). Gentamicin was used as positive controls (Gen). Note that diffusion attributed to the water content of the 3D patches is not marked.

2MH-P30 patches only provoked partial clearance to *E. coli* (29±2 mm) and no inhibition was seen for the gram-positive bacteria, contrary to what was expected from the previous antibacterial activity results (Figure 3.9). As previously demonstrated, no effect was seen in *P. aeruginosa*. As expected, gentamicin control showed the highest inhibition with a full clearance radius (30 mm).

When compared to gentamicin inhibition, it is interesting to note that 3MH-P30 hydrogel can provide around 67% and 57% complete inhibition to *S. epidermidis* and *S. aureus*, respectively. In the wound

healing problematic, a very important point of discussion is the appearance of antibiotic-resistant strains, due to prolonged antibiotic used. However, no MH-resistant strains have been discovered, thus being a good antibacterial agent to be incorporated in wound dressing [59].

These obtained results also reinforce that it is possible to successfully incorporate MH, whilst maintaining its desired properties and that the concentration of MH incorporated can affect the patches' antibacterial effect.

3.3.2. Cell proliferation/cytotoxicity assay

The 3D patches have the main goal of being antibacterial agents, however, it is also important that they do not affect the viability of the cells, during wound healing. For that reason, human dermal fibroblasts (HDF) and human epidermal keratinocytes (HEK), were selected since they play a significant role in the re-epithelialization process during wound healing. A visual optical observation of these cells *in vitro* can be seen in Figure 3.11.

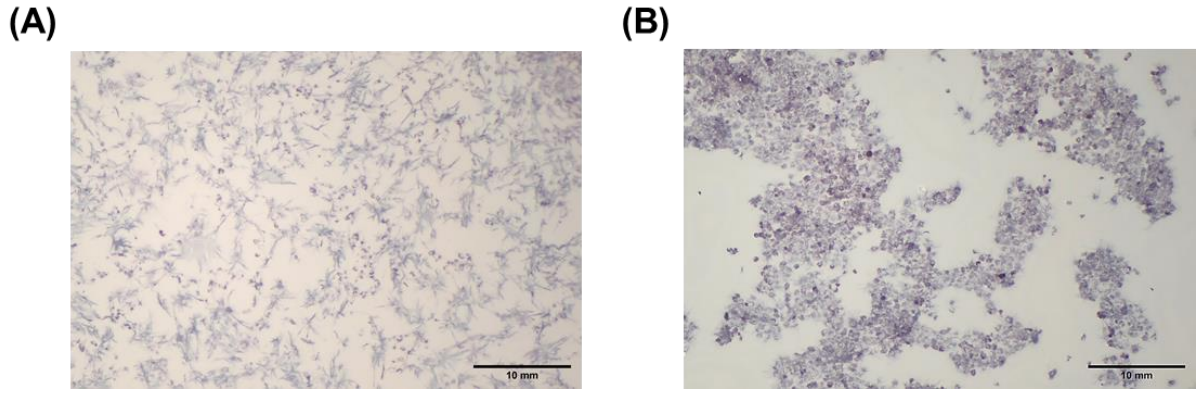

Figure 3.11 - Microscopic observation of human dermal fibroblasts (A) and human epidermal keratinocytes (B) stained with MTT solution at 40x magnification. Scale bar represents 10 mm.

Thus, a cytotoxicity assay was performed, to see the impact of the patches' composition in the 2 cell lines and a detailed microscopic observation of the results for each condition, stained with MTT (Figure 3.12A) and viability results (Figure 3.12B) are exposed in Figure 3.12.

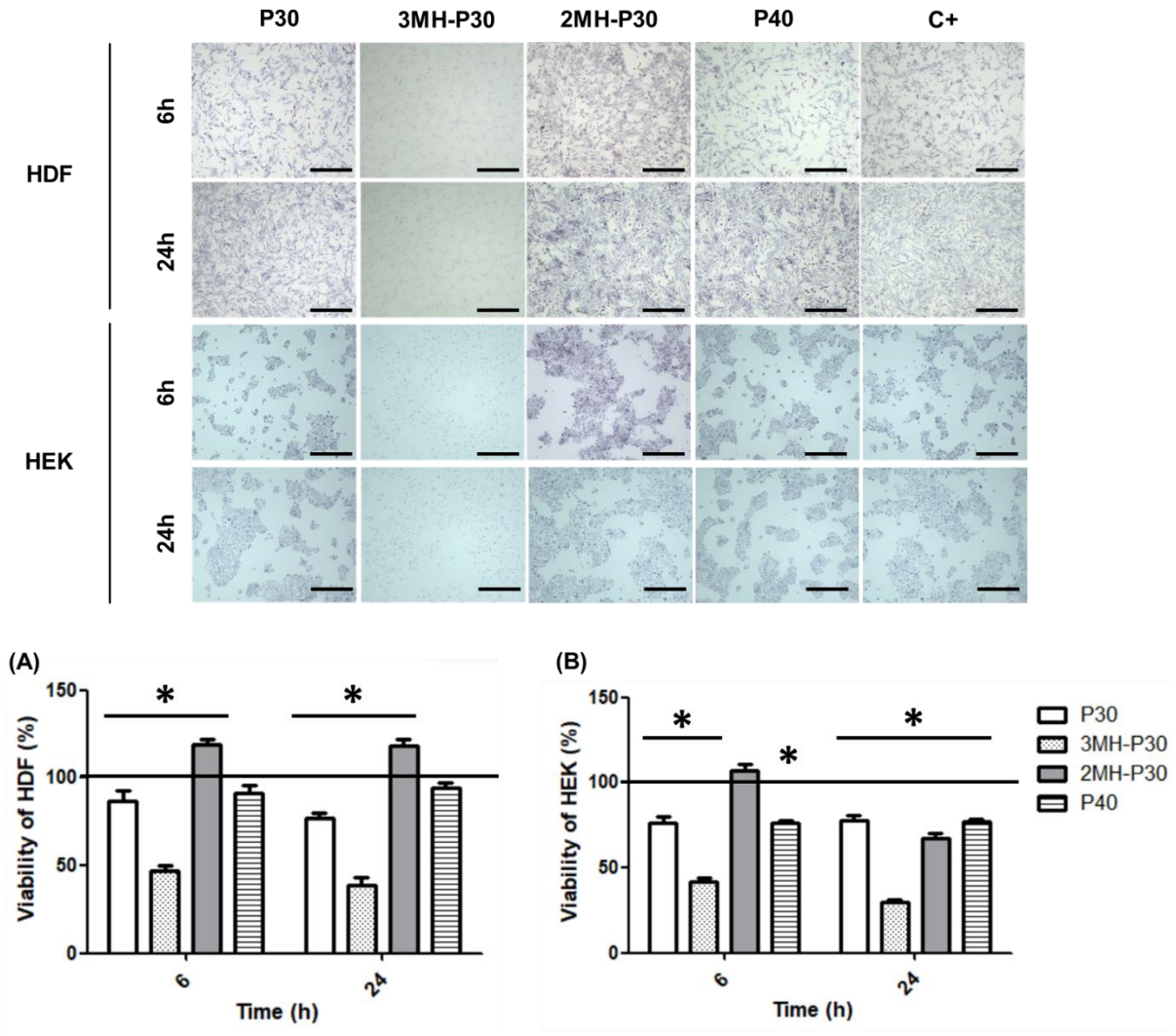

Figure 3.12 - MTT cytotoxicity assay with the patches' leachates. Detailed microscopic observation of each condition, stained with MTT solution and its comparison to the positive control, C^+, with cells grown in normal conditions (A). Viability results - solid line corresponds to the growth of the positive control, C^+, where the cells were incubated under normal conditions; results for human dermal fibroblasts (B1) and human epidermal keratinocytes (B2) are shown. * - Results significantly different from the control (C+) in normal growth medium conditions, at the same time point. Scale bar represents 10 mm.

A detailed appearance at the cytotoxic results for HDF, shows that cells proliferated steadily over the culture time, except for the cells cultured with 3MH-P30 extract, as is visually shown in Figure 3.12A. This patch's composition appears to provoke a reduction in cell viability of approx. 50% in HDF, in both time points. The composition of the 2MH-P30 patch revealed to be the most favourable of all. It even seems to be able to induce cell growth and proliferation of about more 20%, compared to the positive control. The viability reduction observed with the 3-layered patch is no longer seen.

This means that a reduction in honey concentration, leads to a suitable environment for proliferation, or regeneration, in the wound context, and the viability of the cells is not compromised. The remaining extracts, P30 and P40, presented a viability of >77% and >91%, respectively, throughout the whole essay.

In HEK, similar results to HDF can be perceived. Cells proliferated increasingly over the culture time, except for the cells cultured with 3MH-P30 extract, as is visually shown in Figure 3.12A. A reduction of more than 50% in cell viability is also detected, like in HDF. At 6h, the 2MH-P30 extract seems to have the same effect as in the HDF (increase in ~8% viability compared to the control), it seems to create a suitable environment for cell proliferation, possibly meaning regeneration in a wound setting. However, at 24h after incubation this is no longer observed, attaining a viability of ~70%. For P30 and P40 hydrogels' extracts, a viability higher than 76% was attained throughout the essay time.

According to the norm ISO 10993-5:2009, that describes methods to assess the *in vitro* cytotoxicity of medical devices, if viability is reduced to <70% of the positive control, it has a cytotoxic potential [90]. All the hydrogels appear to not provoke a cytotoxic effect in both cell lines, except for the 3MH-P30. The composition of the patch caused the viability of the cells to be reduced to less than 50%. The remaining patches composition can be categorised as non-cytotoxic.

Previous studies have shown that concentrations of MH, as low as 5%, can be cytotoxic *in vitro*. This is hypothesized to be due to the acidic pH of MH and the closed-off environment, leading to a osmolarity deregulation of the medium [85]. In the 3MH-P30 *in vitro* environment this could be happening.

The cytotoxicity of MH in HDF and HEK has been previously described. A study by Elia Ranzato et al. detailed that effective concentrations of 2.07% and 4.74% v/v in HEK produced a cytotoxic effect in 5% (EC_{05}) and 50% (EC_{50}) of the population, respectively [91]. In another study, the same test was performed in HDF and effective concentrations of EC_{05}= ~0.35% v/v and EC_{50} = ~2.18% v/v were obtained [92].

When compared to our results, a cytotoxic effect of ≥ EC_{50} is attained with a concentration of 40%, a much higher concentration. However, it is important to note that the previous exposed results were obtained with the incubation of pure MH. This indicates that within the created patch, high concentrations of MH can be incorporated without creating a toxic effect in the cells. This was also corroborated by the 2MH-P30 patch results. The other patch's components, when honey is incorporated can be lowering the cytotoxic effect on the cells, thus allowing a higher MH incorporation without compromising cell viability.

Another comparison was performed, where the assessment of the irritation potential of the patches' composition *in vitro* was made. The prediction model to assess chemical hazard based on 431 OECD test guidelines uses a viability threshold to classify a substance. A substance is classified as "irritating" or "category 2" when the average viability after skin irritation test obtained using the MTT assay was below 50%. A substance was classified "non-irritating" or "no-category" when the mean viability was above 50% [93]. Similarly, to the previous test, only 3MH-P30 appears to be irritating. The remaining scaffolds composition can be labelled as non-irritating.

The results were also confirmed via immunofluorescence staining. Figure 3.13 shows the results of the Immunofluorescence assay for HDF and Figure 3.14 for HEK, at 24h after incubation with the extracts.

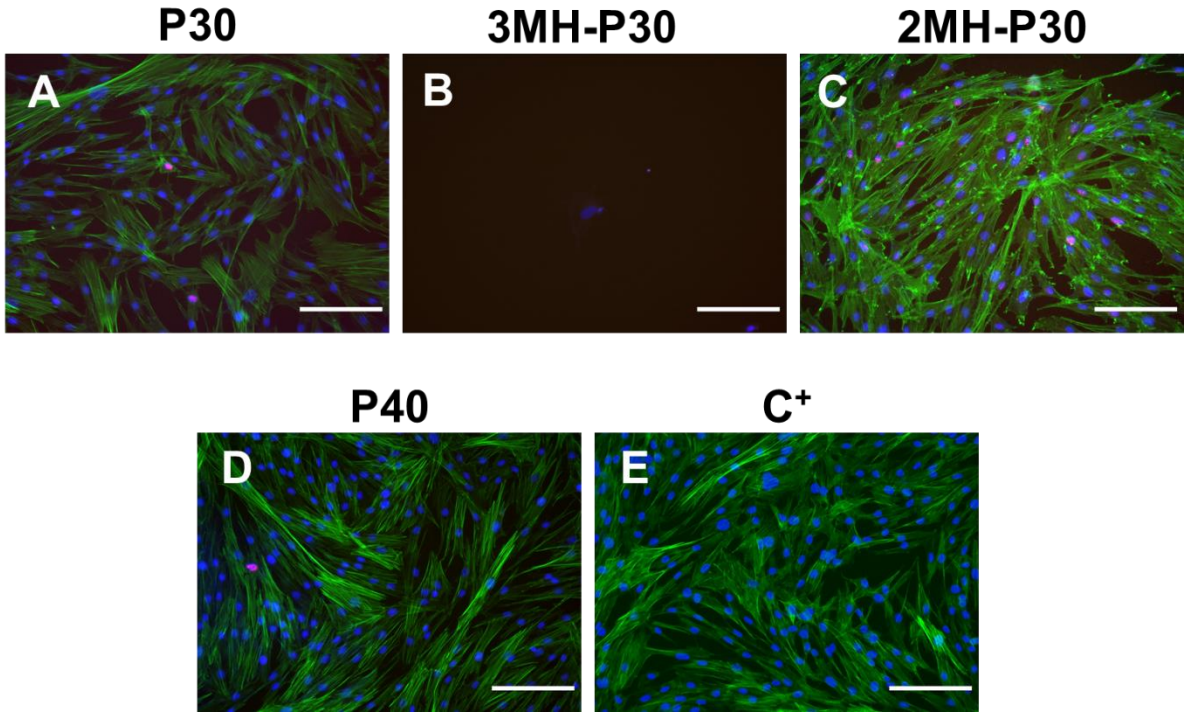

Figure 3.13 - F-actin (green) and nuclei (blue) staining of HDF. Staining of the specific cell marker Ki67 (red) was also performed. Pictures were acquired by fluorescence microscopy; scale bar represents 5 µm.

Cultures of HDF, are accordant with the previous cytotoxic assay, where 3MH-P30 patch appears to be cytotoxic to the cells (Figure 3.13B) and the other samples allow a normal growth (Figure 3.13A, C-E). No Ki67 or actin staining are observed, and cellular nuclei staining is very sparse when the cells are incubated with the 3MH-P30 patch (Figure 3.13B). The F-actin cytoskeleton is a critical cell structure crucial not only in cellular functions (division, gene expression, intracellular transport and signalling pathways) but also in motility and differentiation mechanisms. Due to its importance, F-actin cytoskeleton is considered an early indicator of cytotoxicity [94]. Thus, it was expected to see deleterious effects on this structure, as was confirmed (Figure 3.13B).

Considering cell morphology, HDF in the remaining conditions demonstrated flat, spindle-like, and spreading morphology (Figure 3.13A, C-E). High cellular density with elongated actin filaments between

cells and cell-to-cell contact is also seen, as well as prominent nuclei were also evident (Figure 3.13A, C-E).

A reliable and specific marker for HDF has yet to be found. Other markers for other cell lineages have been used to identify HDFs [95]. Ki67 is a nuclear protein and well-established marker of cell proliferation during wound repair. It is present in actively proliferating cells and lacking in resting cells [96]. The intranuclear staining of Ki67 marker in red can be seen in wells incubated with P30, 2MH-P30 and P40, but not in the control.

This means that the incubation with the patches allows the cells to actively proliferate. A higher Ki67 staining is also noticeable in cells incubated with 2MH-P30 extract, which correlates to the previous results, where a higher proliferation, when compared to the control was observed (Figure 3.12). Thus, for HDF, the 2MH-P30 condition appears to be the most favourable of all.

The time-dependent localization of Ki67 antigen-positive cells in human skin wounds has been previously studied. Fibroblastic cells in the wound area revealed an increased Ki67 staining in 1.5-day-old skin lesion and was found in all specimens aged between 6 days and 1.5 months. It was also observed that the number of Ki67+ fibroblasts decrease with the increased distance from the wound edge, indicating that the fibroblasts directly localized in the edges of the wounds are proliferating and contributing to wound healing [97]. Thus, it is important that the Ki67 marker is present in the incubated cells.

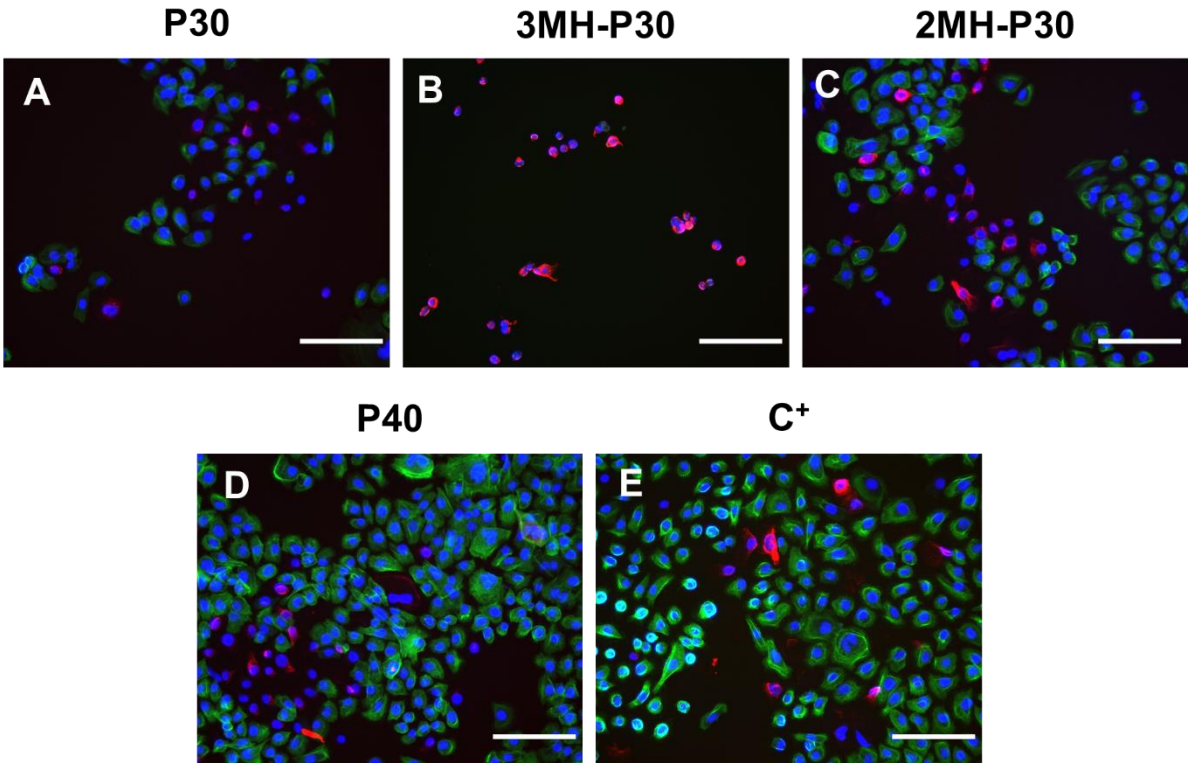

Figure 3.14 - F-actin (green) and nuclei (blue) staining of HEK. Staining of the specific cell marker CK5 (red) was also performed. Pictures were acquired by fluorescence microscopy; scale bar represents 5 µm.

Looking at the results for HEK (Figure 3.14), for every condition except 3MH-P30, the cells form colonies exhibiting the distinctive cobblestone morphology anticipated from primary keratinocytes *in vitro* [98]. Images of triple staining (cytoskeleton, CK5 and nucleus) are consistent with a healthy appearance of the exposed keratinocytes. HEK are significantly smaller cells, when compared to HDF.

As expected, 3MH-P30 shows a significant reduction in cell viability and the cells are dispersed, not forming the typical colonies. It is also interesting to note that the CK5 cytokeratin is expressed in the stained cells, however, the F-actin filaments were not fully developed nor were able to be observed. For the cells incubated with the remaining patches, a proper nuclei, F-actin, and specific cell marker can be seen. Additionally, the cells have staining of the specific cell marker, CK5, meaning their able to proliferate, under the imposed conditions.

The major proteins found in keratinocytes are cytokeratines (CK) and in a healthy epidermal layer, CK5 is expressed in mitotically active basal keratinocytes. This specific cell marker can define the differentiation status of these basal cells. A previous work that compared the histological morphology between normal skin and scar tissue as shown that in scarring epidermis, there were more proliferative keratinocytes present, marked with CK5 [99]. Thus, this means that the hydrogels composition allows a good keratinocyte proliferation, very important during wound healing.

3.3.3. Scratch wound healing Assay

The wound scratch assay was performed to analyse cell migration *in vitro* (Figure 3.15). Since 3MH-P30 patch was deleterious to the cell growth and proliferation, the following test was not performed for this patch. Figure 3.15(A) shows microscopical images of the increase in keratinocyte and fibroblast migration in response to the addition of the patches, after 16 hours (over-night) and 24h. Figure 3.15(B) presents a quantitative measurement of wound closure, during the essay.

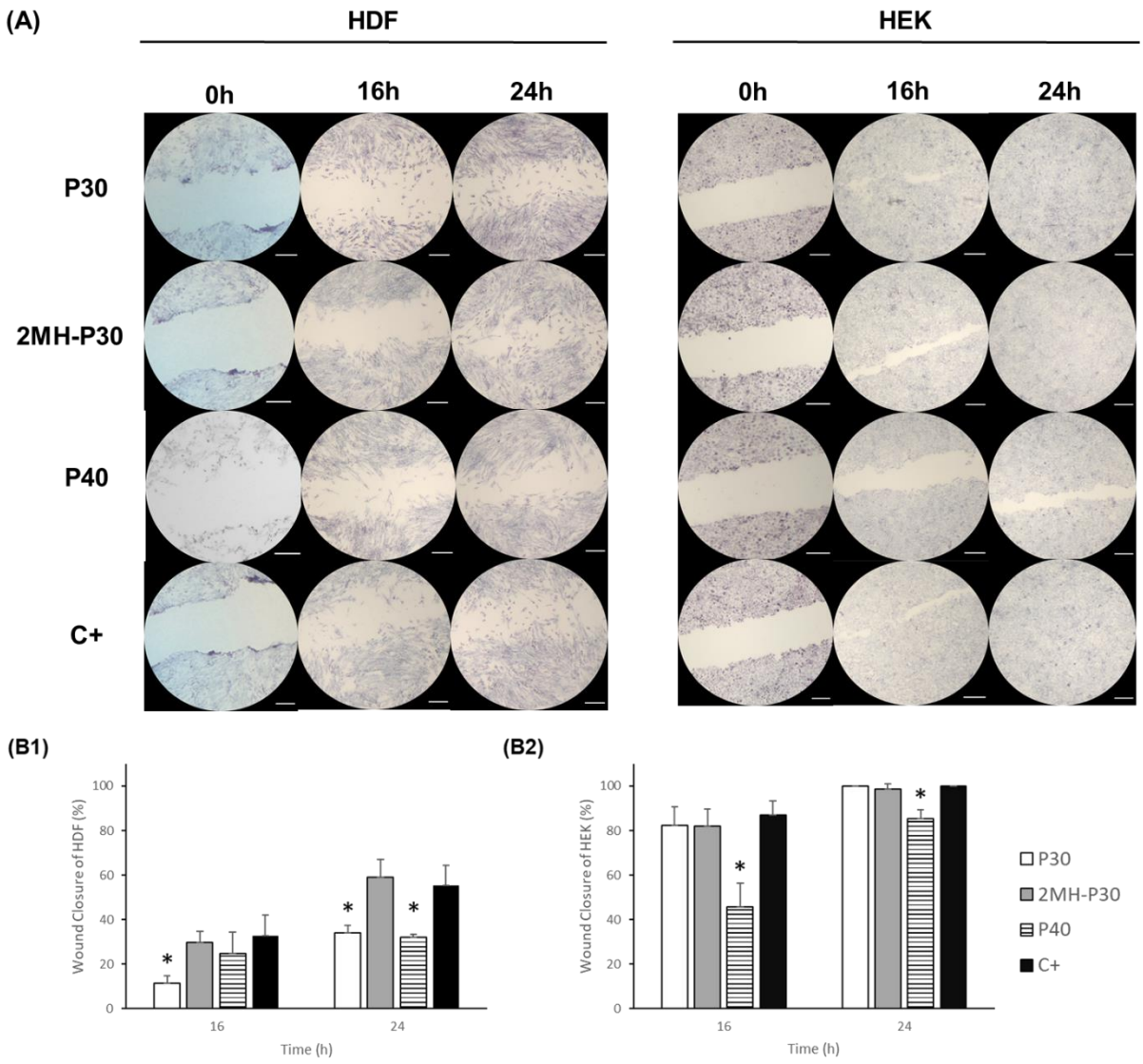

Figure 3.15 - Wound scratch assay *in vitro* in human dermal fibroblasts (HDF) and human epidermal keratinocytes (HEK). Visual representation of the results, where cells were stained with MTT solution. Scale bar represents 5 mm (A); The wound closure was observed and measured at 16h (over-night) and after 24h for HDF (B1) and HEK (B2). * - Significantly different from the positive control (C^+) in normal growth medium, at the same time-point.

It appears that HDF cells have a much slower migration, compared to HEK cells (Figure 3.15A). None of the conditions was able to fully close the wound, during the assay time, as observed in Figure 3.15A. In its normal growth and migration conditions, the wound closure was only ~40% after 16h (C^+). In this essay 2MH-P30 and P40 hydrogels composition seem to allow similar migration rate and wound closure, when compared to the control growth conditions, C^+. At 24h, the cells' migration is also significantly lower than the observed migration in HEK, where only ~60% migration was observed under normal control growth conditions (C^+). However, 2MH-P30 patches' composition permits a similar migration rate and wound closure, when compared to the control, maintaining the same behaviour seen at 16h. Nonetheless, the P40 sample did not maintain its behaviour, showing a delay of ~20%, when compared

to the control. The cells incubated with the P30 patch, always showed a delayed migration of >20%, when compared to the control, throughout the essay.

The cell migration assay revealed that migration of HEKs is very fast, having a coverage of ~87% of the wound after 16h, in normal conditions (C^+). Particularly, the P30 and 2MH-P30 patches composition, seem to provide a similar environment to its normal migration conditions. This means both the used components in the hydrogel base and the introduced honey concentration are not deleterious to the cells and its migration and proliferation abilities. P40 seem to have a delayed cell migration of about 40%, when compared to the normal culture conditions. This could be due to the cells adaptation of the new materials present in the growth medium. After 24h, the wound scratch was fully closed in normal conditions (100%). The behaviour was maintained from 16h, where P30 and 2MH-P30 showed similar cell migration to the control and P40 showed a migration delay (~15%).

Comparing all the results, the assays showed significant variability between patches and between cell lines. However, the 2MH-P30 patch was the only one who maintained the same behaviour between cell lines and was able to provide a similar environment to the control, in every setting.

A study performed by Elia Ranzato et al., where 0.1% v/v MH was directly incubated into the wells after an *in vitro* scratch, has shown that MH improved fibroblast wound repair capabilities and cell motility, after 24h [92]. Even though in this work there was no significant improvement of cell mobility when the cells were incubated with the patches with MH, the patches' composition allowed a similar mobility to the normal conditions and did not reduce cell migration. On the other hand, a different study by Sell et al. showed in an *in vitro* scratch test using HDFs that the results were not impacted by the presence of 1% v/v MH [100], a higher percentage than the previously described research. This goes accordingly to what was obtained in this work, but with lower percentages of MH. It is important to note that different honeys were used in these assays, as well as different concentrations of MH and the test was conducted in different conditions. Moreover, these tests have not been performed for high percentages of MH.

The work presented by Simona Martinotti et al. discovered that the addition of 0.1% and 0.5% pure MH increased the wound closure rate in HEK in ~2.0% and almost 2.5%, respectively, when compared to the used control. These results are not concordant with the here presented since no increased wound closure rate was observed [101]. Another study also investigated the migration of HEK in the presence and absence of 0.1 % MH in several honeys, including MH. Cells exposed to MH also showed significantly higher wound closure rate at 24 hours, almost the double, with respect to controls [91]. However, at 24 hours in the described studies, none of the conditions nor the controls had a full wound closure. The variation of the essay conditions and the use of pure MH instead of incorporated in a patch, could be the cause of these differences, since here at 24 hours the 2MH-P30 patch was able to mimic the control and allow a full wound closure.

When incorporated in a gelatine patch, no previous scratch wound healing tests were discovered. However, the incorporation of MH into other types of patches for wound healing have been described. As an example, the incorporation of 2.5% MH into a methylcellulose foam caused a faster cell migration

in human keratinocyte-like HaCaT cells, when compared to normal conditions [60]. Another study incorporated from 1-10% w/w MH in an alginate-methylcellulose ink and were obtained the same described increasing cell migration in HDF, when compared to the control. The highest cell migration was achieved when 10% MH was incorporated, achieving full closure after only 24h.

Although it was not possible to observe a higher cell migration with the incorporation of MH, as it has been previously described by other authors, it was possible to incorporate a much higher MH concentration than the described in the literature, without impairing cell viability. Moreover, the developed gelatine patch with MH allowed a similar migration to normal conditions.

3.3.4. Antioxidant Activity Assay

As previously mentioned, an excessive amount of reactive oxygen species (ROS) can be deleterious to the cells. Therefore, studying the antioxidant activity of the hydrogels is of extreme importance and the results of the relative fluorescence obtained are presented in Figure 3.16.

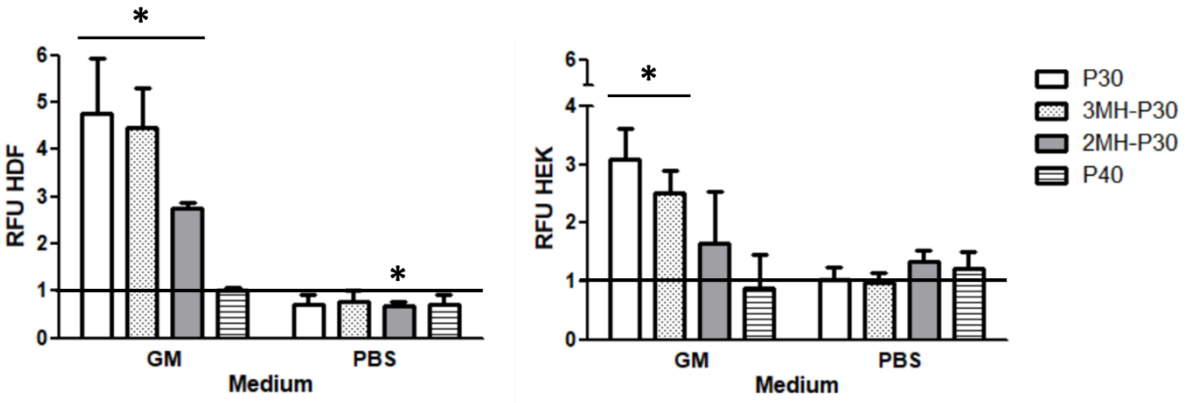

Figure 3.16 - Antioxidant activity of the 3D patches in human dermal fibroblasts (A) and human epidermal keratinocytes (B). The assay was performed under 2 conditions: by incubating the cells with the samples dissolved in growth medium (GM) and PBS (PBS). The results are shown as relative fluorescence units and the solid line dictates the value obtained for ascorbic acid (AA), the positive control, and corresponds to RFU=1. * - Significantly different from the positive control (AA) in normal growth medium, at the same time-point.

Since the growth media have ascorbic acid (AA) present in their composition, and since it is the used positive control in this essay, the same conditions were also tested with the extracts being made in PBS.

When the extracts were prepared in PBS, the results are very uniform, for HDF and HEK, all the samples do not vary significantly in RFU, when compared to ascorbic acid (AA), the positive control used. In HDF the 2MH-P30 patch even seems to provide a slightly higher protection against ROS provoked by the addition of H_2O_2 than AA.

However, in the assay where the extracts were prepared in culture medium, more differences between samples and the control can be seen. First, for HDF, the sample that has more gelatine, P40, seem to

have a higher antioxidant activity and similar to AA. It also provides a higher protection against ROS formation when in comparison with the P30, 3MH-P30 and 2MH-P30. The reduction in honey amount, from 3MH-P30 to 2MH-P30, increases the protection provided by the patches against ROS, thus the latter has a higher antioxidant activity.

For HEK, 2MH-P30 and P40 patches have similar behaviour as the positive control, when incubated in growth medium. The increase in antioxidant activity observed by increasing honey concentration in HDF is no longer observed for HEK, since the results for 3MH-P30 and 2MH-P30 are not statistically different.

The results seem to suggest that the culture medium has an impact in the results, which is plausible since the media themselves have ascorbic acid present (the RFU value was similar to AA), which could be interfering with the results. However, more differences were expected to be observed in the PBS essay, since the interference of AA was not present. Additionally, it would be expected that a higher honey concentration in the patch would provide a higher antioxidant activity to the hydrogel. But the opposite was observed for HDF. This can be explained by the previous cytotoxicity observed in HDF when incubated with 3MH-P30 extracts, also inducing a higher production of ROS by the cells.

MH has a potent capacity to reduce free radicals and it has been previously used in different studies as standard to evaluate the antioxidant capacity of different kinds of honey [58]. MH is viewed as a standard for antioxidant activity due to having one of the highest phenolic contents compared to other honeys [102]. A previous study explored the exposition of HDF to a different oxidative stress, the stressor 2,2'-szobis(2-amidinopropane) dihydrochloride (AAPH). This inductor of the oxidative damage caused lower cell vitality, higher apoptotic and dead cell numbers, intracellular ROS production, among others; all of them indicators of oxidative damage. A pre-treatment of the cells with MH showed significantly lower intracellular ROS levels both compared to control cells and when compared to AAPH-stressed cells [103].

It is also necessary to note that gelatine-based patches blended with other polymers have been developed and used as base for the incorporation of other antioxidant agents. The produced patches demonstrated to be effective against ROS species, while preserving cell viability [104]. However, the antioxidant activity of MH incorporated gelatine hydrogels was not found to be previously studied. Thus, from the present results a strong possible antioxidant activity was possible to be attained with the produced patches.

3.3.5. Irritability and Angiogenesis Tests

For the final portion of this work *in vivo* essays were performed, to test the irritability and angiogenic potential of the patches. Representative images and semi-quantitative score values for the irritability test are shown in Figure 3.17 and the angiogenesis potential is characterized in Figure 3.18.

(A)

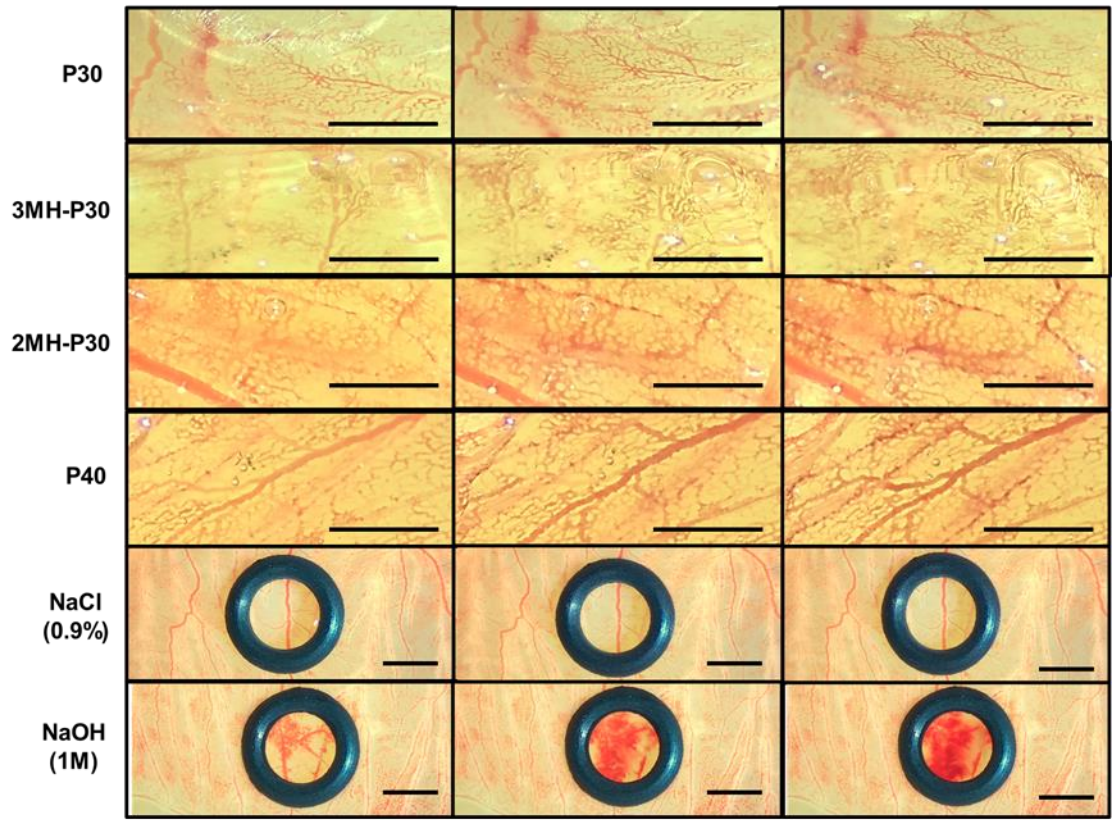

(B)

Sample	Score
P30	0
3MH-P30	0
2MH-P30	0
P40	0
NaCl (0.9%)	0
NaOH (0.5 M)	3

Figure 3.17 - *In vivo* HET-CAM irritation assay. Microscopic representation of the results, after 0.5, 2.0 and 5.0 min of patch incubation and microscopic images of the controls NaCl (0.9%) and NaOH (1M) (A). Classification table with irritation score for the *in vivo* HET-CAM assay after a 5min exposure time with the 3D patches (B). Scale bar represents 10 mm and 5 mm for the incubation with the patches and the controls, respectively.

The CAM membrane that separates the embryo from the inner airspace has no innervations and is highly vascularized. When in contact with a patch, the caused irritation can be studied. On the irritation potential assay, the patches did not induce noticeable adverse vascular alterations, and the results were similar to the negative control (treatment with NaCl, 0.9%) and substantially different of the positive control (treatment with NaOH, 0.5M).

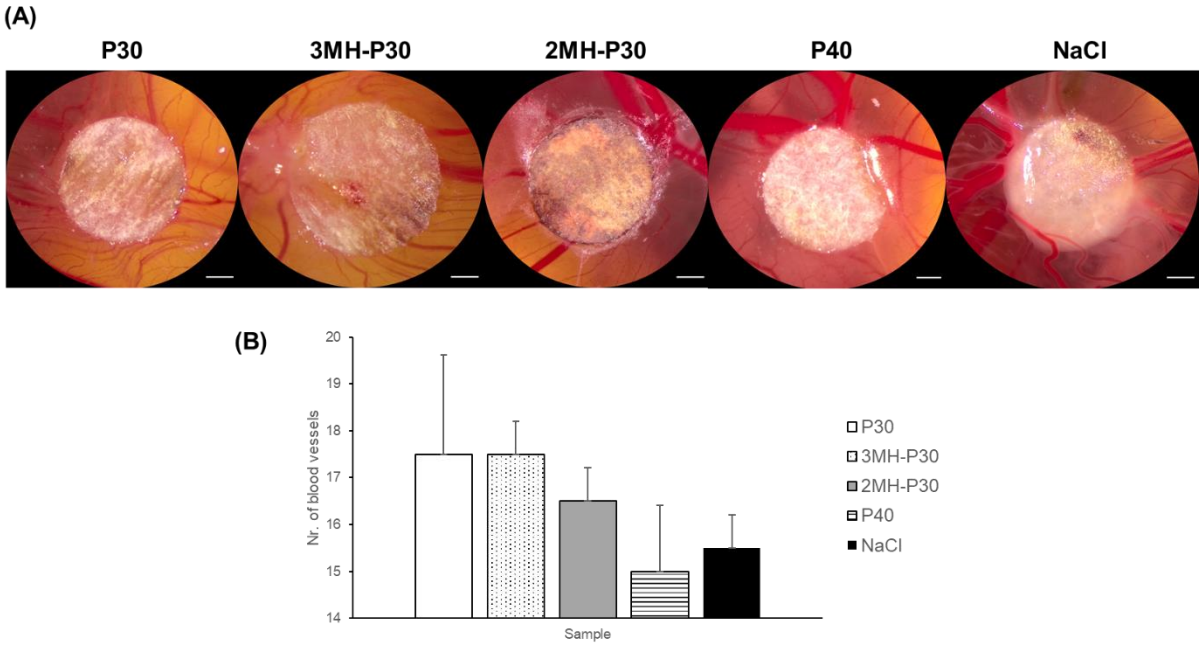

Figure 3.18 - *In vivo* HET-CAM angiogenesis essay. Angiogenic response to the embedded filter with the patches, evaluated by the CAM assay after 3 days post window creation. Microscopic images of the CAM exposed to the extracts and the negative control (0.9% NaCl), where scale bar is 2.5 mm (A). Quantitative evaluation of the number of blood vessels formed during the 3-day incubation period (B).

Concerning the angiogenesis results (Figure 3.18), the filter paper discs embedded with the patch's leachates containing MH, 3MH-P30 and 2MH-P30, appear to have a more brownish colour, probably due to its MH content. None of the patches' composition significantly affected the angiogenic response and behaved similarly after CAM maturation for 3 days, meaning they did not have a significant higher influence on the formation of new blood vessels.

Gelatine-based hydrogels alone and with the incorporation of other polymers have previously demonstrate great potential to serve as an effective delivery system and base for bioagent incorporation, to promote tissue regeneration [39,105]. As an example, the immunocompatibility and non-thrombogenicity of gelatine-based hydrogels with increasing amounts of lysine diisocyanate ethyl ester, have been investigated. The HET-CAM confirmed the patch's compatibility since no bleedings, thrombotic events, or vessel destructions were observed [39]. Another research described a glyoxal-crosslinked chitosan/gelatine hydrogel where it was possible to incorporate human platelet lysate (HPL), a biological material that can exert a positive effect on angiogenesis and provoke post-ischemic vascular modifications, amongst other. The HET-CAM essay revealed that the HPL encapsulation in the structure

was able to stimulate angiogenesis *in ovo* [106]. No previous work was encountered concerning the incorporation of MH in gelatine-based hydrogels, considering the HET-CAM essay. More specifically, no previous studies in HET-CAM essay and related to MH were met.

Even though no significant differences between patches have been observed in the HET-CAM essays, the patches can be considered non-irritable and the patches compatibility to the tissue was observed.

Chapter 4: Conclusions and Future Perspectives

4. Conclusion and Future Perspectives

4.1. Conclusion

In this work, the development of 3D printed gelatine-based hydrogels, incorporated with the bioactive agent Manuka Honey (MH) was presented for applications in wound healing and skin regeneration. The main objectives of the work have been reached: (1) the production of reproducible 3D patches with printing accuracy and high shape fidelity; (2) the successful incorporation of Manuka honey (MH) in the developed 3D patches, whilst preserving its inherent properties, meaning, the MH antibacterial and antioxidant properties, regeneration capacity and angiogenic potential.

Additionally, it can be concluded that an increase in gelatine concentration as well as the addition of MH caused an increase in inks' viscosity, which is preferable for achieving more accurate and reproducible patches. These alterations also impacted the temperature at which printing occurs, increasing from 34 ºC for P30 ink to 43 ºC for MH-P30 and P40 inks. This increase in temperature occurs to avoid nozzle clogging and premature gelation of the ink inside the cartridge. In conclusion, the properties of the developed inks were found to be suitable for extrusion-based printing.

Moreover, mostly properties such as printing temperature, viscosity and excipients concentration showed to significantly influence the printing process and quality of the 3D constructs. By controlling the experimental parameters and achieving the optimal printing conditions, the quality of the 3D printing patches was increased. As observed in this study from drop tests, higher concentration of gelatine and the incorporation of MH allowed less filament spreading, a better printing accuracy, and consequently, more reproducible, and accurate patches were obtained.

Even though microscopically, MH-P30 and P40 patches appear to have similar morphology, SEM characterization showed that MH-P30 patches had more homogeneous filaments, between layers, contrary to P40. Both MH-P30 and P40 patches presented adequate size porous and high porosity, both desirable features in hydrogels for wound healing applications.

Antimicrobial activity of the printed patches was assessed, and the results varied between the tested bacterial strains. As expected, the patches with honey incorporated caused an antibacterial effect on the gram-positive bacteria, *S. aureus* and *S. epidermidis*, and on the gram negative-bacteria *E. coli*. No effect was observed on *P. aeruginosa,* that could be caused by using a MH concentration (40%) very close to the obtained MIC and MBC for this bacterium (35.5 %). No significant differences were observed between the inhibition of 3MH-P30 and 2MH-P30. Interestingly, P40 patch also appears to cause a bacteriostatic and bactericidal effect in the gram-positive bacteria, but this was hypothesized as being due to a slower adaptation of the bacteria to the medium content. Agar diffusion assay confirmed the antimicrobial effect of MH.

Cell viability was also assessed in human dermal fibroblasts (HDF) and human epidermal keratinocytes (HEK) and the 3MH-P30 hydrogel showed to cause an inhibition of >50% in both cell lines. However,

2MH-P30 did not cause significant cytotoxicity in the cells. Moreover, it appeared to promote a higher proliferation and growth of HDF, compared to the control. It is possible to conclude, then, that the cells are sensitive to MH concentration, and that cellular tests should always be investigated, in parallel with the antimicrobial tests. Additionally, a concentration of ~27% of MH was able to be provided in the 2MH-P30 patch without causing cytotoxicity. Regarding the possibility of promotion of the regeneration capacity by MH, although it was not possible to observe a higher cell migration with the incorporation of MH, a much higher MH concentration than the described in the literature was able to be incorporated, without impairing cell viability and proliferation. Moreover, the 2MH-P30 patch allowed a similar migration to normal conditions. The results also indicate that a strong possible antioxidant activity may be attained from the produced patches.

Finally, the HET-CAM irritability and angiogenesis *in vivo* tests, showed that the developed patches did not cause irritation and were also unable to promote angiogenesis.

Thus, the main goals of this project were achieved and was possible to produce 3D printed hydrogels that demonstrate great printability and reproducible results. The added antibacterial substance, MH, showed successful results that justifies its application to improve hydrogel's effectiveness and regeneration ability.

4.2. Future Perspectives

Even though it was possible to achieve the main goals of the proposed work, there is always room for improvement. One of the most important properties that a hydrogel should have is a good swelling capacity. To achieve a better understanding about its water absorption capability, a detailed study on the swelling ratio and water content of the developed 3D patches should be performed.

Moreover, for topical applications, it is important that the produced patches are stable and do not degrade in a very fast paste. In the future, to define the degradation rate of the hydrogels seems important.

As it was previously stated, MH has a very high methylglyoxal (MGO) concentration, which has a huge impact in its antibacterial effect. However, it is known that other MH components also impact its antibacterial effect. Thus, it would be interesting to perform a detailed study on the chemical composition of the used MH and the effect of each component in the antibacterial activity.

The incorporation of other antibacterial compounds to the gelatine-based hydrogel, in addition to MH, should also be considered, to create a synergistic antibacterial effect and to enhance the patch's therapeutic properties. As an example, the addition of metal nanoparticles, such as silver, zinc, and gold, are increasingly being used in wound healing applications. Moreover, another polymer such as chitosan could also be added. Besides its antibacterial activity, it also promotes wound healing and could potentially increase the mechanical properties of the hydrogel.

5. Bibliography

[1] C. K. Sen, “Human Wounds and Its Burden: An Updated Compendium of Estimates,” *Advances in Wound Care*, vol. 8, no. 2. pp. 39–48, Feb. 2019, doi: 10.1089/wound.2019.0946.

[2] I. Matai, G. Kaur, A. Seyedsalehi, A. McClinton, and C. T. Laurencin, “Progress in 3D bioprinting technology for tissue/organ regenerative engineering,” *Biomaterials*, vol. 226, Jan. 2020, doi: 10.1016/j.biomaterials.2019.119536.

[3] M. Takeo, W. Lee and M. Ito, “Wound healing and skin regeneration,” *Cold Spring Harbor Perspectives in Medicine*, vol. 5, no. 1, 2015, doi: 10.1101/CSHPERSPECT.A023267.

[4] M. Rodrigues, N. Kosaric and C. A. Bonham, “Wound Healing: A Cellular Perspective,” *Physiological Reviews.*, vol. 99, no. 1, pp. 665–706, Jan. 2019, doi: 10.1152/PHYSREV.00067.2017.

[5] A. Smandri, A. Nordin, N. M. Hwei, K. Y. Chin, I. Abd Aziz, and M. B. Fauzi, “Natural 3D-printed bioinks for skin regeneration and wound healing: A systematic review,” *Polymers (Basel).*, vol. 12, no. 8, Aug. 2020, doi: 10.3390/polym12081782.

[6] B. D. Pence and J. A. Woods, “Exercise, Obesity, and Cutaneous Wound Healing: Evidence from Rodent and Human Studies,” *Advances in Wound Care*, vol. 3, no. 1, pp. 71–79, Jan. 2014, doi: 10.1089/wound.2012.0377.

[7] D. Simões, S. P. Miguel, M. P. Ribeiro, P. Coutinho, A. G. Mendonça, and I. J. Correia, “Recent advances on antimicrobial wound dressing: A review,” *European Journal of Pharmaceutics and Biopharmaceutics*, vol. 127. Elsevier B.V., pp. 130–141, Jun. 2018, doi: 10.1016/j.ejpb.2018.02.022.

[8] S. Xiong et al., “A Gelatin-sulfonated Silk Composite Scaffold based on 3D Printing Technology Enhances Skin Regeneration by Stimulating Epidermal Growth and Dermal Neovascularization,” Scientific Reports., vol. 7, no. 1, Dec. 2017, doi: 10.1038/s41598-017-04149-y.

[9] R. F. Pereira, “Bioprinting of cell-responsive bioinks for skin tissue engineering,” *ICBAS - Instituto de Ciências Biomédicas Abel Salazar*, Porto, 2018.

[10] P. A. J. Kolarsick, M. A. Kolarsick, and C. Goodwin, “Anatomy and Physiology of the Skin,” *Journal of Dermatology Nurses Association*, vol. 3, no. 4, pp. 203–213, Jul. 2011, doi: 10.1097/JDN.0B013E3182274A98.

[11] A. Dr Yung, “The structure of normal skin | DermNet NZ,” 2007. https://dermnetnz.org/topics/the-structure-of-normal-skin (accessed Nov. 11, 2021).

[12] P. Beldon, “Basic science of wound healing,” *Surgery*, vol. 28, no. 9, pp. 409–412, Sep. 2010, doi: 10.1016/j.mpsur.2010.05.007.

[13] S. Pourshahrestani, E. Zeimaran, N. A. Kadri, N. Mutlu, and A. R. Boccaccini, “Polymeric Hydrogel Systems as Emerging Biomaterial Platforms to Enable Hemostasis and Wound Healing,” *Advanced Healthcare Materials*, vol. 9, no. 20, Oct. 2020, doi: 10.1002/adhm.202000905.

[14] J. M. Reinke and H. Sorg, “Wound repair and regeneration,” *European Surgical Research*, vol. 49, no. 1, pp. 35–43, Aug. 2012, doi: 10.1159/000339613.

[15] Q. Bai et al., “Potential applications of nanomaterials and technology for diabetic wound healing,” *International Journal of Nanomedicine*, vol. 15, pp. 9717–9743, Dec. 2020, doi: 10.2147/IJN.S276001.

[16] S. Wu et al., “Evaluation of gelatin-hyaluronic acid composite hydrogels for accelerating wound healing,” *Journal of Biomaterials Applications*, vol. 31, no. 10, pp. 1380–1390, May 2017, doi: 10.1177/0885328217702526.

[17] J. Juráňová, J. Franková, and J. Ulrichová, “The role of keratinocytes in inflammation,” *Journal Appl. Biomed.*, vol. 15, no. 3, pp. 169–179, Jul. 2017, doi: 10.1016/J.JAB.2017.05.003.

[18] A. M. Wojtowicz, S. Oliveira, M. W. Carlson, A. Zawadzka, C. F. Rousseau, and D. Baksh, “The importance of both fibroblasts and keratinocytes in a bilayered living cellular construct used in wound healing,” *Wound Repair Regen.*, vol. 22, no. 2, p. 246, 2014, doi: 10.1111/WRR.12154.

[19] C. M. Desmet, V. Préat, and B. Gallez, “Nanomedicines and gene therapy for the delivery of growth factors to improve perfusion and oxygenation in wound healing,” *Advanced Drug Delivery Reviews*, vol. 129. Elsevier B.V., pp. 262–284, Apr. 2018, doi: 10.1016/j.addr.2018.02.001.

[20] R. Edwards and K. Harding, “Bacteria and wound healing,” *Current Opinion Infectious Diseases*, vol. 17, no. 2, pp. 91–96, Apr. 2004, doi: 10.1097/00001432-200404000-00004.

[21] S. Guo and L. A. DiPietro, “Factors Affecting Wound Healing,” *Journal of Dental Research*, vol. 89, no. 3, pp. 219-29., Mar. 2019, doi: 10.1177/0022034509359125.

[22] J. L. P. Gemeinder et al., “Gentamicin encapsulated within a biopolymer for the treatment of *Staphylococcus aureus* and *Escherichia coli* infected skin ulcers,” *Journal of Biomaterials Science, Polymer Edition,* , vol. 32, no. 1, pp. 93–111, 2020, doi: 10.1080/09205063.2020.1817667.

[23] M. Pérez et al., “Comparison of Antibacterial Activity and Wound Healing in a Superficial Abrasion Mouse Model of *Staphylococcus aureus* Skin Infection Using Photodynamic Therapy Based on Methylene Blue or Mupirocin or Both,” *Frontiers in Medicine.*, vol. 0, p. 731, May 2021, doi: 10.3389/FMED.2021.673408.

[24] J. S. Ong et al., “*Lactobacillus plantarum* USM8613 Aids in Wound Healing and Suppresses *Staphylococcus aureus* Infection at Wound Sites,” *Probiotics Antimicrobial Proteins 2019 121*, vol. 12, no. 1, pp. 125–137, Jan. 2019, doi: 10.1007/S12602-018-9505-9.

[25] Liu, Michael et al. “Antibiotic-specific differences in the response of Staphylococcus aureus to treatment with antimicrobials combined with manuka honey.” *Frontiers in microbiology*, vol. 5, p. 779, Jan. 2015, doi:10.3389/fmicb.2014.00779

[26] K. Hayashi, A. Fukushima, M. Hayashi-Nishino, and K. Nishino, “Effect of methylglyoxal on multidrug-resistant *Pseudomonas aeruginosa*,” *Frontiers in Microbiology*, vol. 5, Apr. 2014, doi: 10.3389/FMICB.2014.00180.

[27] A. F. Henriques, R. E. Jenkins, N. F. Burton, and R. A. Cooper, “The effect of manuka honey on the structure of *Pseudomonas aeruginosa*,” *European Journal of Clinical Microbiology & Infectious Diseases, 2010 302*, vol. 30, no. 2, pp. 167–171, Oct. 2010, doi: 10.1007/S10096-010-1065-1.

[28] J. Lu et al., “Honey can inhibit and eliminate biofilms produced by *Pseudomonas aeruginosa*,” *Science Reports 2019 91*, vol. 9, no. 1, pp. 1–13, Dec. 2019, doi: 10.1038/s41598-019-54576-2.

[29] N. S. Alharbi et al., “Prevalence of *Escherichia coli* strains resistance to antibiotics in wound infections and raw milk,” *Saudi Journal of Biological Sciences*, vol. 26, no. 7, pp. 1557–1562, Nov. 2019, doi: 10.1016/J.SJBS.2018.11.016.

[30] M. Otto. “*Staphylococcus epidermidis* – the 'accidental' pathogen.” *Nature reviews. Microbiology,* vol. 7, no. 8, pp. 555-67, Aug. 2009, doi:10.1038/nrmicro2182.

[31] M. S. Brescó et al., “Pathogenic Mechanisms and Host Interactions in *Staphylococcus epidermidis* Device-Related Infection,” *Frontiers in Microbiology*, vol. 8, no. AUG, p. 1401, Aug. 2017, doi: 10.3389/FMICB.2017.01401.

[32] E. A. Kamoun, E. R. S. Kenawy, and X. Chen, “A review on polymeric hydrogel membranes for wound dressing applications: PVA-based hydrogel dressings,” *Journal of Advanced Research*, vol. 8, no. 3, pp. 217–233, May 2017, doi: 10.1016/J.JARE.2017.01.005.

[33] H. Liu et al., “A functional chitosan-based hydrogel as a wound dressing and drug delivery system in the treatment of wound healing,” *RSC Adv.*, vol. 8, no. 14, pp. 7533–7549, Feb. 2018, doi: 10.1039/C7RA13510F.

[34] S. Tavakoli and A. S. Klar, “Advanced hydrogels as wound dressings,” *Biomolecules*, vol. 10, no.8, pp. 1–20, Aug. 01, 2020, doi: 10.3390/biom10081169.

[35] S. Afewerki, A. Sheikhi, S. Kannan, S. Ahadian, and A. Khademhosseini, “Gelatin-polysaccharide composite scaffolds for 3D cell culture and tissue engineering: Towards natural therapeutics,” *Bioengineering & Translational Medicine*, vol. 4, no. 1, pp. 96–115, Jan. 2019, doi: 10.1002/btm2.10124.

[36] P. Jaipan, A. Nguyen, and R. J. Narayan, “Gelatin-based hydrogels for biomedical applications,” *MRS Communications*, vol. 7, no. 3, pp. 416–426, Sep. 2017, doi: 10.1557/MRC.2017.92

[37] J. Il Kang and K. M. Park, “Advances in gelatin-based hydrogels for wound management,” *Journal of Materials Chemistry B*, vol. 9, no. 6, pp. 1503–1520, Feb. 2021, doi: 10.1039/D0TB02582H.

[38] B. Sarker et al., “Evaluation of Fibroblasts Adhesion and Proliferation on Alginate-Gelatin Crosslinked Hydrogel,” *PLoS One*, vol. 9, no. 9, p. 107952, Sep. 2014, doi: 10.1371/JOURNAL.PONE.0107952

[39] YY. Hsu, KL. Liu, HH. Yeh, HR. Lin, HL. Wu and JC. Tsai, “Sustained release of recombinant thrombomodulin from cross-linked gelatin/hyaluronic acid hydrogels potentiate wound healing in diabetic mice,” *Eur. J. Pharm. Biopharm.*, vol. 135, pp. 61–71, Feb. 2019, doi: 10.1016/J.EJPB.2018.12.007.

[40] S. S. Athukoralalage, R. Balu, N. K. Dutta and N. R. Choudhury, “3D Bioprinted Nanocellulose-Based Hydrogels for Tissue Engineering Applications: A Brief Review,” *Polymers (Basel).*, vol. 11, no. 5, May 2019, doi: 10.3390/POLYM11050898.

[41] “BioRender.” https://biorender.com/ (accessed Nov. 01, 2021).

[42] J. Li, C. Wu, P. K. Chu, and M. Gelinsky, “3D printing of hydrogels: Rational design strategies and emerging biomedical applications”, Mater. Sci. Eng. R Reports, vol. 140, p. 100543, Apr. 2020, doi: 10.1016/J.MSER.2020.100543.

[43] C. Mandrycky, Z. Wang, K. Kim, DH. Kim, “3D bioprinting for engineering complex tissues,” *Biotechnology Advances*, vol. 34, no. 4, pp. 422–434, Jul. 2016, doi: 10.1016/J.BIOTECHADV.2015.12.011.

[44] T. Jiang, J. G. Munguia-Lopez, S. Flores-Torres, J. Kort-Mascort, and J. M. Kinsella, “Extrusion bioprinting of soft materials: An emerging technique for biological model fabrication,” *Applied Physics Review*, vol. 6, no. 1, p. 011310, Mar. 2019, doi: 10.1063/1.5059393.

[45] X. Wang et al., “Gelatin-Based Hydrogels for Organ 3D Bioprinting,” *Polymers 2017, Vol. 9, Page 401*, vol. 9, no. 9, p. 401, Aug. 2017, doi: 10.3390/POLYM9090401.

[46] H. Li, C. Tan, and L. Li, “Review of 3D printable hydrogels and constructs,” *Materials & Design*, vol. 159, pp. 20–38, Dec. 2018, doi: 10.1016/J.MATDES.2018.08.023.

[47] Y. He, F. Yang, H. Zhao, Q. Gao, B. Xia, and J. Fu, “Research on the printability of hydrogels in 3D bioprinting,” *Science Reports 2016 61*, vol. 6, no. 1, pp. 1–13, Jul. 2016, doi: 10.1038/srep29977.

[48] C. Karavasili et al., “Physico-mechanical and finite element analysis evaluation of 3D printable alginate-methylcellulose inks for wound healing applications,” *CarbohydratePolymers*, vol. 247, p. 116666, Nov. 2020, doi: 10.1016/J.CARBPOL.2020.116666.

[49] J. H. Y. Chung et al., “Bio-ink properties and printability for extrusion printing living cells,” *Biomaterials Science*, vol. 1, no. 7, pp. 763–773, Jun. 2013, doi: 10.1039/C3BM00012E.

[50] D. J. Choi, S. J. Park, B. K. Gu, Y. J. Kim, S. Chung, and C. H. Kim, “Effect of the pore size in a 3D bioprinted gelatin scaffold on fibroblast proliferation,” *Journal of Industrial and Engineering Chemistry*, vol. 67, pp. 388–395, Nov. 2018, doi: 10.1016/J.JIEC.2018.07.013.

[51] S. L. Tomić, J. Nikodinović-Runić, M. Vukomanović, M. M. Babić, and J. S. Vuković, “Novel Hydrogel Scaffolds Based on Alginate, Gelatin, 2-Hydroxyethyl Methacrylate, and Hydroxyapatite,” *Polymers 2021, Vol. 13, Page 932*, vol. 13, no. 6, p. 932, Mar. 2021, doi: 10.3390/POLYM13060932.

[52] J. Liu, J. Chi, K. Wang, X. Liu, J. Liu, and F. Gu, “Full-thickness wound healing using 3D bioprinted gelatin-alginate scaffolds in mice: A histopathological study,” *International Journal of Clinical and Experimental Pathology,* vol. 9, no. 11, Jan. 2016.

[53] F. F. El-Senduny, N. M. Hegazi, G. E. Abd Elghani, and M. A. Farag, “Manuka honey, a unique mono-floral honey. A comprehensive review of its bioactives, metabolism, action mechanisms, and therapeutic merits,” *Food Bioscience*, vol. 42, p. 101038, Aug. 2021, doi: 10.1016/J.FBIO.2021.101038.

[54] M. I. Zainol, K. M. Yusoff, and M. Y. M. Yusof, “Antibacterial activity of selected Malaysian honey,” *BMC Complement. Altern. Med.*, vol. 13, p. 129, Jun. 2013, doi: 10.1186/1472-6882-13-129.

[55] I. Iacopetti, A. Perazzi, T. Martinello, F. Gemignani, and M. Patruno, “Hyaluronic acid, Manuka honey and Acemannan gel: Wound-specific applications for skin lesions,” *Research in Veterinary Science*, vol. 129, pp. 82–89, Apr. 2020, doi: 10.1016/J.RVSC.2020.01.009.

[56] V.C. Nolan, J. Harrison, J.E.E. Wright, J.A.G. Cox, “Clinical Significance of Manuka and Medical-Grade Honey for Antibiotic-Resistant Infections: A Systematic Review,” *Antibiot. (Basel, Switzerland)*, vol. 9, no. 11, pp. 1–24, Nov. 2020, doi: 10.3390/ANTIBIOTICS9110766.

[57] A. F. Henriques, R. E. Jenkins, N. F. Burton, and R. A. Cooper, “The intracellular effects of manuka honey on *Staphylococcus aureus*,” *Eur. J. Clin. Microbiol. Infect. Dis. 2009 291*, vol. 29, no. 1, pp. 45–50, Oct. 2009, doi: 10.1007/S10096-009-0817-2.

[58] J. M. Alvarez-Suarez, M. Gasparrini, T. Y. Forbes-Hernández, L. Mazzoni, and F. Giampieri, “The Composition and Biological Activity of Honey: A Focus on Manuka Honey,” *Foods 2014,* vol. 3, no. 3, pp. 420–432, Jul. 2014, doi: 10.3390/FOODS3030420.

[59] M. Johnston, M. McBride, D. Dahiya, R. Owusu-Apenten, and P. S. Nigam, “Antibacterial activity of Manuka honey and its components: An overview,” *AIMS Microbiology*, vol. 4, no. 4, p. 655, Nov. 2018, doi: 10.3934/MICROBIOL.2018.4.655.

[60] K. Schuhladen, P. Mukoo, L. Liverani, Z. Neščáková and A. R. Boccaccini, , “Manuka honey and bioactive glass impart methylcellulose foams with antibacterial effects for wound-healing applications,” *Biomed. Mater.*, vol. 15, no. 6, Nov. 2020, doi: 10.1088/1748-605X/AB87E5.

[61] P. Nezhad-Mokhtari et al., “Recent advances in honey-based hydrogels for wound healing applications: Towards natural therapeutics,” *Journal of Drug Delivery Science and Technology.*, vol. 66, p. 102789, Dec. 2021, doi: 10.1016/J.JDDST.2021.102789.

[62] F.F. A. El-Malek, A.S. Yousef and S.A. El-Assar, “Hydrogel film loaded with new formula from manuka honey for treatment of chronic wound infections,” *J. Glob. Antimicrob. Resist.*, vol. 11, pp. 171–176, Dec. 2017, doi: 10.1016/J.JGAR.2017.08.007.

[63] K. Schuhladen, V. Bednarzig, N. Rembold, and A. R. Boccaccini, “The effect of borate bioactive glass on the printability of methylcellulose-manuka honey hydrogels,” *J. Mater. Res*., pp. 1–8, Jun. 2021, doi: 10.1557/S43578-021-00256-9.

[64] T. Kreller, T. Distler, S. Heid, S. Gerth, R. Detsch, and A. R. Boccaccini, “Physico-chemical modification of gelatine for the improvement of 3D printability of oxidized alginate-gelatine hydrogels towards cartilage tissue engineering,” *Materials & Design.*, vol. 208, p. 109877, Oct. 2021, doi: 10.1016/J.MATDES.2021.109877.

[65] R.C. Rowe, P.Sheskey and M.Quinn, "Handbook of Pharmaceutical Excipients", Sixth Edit. Pharmaceuticals, 2009.

[66] “Allevi 2 - Allevi.” https://www.allevi3d.com/allevi-2/ (accessed Oct. 06, 2021).

[67] I. Wiegand, K. Hilpert and R. E. W. Hancock, “Agar and broth dilution methods to determine the minimal inhibitory concentration (MIC) of antimicrobial substances,” *Nat. Protoc.*, vol. 3, no. 2, pp. 163–175, Feb. 2008, doi: 10.1038/NPROT.2007.521.

[68] S. B. Almasaudi et al., “Antimicrobial effect of different types of honey on *Staphylococcus aureus*,” *Saudi J. Biol. Sci.*, vol. 24, no. 6, pp. 1255–1261, Sep. 2017, doi: 10.1016/J.SJBS.2016.08.007.

[69] H. Pan, Y. Zhang, G.X. He, N. Katagori, and H. Chen, “A comparison of conventional methods for the quantification of bacterial cells after exposure to metal oxide nanoparticles,” *BMC Microbiology*, vol. 14, no. 1, p. 222, Aug. 2014, doi: 10.1186/S12866-014-0222-6.

[70] P. Costa, A. T. P. C. Gomes, M. Braz, C. Pereira, and A. Almeida, “Application of the Resazurin Cell Viability Assay to *Monitor Escherichia coli* and *Salmonella Typhimurium* Inactivation Mediated by Phages,” *Antibiot. 2021*, vol. 10, no. 8, p. 974, Aug. 2021, doi: 10.3390/ANTIBIOTICS10080974.

[71] National Institutes of Health. ICCVAM-Recommended Test Method Protocol: Hen’s Egg Test–Chorioallantoic Membrane (HETCAM) Test Method (2010).

[72] V. Kokol, Y. B. Pottathara, M. Mihelčič, and L. S. Perše, “Rheological properties of gelatine hydrogels affected by flow- and horizontally-induced cooling rates during 3D cryo-printing,” *Colloids*

Surfaces A Physicochem. Eng. Asp., vol. 616, p. 126356, May 2021, doi: 10.1016/J.COLSURFA.2021.126356.

[73] SH. Hsu and A. M. Jamieson, "Viscoelastic behaviour at the thermal sol-gel transition of gelatin," *Polymer (Guildf).*, vol. 34, no. 12, pp. 2602–2608, Jan. 1993, doi: 10.1016/0032-3861(93)90596-3.

[74] C. Michon, G. Cuvelier, and B. Launay, "Concentration dependence of the critical viscoelastic properties of gelatin at the gel point," *Rheol. Acta Rheol Acta*, vol. 32, pp. 94–103, 1993.

[75] F.F. Cai, S. Heid, and A. R. Boccaccini, "Potential of Laponite® incorporated oxidized alginate–gelatin (ADA-GEL) composite hydrogels for extrusion-based 3D printing," *J. Biomed. Mater. Res. Part B Appl. Biomater*., vol. 109, no. 8, pp. 1090–1104, Aug. 2021, doi: 10.1002/JBM.B.34771.

[76] "Manuka honey is heat sensitive so keep it cool. - Manuka Natural." https://www.manukanatural.com/blog/manuka-honey-is-heat-sensitive-so-keep-it-cool/ (accessed Oct. 21, 2021).

[77] M. Di Giuseppe et al., "Mechanical behaviour of alginate-gelatin hydrogels for 3D bioprinting," *J. Mech. Behav. Biomed. Mater.,* vol. 79, pp. 150–157, Mar. 2018, doi: 10.1016/J.JMBBM.2017.12.018.

[78] S. Bom et al., "Effects of starch incorporation on the physicochemical properties and release kinetics of alginate-based 3D hydrogel patches for topical delivery," Pharmaceutics, vol. 12, no. 8, pp. 1–20, Jul. 2020, doi: 10.3390/pharmaceutics12080719

[79] J. Skopinska-Wisniewska, M. Tuszynska, and E. Olewnik-Kruszkowska, "Comparative Study of Gelatin Hydrogels Modified by Various Crosslinking Agents," *Materials (Basel).*, vol. 14, no. 2, pp. 1–17, Jan. 2021, doi: 10.3390/MA14020396.

[80] E. Mancuso et al., "Potential of Manuka Honey as a Natural Polyelectrolyte to Develop Biomimetic Nanostructured Meshes With Antimicrobial Properties," *Frontiers in Bioengineering and Biotechnology*, vol. 7, p. 344, Dec. 2019, doi: 10.3389/FBIOE.2019.00344.

[81] O. Anjos, M. G. Campos, P. C. Ruiz, and P. Antunes, "Application of FTIR-ATR spectroscopy to the quantification of sugar in honey," *Food Chemistry*, vol. 169, pp. 218–223, Feb. 2015, doi: 10.1016/J.FOODCHEM.2014.07.138.

[82] M.A. Bonifácio et al., "Data on Manuka Honey/Gellan Gum composite hydrogels for cartilage repair," *Data Br.*, vol. 20, pp. 831–839, Oct. 2018, doi: 10.1016/J.DIB.2018.08.155

[83] H. T. Tan et al., "The antibacterial properties of Malaysian tualang honey against wound and enteric microorganisms in comparison to manuka honey," *BMC Complement. Altern. Med. 2009 91*, vol. 9, no. 1, pp. 1–8, Sep. 2009, doi: 10.1186/1472-6882-9-34.

[84] R. Jenkins and R. Cooper, "Improving Antibiotic Activity against Wound Pathogens with Manuka

Honey *In Vitro*," *PLoS One*, vol. 7, no. 9, p. 45600, Sep. 2012, doi: 10.1371/JOURNAL.PONE.0045600.

[85] K. R. Hixon, T. Lu, S. H. McBride-Gagyi, B. E. Janowiak, and S. A. Sell, "A comparison of tissue engineering scaffolds incorporated with Manuka honey of varying UMF," *Biomed Res. Int.*, vol. 2017, 2017, doi: 10.1155/2017/4843065.

[86] N. N. Cokcetin et al., "The Antibacterial Activity of Australian Leptospermum Honey Correlates with Methylglyoxal Levels," *PLoS One*, vol. 11, no. 12, p. e0167780, Dec. 2016, doi: 10.1371/JOURNAL.PONE.0167780.

[87] A. Girma, W. Seo, and R. C. She, "Antibacterial activity of varying UMF-graded Manuka honeys," *PLoS One*, vol. 14, no. 10, p. e0224495, Oct. 2019, doi: 10.1371/JOURNAL.PONE.0224495.

[88] B. A. Minden-Birkenmaier and G. L. Bowlin, "Honey-Based Templates in Wound Healing and Tissue Engineering," *Bioengineering 2018,* vol. 5, no. 2, p. 46, Jun. 2018, doi: 10.3390/BIOENGINEERING5020046.

[89] A. M. N. *Santos* et al., "Physically Cross-Linked Gels of PVA with Natural Polymers as Matrices for Manuka Honey Release in Wound-Care Applications," *Materials (Basel).*, vol. 12, no. 4, Feb. 2019, doi: 10.3390/MA12040559.

[90] "ISO - ISO 10993-5:2009 - Biological evaluation of medical devices — Part 5: Tests for *in vitro* cytotoxicity." https://www.iso.org/standard/36406.html (accessed Oct. 27, 2021).

[91] E. Ranzato, S. Martinotti, and B. Burlando, "Epithelial mesenchymal transition traits in honey-driven keratinocyte wound healing: Comparison among different honeys," *Wound Repair and Regeneration*, vol. 20, no. 5, pp. 778–785, Sep. 2012, doi: 10.1111/J.1524-475X.2012.00825.X.

[92] E. Ranzato, S. Martinotti, and B. Burlando, "Honey exposure stimulates wound repair of human dermal fibroblasts," *Burn. Trauma*, vol. 1, no. 1, p. 32, Jun. 2013, doi: 10.4103/2321-3868.113333.

[93] "Test No. 431: *In vitro* skin corrosion: reconstructed human epidermis (RHE) test method | OECD Guidelines for the Testing of Chemicals, Section 4 : Health Effects | OECD iLibrary." https://www.oecd-ilibrary.org/environment/test-no-431-in-vitro-skin-corrosion-reconstructed-human-epidermis-rhe-test-method_9789264264618-en (accessed Sept. 14, 2021).

[94] C. C. Coelho, L. Grenho, P. S. Gomes, P. A. Quadros, and M. H. Fernandes, "Nano-hydroxyapatite in oral care cosmetics: characterization and cytotoxicity assessment," *Science Reports* 2019 91, vol. 9, no. 1, pp. 1–10, Jul. 2019, doi: 10.1038/s41598-019-47491-z.

[95] T. Goodpaster, A. Legesse-Miller, M. R. Hameed, S. C. Aisner, J. Randolph-Habecker, and H. A. Coller, "An Immunohistochemical Method for Identifying Fibroblasts in Formalin-fixed, Paraffin-embedded Tissue,"*Journal of Histochemistry & Cytochemistry*, vol. 56, no. 4, p. 347, Apr. 2008, doi:

10.1369/JHC.7A7287.2007.

[96] I. Miller et al., “Ki67 is a Graded Rather than a Binary Marker of Proliferation versus Quiescence,” *Cell Rep.*, vol. 24, no. 5, p. 1105, Jul. 2018, doi: 10.1016/J.CELREP.2018.06.110.

[97] P. Betz, A. Nerlich, J. Wilske, J. Tübel, R. Penning and W. Eisenmengen, “The time-dependent localization of Ki67 antigen-positive cells in human skin wounds,” *International Journal of Legal Medicine*, vol. 106, no. 1, pp. 35–40, Jan. 1993, doi: 10.1007/BF01225022.

[98] E. Hunter-Featherstone et al., “Culturing Keratinocytes on Biomimetic Substrates Facilitates Improved Epidermal Assembly *In Vitro*,” *Cells 2021,* vol. 10, no. 5, p. 1177, May 2021, doi: 10.3390/CELLS10051177.

[99] S. W. Yang, ZJ. Geng, K. Ma, XY. Sun and XB. Fu, “Comparison of the histological morphology between normal skin and scar tissue,” *Journal of Huazhong University of Science and Technology [Medical Sciences]* , vol. 36, no. 2, pp. 265–269, Apr. 2016, doi: 10.1007/S11596-016-1578-7.

[100] S. A. Sell et al., “A Preliminary Study on the Potential of Manuka Honey and Platelet-Rich Plasma in Wound Healing,” *International Journal of Biomaterials*, vol. 2012, p. 14, Dec. 2012, doi: 10.1155/2012/313781.

[101] S. Martinotti, U. Laforenza, M. Patrone, F. Moccia, and E. Ranzato, “Honey-Mediated Wound Healing: H_2O_2 Entry through AQP3 Determines Extracellular Ca^{2+} Influx,” *Int. J. Mol. Sci.*, vol. 20, no. 3, Dec. 2019, doi: 10.3390/IJMS20030764.

[102] H. A. Alzahrani, R. Alsabehi, L. Boukraâ, F. Abdellah, Y. Bellik, and B. A. Bakhotmah, “Antibacterial and Antioxidant Potency of Floral Honeys from Different Botanical and Geographical Origins,” *Molecules 2012*, vol. 17, no. 9, pp. 10540–10549, Sep. 2012, doi: 10.3390/MOLECULES170910540.

[103] J. M. Alvarez-Suarez et al., “Activation of AMPK/Nrf2 signalling by Manuka honey protects human dermal fibroblasts against oxidative damage by improving antioxidant response and mitochondrial function promoting wound healing,” *Journal of Functional Foods*, vol. 25, pp. 38–49, Aug. 2016, doi: 10.1016/J.JFF.2016.05.008.

[104] S. Patel, S. Srivastava, M. R. Singh, and D. Singh, “Preparation and optimization of chitosan-gelatin films for sustained delivery of lupeol for wound healing,” *International Journal of Biological Macromolecules*, vol. 107, pp. 1888–1897, Feb. 2018, doi: 10.1016/J.IJBIOMAC.2017.10.056.

[105] W. Schuurman et al., “Gelatin-methacrylamide hydrogels as potential biomaterials for fabrication of tissue-engineered cartilage constructs,” *Macromol. Biosci.*, vol. 13, no. 5, pp. 551–561, May 2013, doi: 10.1002/MABI.201200471.

[106] C.C. Tsai, TH. Young, G.S. Chen, and N.C. Cheng, “Developing a Glyoxal-Crosslinked Chitosan/Gelatin Hydrogel for Sustained Release of Human Platelet Lysate to Promote Tissue Regeneration,” *International Journal of Molecular Sciences* vol. 22,12 6451. 16 Jun. 2021, doi:10.3390/ijms22126451

6. Appendix

6.1. Appendix A1 - Results and Discussion

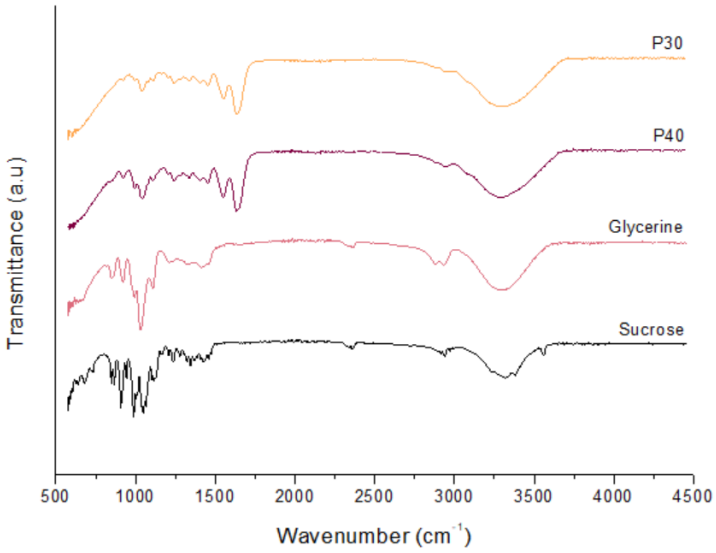

Figure A 1 - Comparison between the ATR-FTIR spectra of glycerine, sucrose powder, P30 and P40 patches.

6.2. Appendix A2 - Results and Discussion

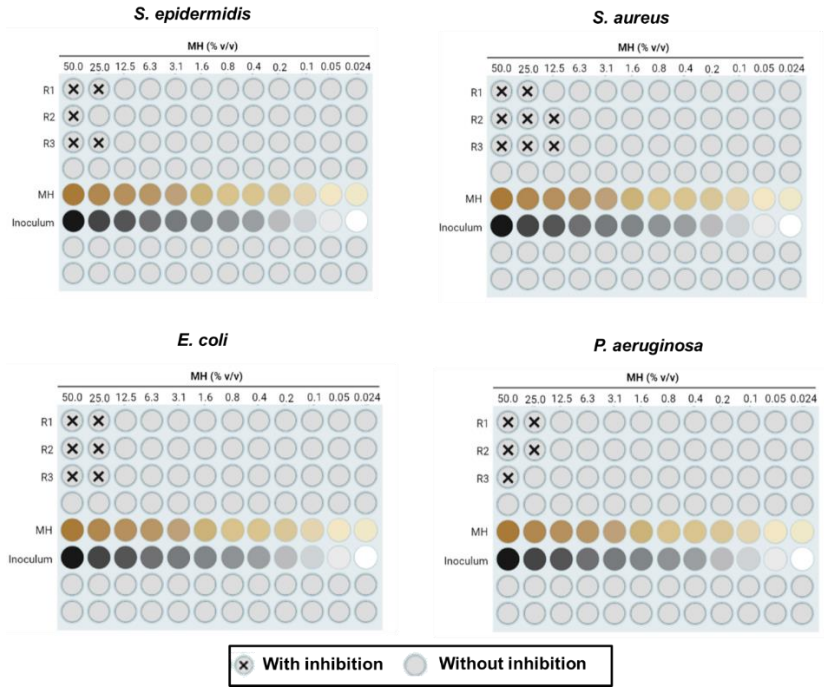

Appendix A 1 - Minimum Inhibitory Concentration (MIC) of Manuka honey (MH) obtained for each studied strain, *S. aureus, S. epidermidis, E. coli* and *P. aeruginosa.* The test was performed in triplicates and the obtained values were decided when at least 2 replicas showed bacterial inhibition after 24h.

6.3. Appendix A3 – Results and Discussion

Calculation of methylglyoxal content (MGO) in the studied Manuka Honey (MH) with a MGO of 300+ mg MGO/kg MH, for a MIC of 35.5% w/v.

$$300\ \frac{mg\ MGO}{kg\ MH} \Rightarrow\ 0.3\ \frac{mg\ MGO}{g\ MH}\ x\ \frac{35.5\ g\ MH}{100\ mL}\ =\ 0.1065\ \frac{mg\ MGO}{mL} \cong 106\ \mu g\ MGO/mL$$